TECHNISCHE UNIVERSITÄT MÜNCHEN

PHYSIK-DEPARTMENT

THEORETISCHE PHYSIK T70

# Right-handed Neutrinos: From the Early Universe to Experiments

Juraj KLARIĆ

Vollständiger Abdruck der von der Fakultät für Physik der Technischen Universität München zur Erlangung des akademischen Grades eines

Doktors der Naturwissenschaften (Dr. rer. nat.)

genehmigten Dissertation.

| | |
|---|---|
| Vorsitzender: | Prof. Dr. Bastian Märkisch |
| Prüfer der Dissertation: | 1. Prof. Dr. Björn Garbrecht<br>2. apl. Prof. Dr. Antonio Vairo |

Die Dissertation wurde am 11.02.2019 bei der Technischen Universität München eingereicht und durch die Fakultät für Physik am 21.05.2019 angenommen.

# Contents


**1 Introduction** **7**

**2 The Low Scale Seesaw Mechanism** **11**
2.1 The Type-I Seesaw Mechanism . . . . . 13
2.1.1 The Casas-Ibarra Parametrization . . . . . 16
2.2 Symmetry protected scenario . . . . . 17
2.3 Constraints on the Properties of Heavy Neutrinos . . . . . 19

**3 Out-of-Equilibrium Fields in the Early Universe** **26**
3.1 Derivation of the Evolution Equations . . . . . 28
3.1.1 Correlation functions . . . . . 28
3.1.2 Wigner space and the gradient expansion . . . . . 29
3.1.3 Evolution equations for heavy neutrinos . . . . . 32
3.2 Quantum Boltzmann equations for heavy neutrinos . . . . . 35
3.3 Boltzmann equations for active leptons . . . . . 36
3.3.1 Spectator Processes . . . . . 38
3.4 Expansion of the Universe . . . . . 39

**4 Baryogenesis Through Leptogenesis** **41**
4.1 Vanilla Leptogenesis . . . . . 42
4.2 Evolution Equations for Leptogenesis . . . . . 44
4.3 Resonant leptogenesis . . . . . 45
4.3.1 Non-Relativistic Approximations . . . . . 45
4.3.2 Strong Washout Regime . . . . . 47
4.3.3 Applicability of approximations . . . . . 48
4.4 Leptogenesis Through Neutrino Oscillations . . . . . 54
4.4.1 Ultra-Relativistic Approximations . . . . . 54
4.4.2 Analytic Expansions for Leptogenesis Through Neutrino Oscillations . . . . . 58
4.4.3 The Role of Lepton Number Violating Processes . . . . . 79

**5 Testing the Low-scale Seesaw and Leptogenesis** **85**
5.1 Parameter Space in Absence of the $\tilde{L}NV$ Processes . . . . . . . . . . . 86
5.2 Parameter Space With the $\tilde{L}NV$ Processes . . . . . . . . . . . . . . . . . 92
5.2.1 Measurement of Leptogenesis Parameters at Future Lepton Colliders . . . . . . . . . . . . . . . . . . . . . . . . . . . . 92
5.2.2 Results of the Parameter Scan . . . . . . . . . . . . . . . . . . . . 97

**6 Conclusion** **109**

**A Heavy neutrino mixing angles** **112**

**B The Metropolis-Hastings sampling algorithm** **115**

**C Definitions and relations between the two-point functions** **116**

**D Equilibrium Green functions** **117**

**E Majorana Neutrino Self-Energy** **119**
E.1 Relation between the collision terms of the heavy and doublet neutrinos . . . . . . . . . . . . . . . . . . . . . . . . . . . . . . . . 120

**F Precision of measuring flavour mixing ratios** **122**
F.1 Probability distribution for $N_{\rm sl}$ semileptonic events with $N_\alpha$ of them in flavour $\alpha$. . . . . . . . . . . . . . . . . . . . . . . . . . . . . 122
F.2 Precision of measuring $U_\alpha^2/U^2$. . . . . . . . . . . . . . . . . . . . . . . . 123

# Acknowledgements

I would like to express my enormous gratitude to my supervisor, Prof. Björn Garbrecht, for providing a friendly and motivating work environment. Thanks to him, I had the fortune not only to work on topics I found interesting, but to have great fun while doing so. I am especially grateful for the patience and understanding he showed me from the beginning to the very end of my time at TUM.

I am sincerely thankful to Prof. Marco Drewes, for the long discussions, for always being happy to help and give advice with the many questions a PhD student can have. Furthermore, I have to mention Dario Gueter, to whom I grateful for all the peanut kit-kats[1] we shared, for the excellent teamwork on several projects, and for showing me the meaning of the phrase "two heads are better than one".

I would like to thank Prof. Stefan Antusch, Dr. Oliver Fischer, Eros Cazzato, Dr. Mathias Garny and Dr. Florian Gautier for the fun and interesting collaboration during the different stages of my PhD.

Life of a PhD student would not be complete with other PhD students, postdocs and master students to share coffee and thoughts with. For this I am especially grateful to Yi Zhu, Peter Millington, Philipp Klose, Wenyuan Ai, Carlos Tamarit, Juan Sebastian Cruz, Jamie McDonald and Giovanni Zattara. I would also like to thank Laura Darabas for the support with all of the paperwork and logistics at the TUM. A large part of my work relied on the excellent IT infrastructure TUM has, and for this I have to extend my gratitude to Dr. Stefan Recksiegel, who helped me with any hurdles or questions I ran into.

I thank my parents Vlasta and Marin, for all the support and always being there for me. I am also grateful to my siblings, Ana, Magda, Mislav and Lovro, for visiting me many times while I was here, and making Munich feel even more like home.

Of course, I am especially grateful to my wife, Tea, who supported me throughout my PhD, and happily tolerated my late evenings (and sometimes nights), as well as my occasional zoning-out in the middle of the conversation if my mind somehow wandered away to physics.

[1] Not a sponsor.

# Publications

This manuscript is based on several publications that were written during this PhD thesis, listed below:

- B. Garbrecht, F. Gautier and J. Klaric *Strong Washout Approximation to Resonant Leptogenesis*, JCAP **1409** (2014) no.09, 033
- M. Drewes, B. Garbrecht, D. Gueter and J. Klaric *Leptogenesis from Oscillations of Heavy Neutrinos with Large Mixing Angles*, JHEP **1612** (2016) 150
- M. Drewes, B. Garbrecht, D. Gueter and J. Klaric *Testing the low scale seesaw and leptogenesis*, JHEP **1708** (2017) 018
- S. Antusch, E. Cazzato, M. Drewes, O. Fischer, B. Garbrecht, D. Gueter and J. Klaric *Probing Leptogenesis at Future Colliders*, JHEP **1809** (2018) 124
- B. Dev, M. Garny, J. Klaric, P. Millington and D. Teresi, *Resonant enhancement in leptogenesis*, Int. J. Mod. Phys. A **33** (2018) 1842003
- M. Drewes, J. Hajer, J. Klaric and G. Lanfranchi, *NA62 sensitivity to heavy neutral leptons in the low scale seesaw model*, JHEP **1807** (2018) 105

# Chapter 1

# Introduction

Almost all phenomena in nature can be explained by the standard model of particle physics (SM). The only well established experimental sign of physics beyond the standard model (BSM) are the *neutrino flavour oscillations*, which imply the existence of neutrino masses. The neutrino masses cannot be generated with the fields available in the standard model alone.

Besides neutrino oscillations, there are several hints of new physics coming from cosmology. One of the most compelling signs of physics beyond the standard model is the observed baryon asymmetry of the Universe (BAU). We quantify the size of the BAU through the ratio of baryon number to entropy [1–4]

$$Y_B^{\text{obs}} = (8.6 \pm 0.1) \times 10^{-11} \,. \tag{1.1}$$

Mechanisms of producing the excess of baryons over antibaryons are known by the umbrella term *baryogenesis*. The conditions necessary for producing such an asymmetry were first laid out by Sakharov in 1967 [5], known as the *Sakharov conditions*:

- baryon number violation $\not{B}$
- violation of $C$ and $CP$ symmetries
- deviation from thermal equilibrium.

It is interesting that all three of these Sakharov conditions are realized in the standard model. Baryon number is violated by the so-called *sphaleron* processes, which violate the sum of baryon and lepton numbers $B + L$, but conserve their difference $B - L$. The $C$ and $CP$ symmetries are violated in the quark sector through the phases in the Cabbibo-Kobayashi-Makasawa (CKM) matrix. However, even if the electroweak phase transition was first-order, giving a sizeable deviation from equilibrium, the standard model would fall short of the observed BAU by more than 16

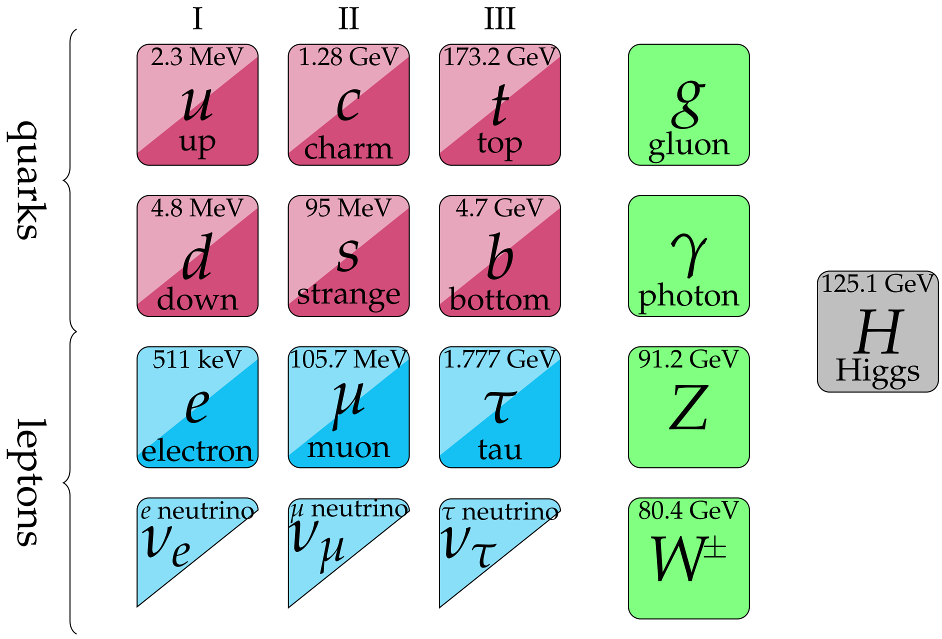


Figure 1.1: The standard model of particle physics. Note that all standard model particles appear in left and right-handed chiralities except for neutrinos.

orders of magnitude [6–8]. Therefore, any scenario that could explain the observed BAU has to rely on phenomena beyond the standard model.

In the SM all fermions appear as both right-handed (RH) and left-handed (LH) chiral particles. The only exception are the neutrinos, which appear only as left-handed (*c.f.* Fig. 1.1).

If we extend the standard model by right-handed neutrinos, we can solve both problems, the neutrino masses can be generated through the so-called *seesaw mechanism* [9–14], and the baryon asymmetry of the universe can arise through a process called *leptogenesis* [15].

The neutrino masses are significantly smaller than any of the other fermion masses in the standard model. Current limits from the Planck collaboration [4], imply that the sum of neutrino masses is smaller than $\sum_i m_i < 0.12\,\mathrm{eV}$. If neutrino masses are generated only through the Higgs mechanism, their Yukawa couplings would need to be more than 6 orders of magnitude smaller than those of the electron.

However, neutrinos have another trick up their sleeve. Right-handed neutrinos are standard model gauge singlets. As such, in addition to the usual Dirac masses generated through the Higgs mechanism, they can also have Majorana masses. The Majorana masses are free parameters and are not constrained by the observed neutrino masses. In the usual seesaw mechanism, the Majorana masses $M$ are assumed to be much larger than the electroweak scale $\sim v = 174\,\text{GeV}$, which suppresses the observed neutrino masses by a factor $v/M$.

On the other hand, Majorana masses below the electroweak scale are phenomenologically motivated, as the existence of right-handed neutrinos could be tested experimentally. For Majorana masses below 5 GeV, right-handed neutrinos could be found in current experiments like the NA62 experiment [16, 17], T2K [18], or, in the future, the SHiP experiment [19, 20]. Existing LHC experiments such as ATLAS [21–23], CMS [24–26] and LHCb [27, 28] are already performing searches for right-handed neutrinos with Majorana masses between 5 GeV and the $W$ gauge boson mass. Sensitivity to right-handed neutrinos can be significantly enhanced with the inclusion of more signatures and improved triggers [29–35], or with additional detectors [36–38]. Higher sensitivity could be achieved at future lepton colliders [20, 39–46].

Besides phenomenological considerations, Majorana masses below the electroweak scale can also be motivated on theoretical grounds. Right-handed neutrinos with superheavy Majorana masses could potentially destabilize the Higgs mass [47], which is not a problem for Majorana masses below the EW scale [48]. Furthermore, it is also possible that the Majorana masses and the electroweak scale have a common origin [49–52]. Light Majorana masses are also realised in models with an approximate $B - L$ symmetry. The smallness of the observed neutrino masses is then not due to the seesaw mechanism, but is instead determined by the amount of violation of the approximate "lepton-number"-like symmetry. Examples of such models include the "inverse seesaw models" [53–56], "linear seesaw models" [57–60] (see also [61–65]), and "minimal flavour violation" [66, 67]. For numerical implementations of different models that include radiative corrections see [68, 69]. In this work we remain agnostic to the origin of this approximate symmetry, and only consider SM extended with two right-handed neutrinos. This scenario effectively corresponds to the *Neutrino Minimal Standard Model* ($\nu$-MSM) [70, 71], where two of the right-handed neutrinos are responsible for the light neutrino masses and the BAU, while a third right-handed neutrino almost decouples, and acts as a dark matter candidate. [1]

Leptogenesis [15] is a mechanism of producing a lepton asymmetry in the early universe. This lepton asymmetry is converted to a baryon asymmetry through the electroweak sphaleron processes [74], solving the puzzle of the observed BAU. In the simplest realization, the lepton asymmetry is generated through the $CP$ violating decays of a heavy Majorana neutrino in the early universe. The majority of the lepton asymmetry is produced at temperatures $T \sim M$, when the heavy Majorana neutrino is freezing out of equilibrium. Such a scenario requires large right-handed neutrino Majorana masses $M \sim 10^9$ GeV [75–79], which are out of reach for any

[1] For a more detailed descriptions of the $\nu$MSM see *e.g.* refs. [72, 73].

present or near future experiments.

This bound can be significantly relaxed if at least two of the Majorana masses are close to being degenerate, as the decay asymmetry becomes resonantly enhanced [80–86], which is known as *resonant leptogenesis*. In this scenario the lower bound comes from the requirement that the heavy neutrino decays before the sphaleron freeze-out at $T \sim 130$ GeV [87].

For even lighter (GeV-scale) right-handed neutrino Majorana masses, instead of relying on freeze-out, leptogenesis can occur during the production and oscillations of the right-handed Majorana neutrinos [71, 88], known as *leptogenesis through neutrino oscillations*.

In this work we develop numerical and analytic methods to study these two leptogenesis mechanisms, and discuss the relevant phenomenological implications.

# Chapter 2

# The Low Scale Seesaw Mechanism

In this chapter we briefly review the phenomenology of neutrino masses, and the type-I seesaw model. Neutrino oscillations are the only well established experimental signal of physics beyond the SM. The interactions of neutrinos $\nu_L$ with the rest of the standard model is described by the Lagrangian

$$-\frac{g}{\sqrt{2}}\bar{\nu_L}\gamma^\mu e_L W^+_\mu - \frac{g}{\sqrt{2}}\bar{e_L}\gamma^\mu \nu_L W^-_\mu - \frac{g}{2\cos\theta_W}\bar{\nu_L}\gamma^\mu \nu_L Z_\mu\,, \tag{2.1}$$

which defines the interaction eigenstates $\nu_e$, $\nu_\mu$ and $\nu_\tau$. Significant evidence for neutrino oscillations, which imply neutrino masses, was found in experiments involving solar, atmospheric and reactor neutrinos. The oscillations of neutrinos are then explained by a mismatch between the neutrino interaction and mass bases, *i.e.* each of the flavour eigenstates $\nu_\alpha$ can be written as a superposition of mass eigenstates

$$\nu_\alpha(x) = \sum_\beta (U_\nu)_{\alpha\beta}\nu_\beta(x)\,, \tag{2.2}$$

where $U_\nu$ is the unitary Pontecorvo-Maki-Nakagawa-Sakata (PMNS) matrix, for which we use the standard parametrization [89]

$$U_\nu = V^{(23)}U_\delta V^{(13)}U_{-\delta}V^{(12)}\mathrm{diag}(e^{\mathrm{i}\alpha_1/2},\, e^{\mathrm{i}\alpha_2/2},\, 1)\,, \tag{2.3}$$

where $U_{\pm\delta} = \mathrm{diag}(1,\, e^{\mp\mathrm{i}\delta/2},\, e^{\pm\mathrm{i}\delta/2})$, and the non-vanishing entries of $V^{(\alpha\beta)}$ for $\alpha = e,\, \mu,\, \tau$ are

$$V^{(\alpha\beta)}_{aa} = V^{(\alpha\beta)}_{bb} = \cos\theta_{\alpha\beta}\,, \quad V^{(\alpha\beta)}_{\alpha\beta} = -V^{(\alpha\beta)}_{\beta\alpha} = \sin\theta_{\alpha\beta}\,, \quad V^{(\alpha\beta)}_{\gamma\gamma}|_{\gamma\neq\alpha,\beta} = 1\,. \tag{2.4}$$

The elements of the PMNS matrix, as well as two of the neutrino mass differences have been measured by the neutrino oscillation experiments. The smaller of the two mass differences is the "solar mass difference" $\Delta m^2_{\mathrm{sol}} \equiv m_2^2 - m_1^2$, where $m_2$ is the heavier of the two neutrinos. The mass difference, between $m_1$ and $m_3$, is for historical reasons known as the "atmospheric mass difference" $\Delta m^2_{\mathrm{atm}} \equiv |m_3^2 - m_1^2|$. The third mass eigenstate can either be heavier than $m_1$ and $m_2$, in what we call "normal neutrino mass ordering" (NO), or lighter, which corresponds to the "inverted ordering" (IO). We summarize these definitions in table 2.1.

The parameters of the PMNS matrix can be determined by combining results of several different experiments. In the following, we take the best fit values provided by the $\nu$-fit collaboration [90, 91], cf. Table 2.2.

| Variables | | NO | IO |
|---|---|---|---|
| Masses | $m_1^2$ | $m_{\text{lightest}}^2$ | $m_{\text{lightest}}^2 - \Delta m_{32}^2 - \Delta m_{\text{sol}}^2$ |
| | $m_2^2$ | $m_{\text{lightest}}^2 + \Delta m_{\text{sol}}^2$ | $m_{\text{lightest}}^2 - \Delta m_{32}^2$ |
| | $m_3^2$ | $m_{\text{lightest}}^2 + \Delta m_{31}^2$ | $m_{\text{lightest}}^2$ |
| Differences | larger $\Delta m^2$ | $\Delta m_{31}^2 = m_3^2 - m_1^2$ | $\Delta m_{32}^2 = m_3^2 - m_2^2$ |
| | $(n_s = 2)$ $\Delta m_{\text{atm}}^2$ | $m_3^2$ | $m_1^2 \equiv m_2^2 + \mathcal{O}(\Delta m_{\text{sol}}^2 / \Delta m_{\text{atm}}^2)$ |

Table 2.1: The naming convention for neutrino masses and their differences in the cases of normal (NO) and inverted orderings (IO). The "solar mass difference" is the smaller mass difference, defined as the difference $\Delta m_{\text{sol}}^2 = m_2^2 - m_1^2$ regardless of the neutrino mass ordering. The larger mass difference is known as the "atmospheric mass difference", and it is defined as $\Delta m_{\text{atm}}^2 = |m_3^2 - m_1^2|$. The lightest neutrino is massless ($m_{\text{lightest}} = 0$) in the minimal scenario $(n_s = 2)$ and the atmospheric mass splitting $\Delta m_{\text{atm}}^2$ can clearly be identified with one of the neutrino masses.

## 2.1 The Type-I Seesaw Mechanism

The type-I seesaw model is the extension of the standard model by $n_s$ right-handed neutrinos (RHN) $\nu_{\mathrm{R}\,\mathrm{i}}$ ($i = 1 \ldots n_s$) and is described by the Lagrangian

$$\mathcal{L} = \mathcal{L}_{\text{SM}} + \mathrm{i}\overline{\nu_{\mathrm{R}i}}\partial\!\!\!/\,\nu_{\mathrm{R}i} - \frac{1}{2}(\overline{\nu^c_{\mathrm{R}i}} M_{ij} \nu_{\mathrm{R}j} + \overline{\nu_{\mathrm{R}i}} M^*_{ji} \nu^c_{\mathrm{R}j}) - Y^*_{i\alpha} \overline{\ell_\alpha} \varepsilon \phi \nu_{\mathrm{R}i} - Y_{i\alpha} \overline{\nu_{\mathrm{R}i}} \phi^\dagger \varepsilon^\dagger \ell_\alpha\,, \tag{2.5}$$

where $\mathcal{L}_{\text{SM}}$ is the Lagrangian of the SM. The only interaction between the right-handed neutrinos and the SM is through the Yukawa couplings $Y$ to the SM lepton

| Variables | | NO | IO |
|---|---|---|---|
| Differences | smaller $\Delta m_{\text{sol}}^2$ | $7.40 \times 10^{-5}\,\text{eV}^2$ | $7.40 \times 10^{-5}\,\text{eV}^2$ |
| | larger $\Delta m^2$ | $2.494 \times 10^{-3}\,\text{eV}^2$ | $-2.465 \times 10^{-3}\,\text{eV}^2$ |
| Angles | $\sin^2\theta_{12}$ | 0.307 | 0.307 |
| | $\sin^2\theta_{13}$ | 0.02206 | 0.02227 |
| | $\sin^2\theta_{23}$ | 0.538 | 0.554 |

Table 2.2: Best fit values of neutrino mixing angles and mass differences from the NuFIT 3.2 release by the $\nu$-fit collaboration [90, 91], for "normal ordering" (NO) and "inverted ordering" (IO). The mass differences are defined in Table 2.1.

doublets $\ell_\alpha$ ($\alpha = e, \mu, \tau$) and the Higgs field $\phi$, where $\varepsilon$ is the antisymmetric SU(2)-invariant tensor with $\varepsilon^{12} = 1$. The superscript $c$ appearing on the RHN spinors denotes charge conjugation. The matrix $M_{ij}$ is the Majorana mass matrix of the RHN.

After electroweak symmetry breaking (EWSB) the Higgs field obtains an expectation value $v = 174\,\text{GeV}$. The Yukawa interaction term $Y^*_{ia}\overline{\ell_a}\varepsilon\phi\nu_{\text{R}i}$ gives us the Dirac mass term $\overline{\nu_{L\alpha}}(m_D)_{\alpha i}\nu_{Ri}$, with the Dirac mass

$$(m_D)_{\alpha i} = v\left(Y^\dagger\right)_{\alpha i}. \tag{2.6}$$

After EWSB we can write the mass term of the neutrinos in the block-matrix form

$$\mathcal{L} \supset -\frac{1}{2}\begin{pmatrix}\bar{\nu_L} & \bar{\nu^c_R}\end{pmatrix}\begin{pmatrix}0 & m_D \\ m_D^T & M\end{pmatrix}\begin{pmatrix}\nu^c_L \\ \nu_R\end{pmatrix}. \tag{2.7}$$

Assuming a hierarchy between the Majorana and Dirac masses, $M \gg m_D$ we can block-diagonalize the mass matrix (2.7). We find light and heavy mass eigenstates described by the Majorana spinors

$$\nu_i = \left[V_\nu^\dagger \nu_L - U_\nu^\dagger \theta \nu_R^c + V_\nu^T \nu_L^c - U_\nu^T \theta \nu_R\right]_i, \quad N_i = \left[V_N^\dagger \nu_R + \Theta^T \nu_L^c + V_N^T \nu_R^c + \Theta^\dagger \nu_L\right]_i, \tag{2.8}$$

respectively. The mixing matrix between the light and heavy states is approximately

$$\theta \approx m_D M^{-1}. \tag{2.9}$$

The light neutrino mixing matrix $V_\nu = \left(1 - \frac{1}{2}\theta\theta^\dagger\right)U_\nu$ diagonalises the light neutrino mass matrix $m_\nu$ and the unitary part $U_\nu$ is the PMNS matrix. The heavy neutrino mass matrix is diagonalized by $V_N = \left(1 - \frac{1}{2}\theta^T\theta^*\right)U_N$. The mixing angle $\Theta$ is given by $\Theta = \theta U_N^*$. The light neutrino mass matrix after EWSB is to a very good approximation given by

$$m_\nu \approx -m_D M^{-1} m_D^T = -v^2 Y^\dagger M^{-1} Y^* = -\theta M \theta^T, \tag{2.10}$$

while the heavy neutrino mass matrix is

$$M_N = M + \frac{1}{2}\left(\theta^\dagger\theta M + M^T\theta^T\theta^*\right). \tag{2.11}$$

Note that although the correction to the heavy neutrino mass matrix appears negligible, it can play a crucial role in leptogenesis, as well as lepton number violating signatures at collider experiments if the masses in $M$ are close to being degenerate. The difference between the heavy neutrino mass eigenstates will then be given by:

$$\Delta M_{\text{phys}} = \sqrt{\Delta M^2 + \Delta M_{\theta\theta}^2 - 2\Delta M \Delta M_{\theta\theta} \cos(2\text{Re}\omega)}\,, \tag{2.12}$$

where $\Delta M_{\theta\theta} = m_2 - m_3$ for normal ordering and $\Delta M_{\theta\theta} = m_1 - m_2$ for inverted ordering. As a result of the type-I seesaw mechanism, the previously massless light neutrinos obtain a finite mass, and the heavy neutrinos obtain a $\theta$-suppressed weak interaction. The size of this suppression $\theta$ is an important quantity from the point of view of experimental searches, as the heavy neutrino then takes part in all interactions as the light neutrino, but with the cross-section suppressed by a factor $|\theta_{i\alpha}|^2$. Therefore it is useful to introduce the quantities

$$U_{i\alpha}^2 \equiv |\theta_{i\alpha}|^2\,, \qquad U_{\alpha}^2 \equiv \sum_i |\theta_{i\alpha}|^2\,, \tag{2.13}$$

$$U_i^2 \equiv \sum_\alpha |\theta_{i\alpha}|^2\,, \qquad U^2 \equiv \sum_{i,\alpha} |\theta_{i\alpha}|^2\,. \tag{2.14}$$

Within the type-I seesaw model, there are two ways to explain the observed smallness of the neutrino masses $m_\nu$. One possibility is that the scale of the Majorana masses $M$ is much larger than the electroweak scale $\sim v = 174\,\text{GeV}$, and the neutrino Yukawa couplings are of $Y \sim \mathcal{O}(1)$. The smallness of the light neutrino masses is then realized via the suppression factor $v/M$. This conventional scenario is only viable for heavy neutrinos with masses above the electroweak scale $M \gg v$. The other possibility, that the Yukawa couplings are small $Y \ll 1$, is also quite interesting from an experimental point of view, as the heavy neutrino masses could be below the electroweak scale and therefore accessible to current or near future experiments. If we assume that all heavy neutrinos have roughly the same mass $M_{ij} = \bar{M}$ and Yukawa couplings $Y_{i\alpha} = Y_0$, and neglect the differences between the flavour and mass eigenstates of the light neutrinos, we find the expected size of the Yukawa couplings through the "naive seesaw" relation

$$|Y_{i\alpha}|^2 \sim Y_0^2 \equiv \frac{\bar{M}}{v^2}\sqrt{\Delta m_{\text{atm}}^2 + m_{\text{lightest}}^2}\,, \tag{2.15}$$

where $\Delta m_{\text{atm}}^2$ is the larger of the observed mass differences, and $m_{\text{lightest}}$ is the mass of the lightest neutrino which has not been experimentally measured to this date. The above relation also implies the size of the mixing angle between the heavy and light neutrinos

$$U_0^2 = \frac{1}{\bar{M}}\sqrt{\Delta m_{\text{atm}}^2 + m_{\text{lightest}}^2}\,. \tag{2.16}$$

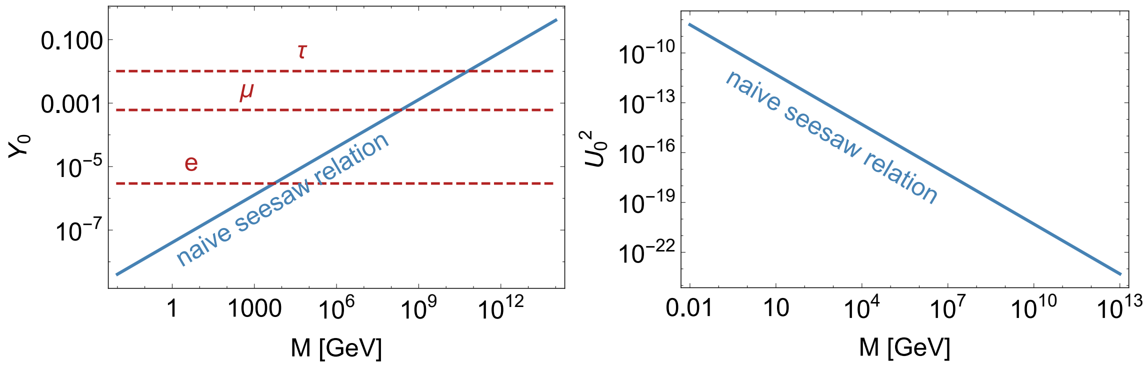


Figure 2.1: The range of Yukawa couplings (left panel) and mixing angles (right panel) consistent with the naive seesaw relation (2.15) (blue), where we assumed $m_{\text{lightest}} = 0$. The Standard Model lepton Yukawa couplings are also presented (red, dashed) for comparison. For heavy neutrinos at the GeV scale the naive Yukawa couplings are a few orders of magnitude smaller than the electron Yukawa couplings. On the other hand, GeV-scale heavy neutrino masses also imply large mixing angles, which increases the chances of testing the model at near future experiments (right panel).

These naive estimates can easily be avoided if there are cancellations between entries of the Dirac mass matrix $m_D$, which can allow for Yukawa couplings and mixing angles much larger than the naive estimates $|Y_{i\alpha}| \gg Y_0$ and $U_{i\alpha}^2 \gg U_0^2$. We will discuss such a scenario in more detail in Section 2.2.

### 2.1.1 The Casas-Ibarra Parametrization

The Lagrangian (2.5) has $7n_s - 3$ unknown parameters, with $n_s$ of them corresponding to the heavy neutrino masses. The remaining parameters are already constrained by the light neutrino oscillation data.

At tree-level, the connection between the Yukawa couplings and the light neutrino masses is conveniently given by the Casas-Ibarra parametrization [92]. The parametrization was generalized in [93] to include radiative corrections to the neutrino masses, which we neglect in the present discussion. The neutrino Yukawa couplings can then be parametrized as

$$Y^\dagger = \frac{\mathrm{i}}{v} U_\nu \sqrt{m_\nu^{\text{diag}}} \mathcal{R} \sqrt{M^{\text{diag}}} \,. \tag{2.17}$$

The matrix $M^{\text{diag}}$ is the Majorana mass matrix from (2.5), and $m_\nu^{\text{diag}}$ are the eigenvalues of the light neutrino mass matrix $m_\nu$. The number of massive light neutrinos cannot be larger than $n_s$. With the two observed neutrino mass differences, this model requires at least two heavy neutrinos if $m_{\text{lightest}} = 0$ and $n_s = 3$ heavy neutrinos if $m_{\text{lightest}} \neq 0$. $\mathcal{R}$ is a complex orthogonal matrix that satisfies $\mathcal{R}\mathcal{R}^T = 1$. In the case of $n_s = 3$, it can be expressed through the Euler parametrization:

$$\mathcal{R} = \mathcal{R}^{(23)}\mathcal{R}^{(13)}\mathcal{R}^{(12)}\,, \tag{2.18}$$

where the non-zero elements of $\mathcal{R}^{(ij)}$ are

$$\mathcal{R}^{(ij)}_{ii} = \mathcal{R}^{(ij)}_{jj} = \cos\omega_{ij}\,, \qquad \mathcal{R}^{(ij)}_{kk}|_{k\neq i,j} = 1\,, \tag{2.19}$$

$$\mathcal{R}^{(ij)}_{ij} = \sin\omega_{ij}\,, \qquad \mathcal{R}^{(ij)}_{ji} = -\sin\omega_{ij}\,, \tag{2.20}$$

where $\omega_{ij}$ are complex angles. In the minimal case with only two heavy neutrinos $n_s = 2$, the matrices are instead given by

$$\mathcal{R}^{\text{NO}} = \begin{pmatrix} 0 & 0 \\ \cos\omega & \sin\omega \\ -\xi\sin\omega & \xi\cos\omega \end{pmatrix}, \qquad \mathcal{R}^{\text{IO}} = \begin{pmatrix} \cos\omega & \sin\omega \\ -\xi\sin\omega & \xi\cos\omega \\ 0 & 0 \end{pmatrix}, \tag{2.21}$$

where superscripts (NO) and (IO) indicate normal or inverted neutrino mass ordering, $\omega = \text{Re}\,\omega + \text{i}\,\text{Im}\,\omega$ is a complex angle and $\xi = \pm 1$. For large values $|\,\text{Im}\,\omega| \gg 1$ we can expand the trigonometric functions to obtain the useful expansion

$$\mathcal{R}^{\text{NH}}_{|\,\text{Im}\,\omega|\gg 1} = \frac{1}{2}\text{e}^{\text{Im}\,\omega}\text{e}^{-\text{i}\,\text{Re}\,\omega}\begin{pmatrix} 0 & 0 \\ 1 & \text{i} \\ -\xi\text{i} & \xi \end{pmatrix}, \qquad \mathcal{R}^{\text{IH}}_{|\,\text{Im}\,\omega|\gg 1} = \frac{1}{2}\text{e}^{\text{Im}\,\omega}\text{e}^{-\text{i}\,\text{Re}\,\omega}\begin{pmatrix} 1 & \text{i} \\ -\xi\text{i} & \xi \\ 0 & 0 \end{pmatrix}. \tag{2.22}$$

## 2.2 Symmetry protected scenario

Low-scale seesaw models are often motivated by an approximate "lepton number"-like symmetry, that allows for small heavy neutrino masses $M$ simultaneously with sizeable neutrino Yukawa couplings that are technically natural. Such scenarios are often referred to as *symmetry protected scenarios*.

This limit can be motivated by extensions of the type-I seesaw model, such as the "inverse seesaw", the "linear seesaw", scale invariant models [51], some technicolour-type models [94, 95], models with "minimal flavour violation"[66, 67] or the $\nu$MSM [96].

Perhaps the most attractive feature of this class of models is that the mixings $U^2_{i\alpha}$ can be sufficiently larger than the naive estimate (2.16), making it accessible to experimental searches. In the following, we consider the minimal scenario with two heavy neutrinos $n_s = 2$.

Let us examine mass and Yukawa matrices with the form

$$M = \bar{M}\begin{pmatrix} \mu & 1 \\ 1 & \mu \end{pmatrix}, \qquad Y = \begin{pmatrix} F_e & F_\mu & F_\tau \\ \varepsilon_e & \varepsilon_\mu & \varepsilon_\tau \end{pmatrix}, \tag{2.23}$$

where $\mu$ and $\varepsilon$ are small parameters. The mass matrix of the light neutrinos

$$m_\nu = v^2 Y^\dagger M^{-1} Y^* = \mathcal{O}(\varepsilon) + \mathcal{O}(\mu) \tag{2.24}$$

vanishes at zeroth order in $\mu$ and $\varepsilon$. This means that the Yukawa couplings $F_\alpha$ can be as large as the electron Yukawa coupling without requiring large Majorana masses, as long as $\varepsilon_\alpha$ and $\mu$ are sufficiently small. The small parameters in (2.23) are consistent with the Casas-Ibarra parametrization, which becomes evident if we multiply the Yukawa matrix from (2.17) by the matrix

$$U_{B-L} = \frac{1}{\sqrt{2}}\begin{pmatrix} 1 & \mathrm{i} \\ 1 & -\mathrm{i} \end{pmatrix}, \tag{2.25}$$

where we can identify

$$F_\alpha = \frac{1}{\sqrt{2}}\left(Y_{1\alpha} + \mathrm{i}Y_{2\alpha}\right), \qquad \varepsilon_\alpha = \frac{1}{\sqrt{2}}\left(Y_{1\alpha} + \mathrm{i}Y_{2\alpha}\right), \tag{2.26}$$

as well as

$$\mu = \frac{M_1 - M_2}{M_1 + M_2}. \tag{2.27}$$

Furthermore, we find that parameter

$$\epsilon = \mathrm{e}^{-2\,\mathrm{Im}\,\omega}, \tag{2.28}$$

determines the size of the Yukawa couplings

$$|F_\alpha| \sim Y_0/\sqrt{\epsilon}, \qquad |\varepsilon_\alpha| \sim \sqrt{\epsilon}Y_0. \tag{2.29}$$

Therefore, we can associate small values of $\epsilon$ with large imaginary parts of the complex angle $\omega$. Note we cannot take the exact limit $\epsilon \to 0$, as $|F_\alpha|$ would grow to be infinitely large.

**Approximate $\bar{L}$ conservation** This parametrization is, of course, more than just a mathematical trick. The transformation $U_{B-L}$ is not only applied to the Yukawa matrices, but to the spinors $\nu_R$. Through this transformation, we find the states

$$\nu_{R\mathrm{s}} = \frac{1}{\sqrt{2}}(\nu_{R1} + \mathrm{i}\nu_{R2}), \qquad \nu_{R\mathrm{w}} = \frac{1}{\sqrt{2}}(\nu_{R1} - \mathrm{i}\nu_{R2}), \tag{2.30}$$

where $\nu_{Ri}$ are the flavour eigenstates of $M$. In the limit $\mu, \varepsilon \to 0$, the weak state $\nu_{R\mathrm{w}}$ decouples, and we can assign a lepton number $+1$ to $\nu_{R\mathrm{s}}$ and $-1$ to $\nu_{R\mathrm{w}}$. In this limit, we can construct a Dirac spinor $\psi_N = (\nu_{R\mathrm{s}} + \nu_{R\mathrm{w}}^c)$, and rewrite the Lagrangian as

$$\begin{aligned}\mathcal{L} &= \mathcal{L}_{\mathrm{SM}} + \overline{\psi_N}(\mathrm{i}\partial\!\!\!/ - \bar{M})\psi_N - F_\alpha \overline{\psi_N}\phi^\dagger \varepsilon^\dagger P_L \ell_\alpha - F_\alpha^* \overline{\ell}_\alpha \varepsilon \phi P_R \psi_N \\ &\quad - \varepsilon_\alpha \overline{\psi_N^c}\phi^\dagger \varepsilon^\dagger P_L \ell_\alpha - \varepsilon_\alpha^* \overline{\ell}_\alpha \varepsilon \phi P_R \psi_N^c - \tfrac{1}{2}\mu \bar{M}\left(\overline{\psi_N^c}\psi_N + \overline{\psi_N}\psi_N^c\right) . \qquad (2.31)\end{aligned}$$

This limit is often called the pseudo-Dirac scenario, and in the limit $\mu, \varepsilon \to 0$ lepton number becomes conserved, and the light neutrino masses vanish. The $\bar{L}NV$ terms are summarized in the second line of Eq. (2.31).

**Approximate $\tilde{L}$ conservation** Another approximate symmetry arises at temperatures $T \gg M$, where the Majorana masses are negligible. In such a regime, we may assign an approximate lepton number $\tilde{L}$ to the helicity states of the heavy neutrinos, $\tilde{L} = +1$ to the positive helicity, and $\tilde{L} = -1$ for negative helicity.

This lepton number remains approximately conserved in leptogenesis through neutrino oscillations.[1] It is important to differentiate this lepton number from the one associated with pseudo-Dirac neutrinos described above. It is interesting that both of these symmetries can appear in the leptogenesis through neutrino oscillations, as the heavy neutrinos can be both pseudo-Dirac and relativistic simultaneously.

## 2.3 Constraints on the Properties of Heavy Neutrinos

As mentioned earlier, the mixings $U_{i\alpha}^2$ of the heavy neutrinos are one of the most important properties when we consider experimental searches, as they approximately quantify the suppression of the cross section for a process $X \to N_i$ compared to $X \to \nu_\alpha$.

In the minimal scenario with two heavy neutrinos, the total interaction strength $U^2$ of the heavy neutrinos can conveniently be expressed in terms of the small parameters $\epsilon$ from (2.28), and $\mu$ defined in (2.27) as

$$U^2 = \frac{1}{1-\mu^2}\left[2\mu\cos(2\,\mathrm{Re}\,\omega)\frac{\Delta m}{\overline{M}} + \left(\epsilon + \frac{1}{\epsilon}\right)\frac{\overline{m}}{\overline{M}}\right] , \qquad (2.32a)$$

where

$$\Delta m = \frac{1}{2}\begin{cases} m_2 - m_3 & \text{for NO} \\ m_1 - m_2 & \text{for IO}\end{cases} , \qquad \overline{m} = \frac{1}{2}\begin{cases} m_2 + m_3 & \text{for NO} \\ m_1 + m_2 & \text{for IO}\end{cases} . \qquad (2.32b)$$

[1] In the recent years the importance of terms that violate this approximate lepton number in the case of leptogenesis through neutrino oscillations has been studied by several authors [46, 97–100].

The ratios of the flavoured mixing angles $U_{i\alpha}^2/U^2$ to the total interaction strength is mostly determined by the parameters in the PMNS matrix $U_\nu$ [67, 93, 101–105]. In the *symmetric limit* defined by $\mu \to 0$, and $\epsilon \ll 1$, we find that the two heavy neutrinos have mixings of the same size

$$U_{1\alpha}^2 = U_{2\alpha}^2 = \frac{1}{2}U_\alpha^2 . \tag{2.33}$$

We can express the mixings $U_\alpha^2$ to leading order in $\sqrt{\Delta m_{\rm sol}/\Delta m_{\rm atm}}$ and $\theta_{13}$ [67, 104–107] as

$$\left.\begin{aligned} U_e^2/U^2 &\approx \left|s_{12}\sqrt{\tfrac{m_2}{m_3}}e^{i\alpha_2/2} - i\, s_{13}e^{-i\delta}\xi\right|^2 \\ U_\mu^2/U^2 &\approx \left|c_{12}c_{23}\sqrt{\tfrac{m_2}{m_3}}e^{i\alpha_2/2} - i\, s_{23}\xi\right|^2 \\ U_\tau^2/U^2 &\approx \left|c_{12}s_{23}\sqrt{\tfrac{m_2}{m_3}}e^{i\alpha_2/2} + i\, c_{23}\xi\right|^2 \end{aligned}\right\}\text{ for NO,} \tag{2.34}$$

$$\left.\begin{aligned} U_e^2/U^2 &\approx \tfrac{1}{2}\left|c_{12} - is_{12}e^{i(\alpha_2-\alpha_1)/2}\right|^2 \\ U_\mu^2/U^2 &\approx \tfrac{1}{2}\left|s_{12}c_{23} + c_{12}s_{13}s_{23}e^{i\delta} + i(c_{12}c_{23} - e^{i\delta}s_{12}s_{13}s_{23})e^{i(\alpha_2-\alpha_1)/2}\xi\right|^2 \\ U_\tau^2/U^2 &\approx \tfrac{1}{2}\left|s_{12}s_{23} - c_{12}s_{13}c_{23}e^{i\delta} + i(c_{12}s_{23} + e^{i\delta}s_{12}s_{13}c_{23})e^{i(\alpha_2-\alpha_1)/2}\xi\right|^2 \end{aligned}\right\}\text{ for IO.} \tag{2.35}$$

We present the full expressions for the mixing angles in appendix A. The allowed range of parameters $U_{i\alpha}^2/U^2$ is a useful quantity when one estimates the potential of different experiments to find heavy neutrinos. To estimate this range we fix the measured low-energy neutrino parameters to the best fit values from from Table 2.2, and vary the remaining Casas-Ibarra parameters $\omega$, $\delta$, $\alpha$, $\bar{M}$ and $\mu$. The allowed regions are presented in Fig. 2.2.

We find that in the case of large mixing angles $U_i^2 > 10^{-11}\frac{\rm GeV}{M_i}$, the range of allowed $U_{i\alpha}^2/U_i^2$ corresponds to the range predicted by the symmetric limit *c.f.* Fig. 2.3.

If we constrain ourselves to the symmetric limit, where the mixing ratios are completely determined by the parameters $\alpha$ and $\delta$, we can impose even stronger constraints on the mixing ratios. Current neutrino oscillation data already excludes certain values of the phase $\delta$. The various neutrino oscillation experiments can be combined into a global fit, which gives us $\Delta\chi^2$ as a function of the low-energy parameters. We use the results of the global fit NuFIT 3.2 provided by the $\nu$-fit collaboration [90, 91], which allows us to determine the $\Delta\chi^2$ for $\Delta m_{31}^2$, $\Delta m_{32}^2$ and

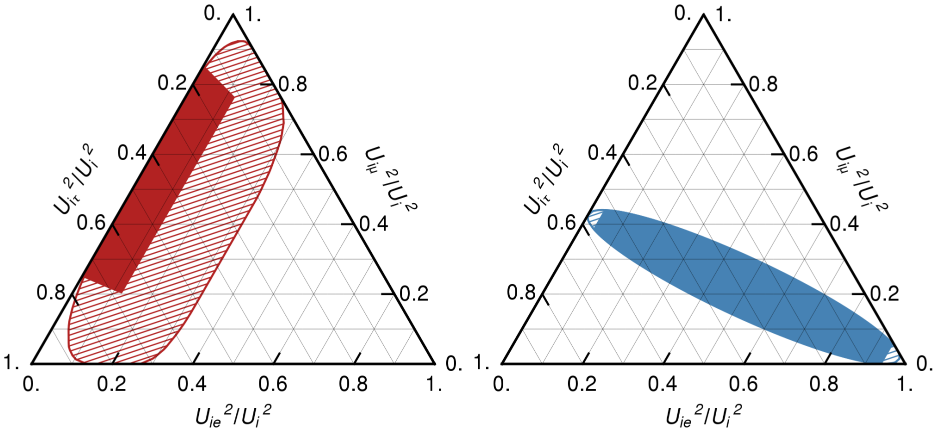


(a) Normal ordering. (b) Inverted ordering.

Figure 2.2: Allowed range of the mixing ratios $U_\alpha^2/U^2$ in the $n_s = 2$ model for arbitrary parameter choices (hashed region) compared to the symmetric limit (filled region) for normal ordering in Panel (a) and inverted ordering in Panel (b) of light neutrino masses. The extended hashed regions are only consistent with light neutrino oscillation data if the total mixing satisfies $U_i^2 \times M_i/\mathrm{GeV} < 10^{-11}$, cf. Figure 2.3. Figure taken from [17].

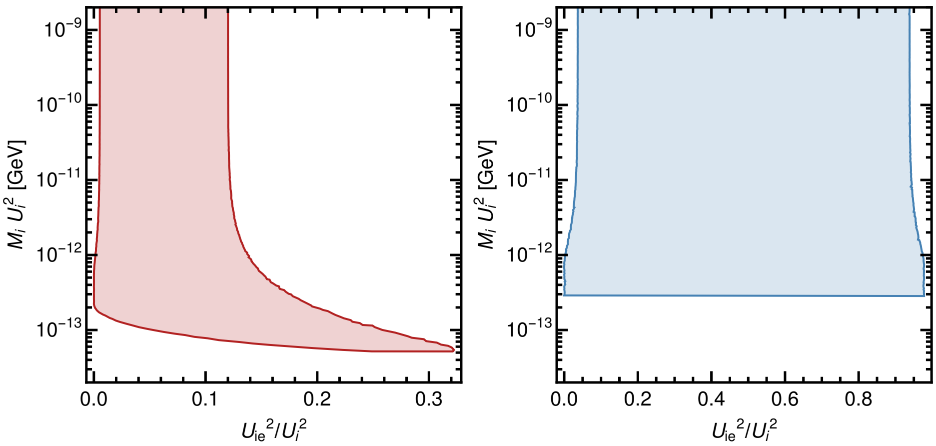


(a) Normal ordering. (b) Inverted ordering.

Figure 2.3: We can illustrate the applicability of the symmetric limit by plotting the allowed range of $U_{ei}^2/U_i^2$ for different values of $U_i^2 M_i$, which is in good approximation independent of $M_i$. For both, normal ordering shown in Panel (a) and inverted ordering shown in Panel (b), we find that the allowed range of $U_{ei}^2/U_i^2$ becomes independent of $U_i^2 M_i$ for values of $U_i^2 > 10^{-11} \frac{\mathrm{GeV}}{M_i}$. Figure taken from [17].

all parameters in $U_\nu$ with the exception of the Majorana phase $\alpha$. We use a one-dimensional projection for all low-energy parameters except for $\theta_{23}$ and $\delta$, where have a large deviation from the Gaussian limit, and use a two-dimensional $\Delta\chi^2$ projection instead. For a set of parameters we sum over the individual $\Delta\chi^2$ to obtain the total $\Delta\chi^2$.

To identify the preferred mixing ratios, we use a simple implementation of the Metropolis-Hastings algorithm [108, 109], which we describe in appendix B. Our analysis depends on parameters, which we arrange in the vector $x = (\Delta m^2_{31}, \Delta m^2_{32}, s_{12}, s_{13}, s_{23}, \delta, \alpha)$. To generate the sample we assume the log-likelihood function

$$\log \mathscr{L} = -\frac{1}{2}\Delta\chi^2 . \tag{2.36}$$

We assume flat priors for the mass differences, the sines of the angles $s_{ij} = \sin\theta_{ij}$, and the CP phase $\delta$. For the parameter $\alpha$, which is experimentally unconstrained, we choose two different priors, the first one is a flat prior, distributed between 0 and $4\pi$. The second choice of prior is chosen as "flat" in $U_e^2/U^2$. We achieve this by choosing $\alpha$ from a flat distribution in $\sin(\alpha/2 + \delta)$ for normal hierarchy and $\sin(\alpha/2)$ for inverted hierarchy according to relations (A.2) and (A.4).

The resulting likelihoods for the ratios $U_\alpha^2/U^2$ are shown in figures 2.4 and 2.5 for the two different choices of prior. The DUNE experiment is expected to determine the CP violating phase $\delta$ to an even higher accuracy. We show the expected improvement to the limits from Fig. 2.4 in Fig. 2.6. With an even more precise determination of the phase $\delta$ we can expect these areas to shrink further. If heavy neutral leptons are found at a future experiment, we can compare their mixing ratios with these predictions as a first test of the minimal type-I seesaw mechanism.

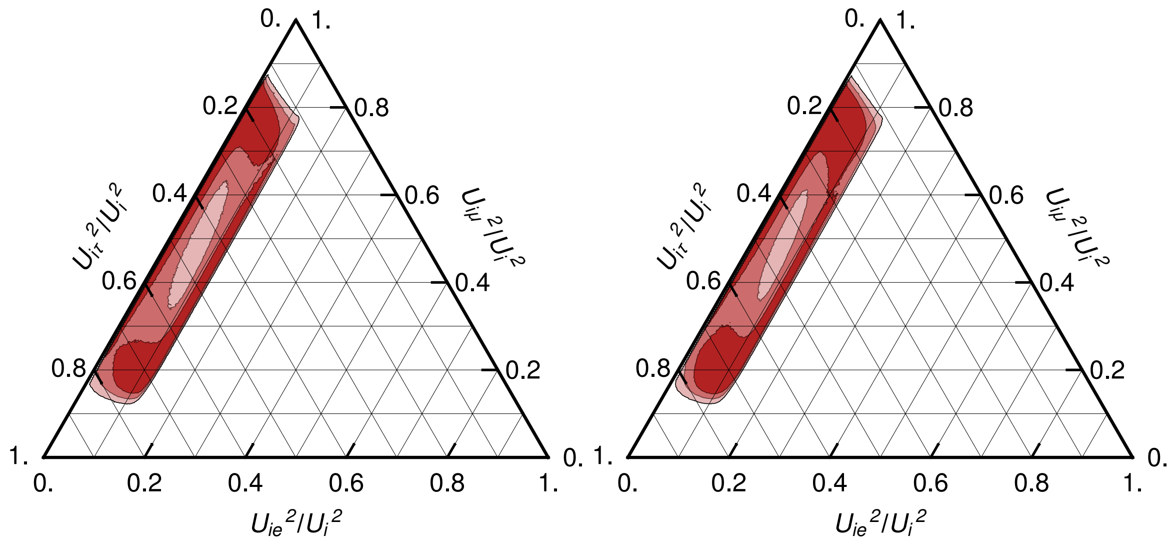


(a) Flat prior on $\alpha$.

(b) Flat prior on $\sin(\alpha/2+\delta)$.

Figure 2.4: Probability contours for the ratios $U_\alpha^2/U^2$ for $n_s = 2$ and NO that can be obtained from present neutrino oscillation data. The shades indicate the $1\sigma$ (darkest), $2\sigma$ and $3\sigma$ (lightest) probability contours for the ratios $U_a^2/U^2$ for $n = 2$ and NO that can be obtained from present neutrino oscillation data. In Panel (a) we assume a flat prior in $\alpha$ and in Panel (b) we assume a flat prior in $\sin(\alpha/2+\delta)$. Figure taken from [17].

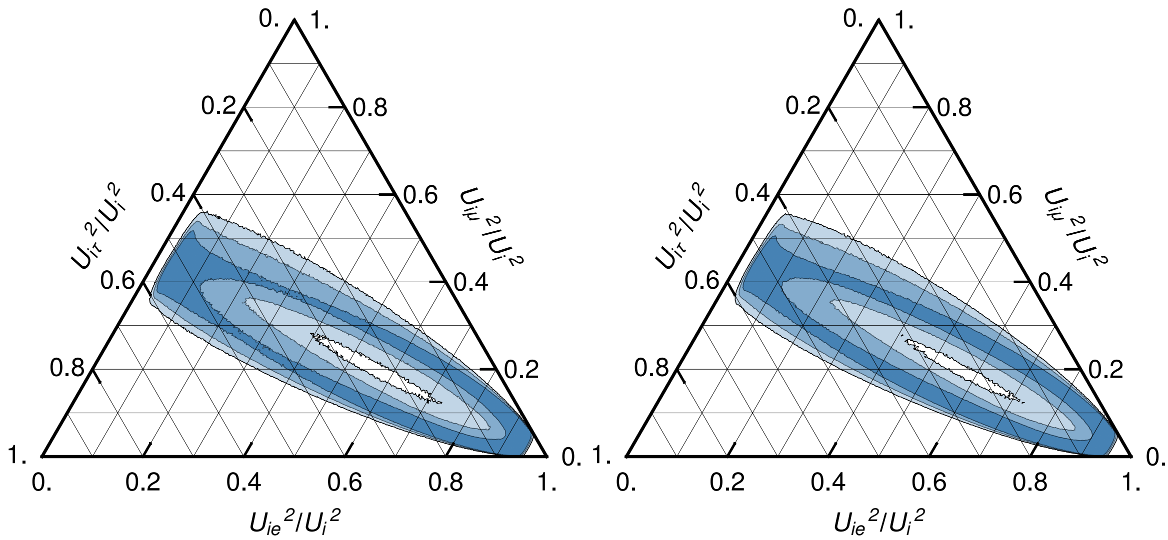


(a) Flat prior on $\alpha$.

(b) Flat prior on $\sin(\alpha/2)$.

Figure 2.5: Probability contours for the ratios $U_\alpha^2/U^2$ for $n_s = 2$ and IO that can be obtained from present neutrino oscillation data. The shades indicate the $1\sigma$ (darkest), $2\sigma$ and $3\sigma$ (lightest) probability contours for the ratios $U_a^2/U^2$ for $n = 2$ and IO that can be obtained from present neutrino oscillation data. In Panel (a) we assume a flat prior in $\alpha$ and in Panel (b) we assume a flat prior in $\sin(\alpha/2)$. Figure taken from [17].

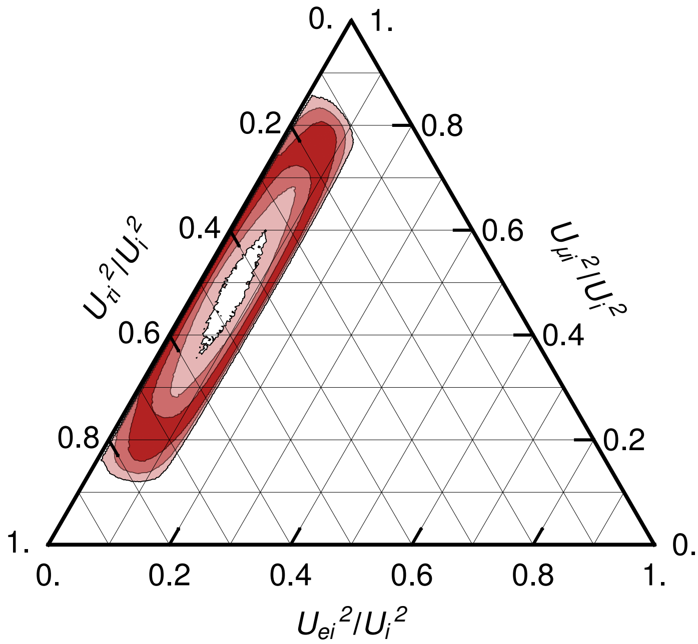


Figure 2.6: In this figure we show the expected improvement to the limits from Fig. 2.4 with DUNE [110]. For the parameter $\delta$ we assume Gaussian errors around the value $\delta = -\pi/2 \pm \pi/9$ used as benchmarks in [111]. For the remaining parameters we take the one dimensional $\chi^2$ projections from NuFIT 3.2. We assume flat priors on the parameter $\alpha$. Note that this is a conservative estimate, as in reality we can expect even stronger constraints as all low-energy parameters will be measured with a higher precision (here we assumed an improvement in $\delta$ alone). Figure taken from [17].

# Chapter 3

# Out-of-Equilibrium Fields in the Early Universe

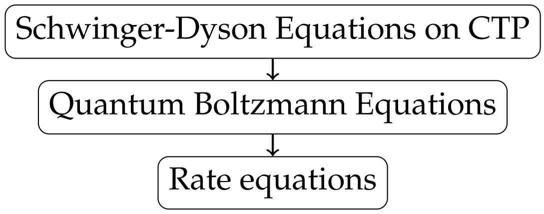


Figure 3.1: The approximation scheme used to derive the quantum Boltzmann equations used for leptogenesis.

In this chapter we derive evolution equations for out-of-equilibrium fields in the early Universe. We start by deriving the equations for particles in a Minkowski spacetime, and later generalize to a Friedmann-Lemaître-Robertson-Walker (FLRW) metric. As this chapter focuses on the formal aspects of the leptogenesis calculations, we direct the phenomenologically oriented reader to Chapter 4.

Standard leptogenesis calculations typically combine $S$-matrix elements calculated in the *in-out formalism* with classical Boltzmann equations. The downside of this approach is that in a medium the asymptotic *in-* and *out-* states are not well defined, as the particles under consideration keep interacting with the background. Furthermore, the properties of quasiparticles can significantly differ from the particle properties in vacuum.

In the Closed-Time-Path (CTP) formalism [1] developed by Schwinger, Keldysh and others [114–116] we instead consider the time-evolution of expectation values, such as 2-point functions. This way, we do not need to make reference to the particle states, as observables, such as number densities are encoded within 2-point functions. We will use these methods to derive the quantum kinetic equations for heavy neutrino number densities, and their correlations. Our derivation follows the ones described in [117] and [118].

[1] For a pedagogical review see *e.g.* Refs[112, 113].

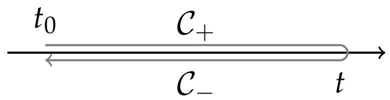


Figure 3.2: The complex time contour for the Schwinger-Keldysh formalism.

## 3.1 Derivation of the Evolution Equations

### 3.1.1 Correlation functions

The key quantities in the CTP description are the Green functions on the closed time path, which are defined as:

$$\mathrm{i}S^{T}_{\alpha\beta}(x_1,x_2) \equiv \mathrm{i}S^{++}_{\alpha\beta}(x_1,x_2) = \langle T[\psi_\alpha(x)\bar{\psi}_\beta(x_2)]\rangle\,, \tag{3.1}$$

$$\mathrm{i}S^{\bar{T}}_{\alpha\beta}(x_1,x_2) \equiv \mathrm{i}S^{--}_{\alpha\beta}(x_1,x_2) = \langle \bar{T}[\psi_\alpha(x)\bar{\psi}_\beta(x_2)]\rangle\,, \tag{3.2}$$

$$\mathrm{i}S^{<}_{\alpha\beta}(x_1,x_2) \equiv \mathrm{i}S^{+-}_{\alpha\beta}(x_1,x_2) = -\langle \bar{\psi}_\beta(x_2)\psi_\alpha(x)\rangle\,, \tag{3.3}$$

$$\mathrm{i}S^{>}_{\alpha\beta}(x_1,x_2) \equiv \mathrm{i}S^{-+}_{\alpha\beta}(x_1,x_2) = \langle \psi_\alpha(x)\bar{\psi}_\beta(x_2)\rangle\,, \tag{3.4}$$

where the indices $+$ and $-$ indicate the branch of the closed time path contour illustrated in Fig. 3.2. On the upper branch $\mathcal{C}_+$ we have normal time ordering $T$, while the lower branch $\mathcal{C}_-$, which runs backwards in time has anti-time ordering $\bar{T}$. All times on the upper branch $\mathcal{C}_+$ precede the lower branch $\mathcal{C}_-$. The $\langle\cdots\rangle$ describes the usual quantum statistical average of a system, *i.e.* for a system described by a density matrix $\varrho$, the average is obtained by taking the trace $\langle\cdots\rangle = \mathrm{Tr}(\varrho\cdots)$. The choice of $\varrho$ corresponds to the initial condition, *i.e.* we may consider

$$\varrho = \varrho^{\mathrm{eq}}_{SM} \otimes \varrho_N\,, \tag{3.5}$$

where $\varrho_N$ is the density matrix of the heavy neutrinos, that can correspond to equilibrium (for standard leptogenesis) or vacuum initial conditions (for leptogenesis through neutrino oscillations).

The functions $S^>$ and $S^<$ are known as the Wightmann functions, and can be combined to obtain the spectral and statistical functions:

$$S^{\mathcal{A}}(x_1,x_2) = \frac{\mathrm{i}}{2}\left(S^>(x_1,x_2) - S^<(x_1,x_2)\right)\,, \tag{3.6}$$

$$S^{F}(x_1,x_2) = \frac{1}{2}\left(S^>(x_1,x_2) + S^<(x_1,x_2)\right)\,, \tag{3.7}$$

which have intuitive physical interpretations. The statistical function $S^F$ contains the information about the occupation numbers, while the spectral function $S^{\mathcal{A}}$ determines the spectrum of the quasi-particles in the plasma.

The retarded, advanced and Hermitian are defined as:

$$\mathrm{i}S^R(x_1,x_2) = 2\theta(t_1-t_2)S^{\mathcal{A}}(x_1,x_2)\,, \tag{3.8}$$

$$\mathrm{i}S^A(x_1,x_2) = -2\theta(t_2-t_1)S^{\mathcal{A}}(x_1,x_2)\,, \tag{3.9}$$

$$S^H(x_1,x_2) = \frac{1}{2}\left[S^R(x_1,x_2) - S^A(x_1,x_2)\right] = -\mathrm{i}\,\mathrm{sgn}(t_1-t_2)S^{\mathcal{A}}(x_1,x_2)\,. \tag{3.10}$$

The Greens functions on the CTP satisfy the Schwinger-Dyson equations:

$$(\mathrm{i}\partial\!\!\!/_{x_1} - M)S^{\mathcal{A}}(x_1,x_2) = 2\mathrm{i}\int_{t_1}^{t_2}\mathrm{d}t'\int \mathrm{d}^3\mathbf{x}'\,\Sigma^{\mathcal{A}}(x_1,x')S^{\mathcal{A}}(x',x_2)\,, \tag{3.11}$$

$$\begin{aligned}(\mathrm{i}\partial\!\!\!/_{x_1} - M)S^{F}(x_1,x_2) &= 2\mathrm{i}\int_{t_0}^{t_2}\mathrm{d}t'\int \mathrm{d}^3\mathbf{x}'\,\Sigma^{F}(x_1,x')S^{\mathcal{A}}(x',x_2)\\ &\quad - 2\mathrm{i}\int_{t_0}^{t_1}\mathrm{d}t'\int \mathrm{d}^3\mathbf{x}'\,\Sigma^{\mathcal{A}}(x_1,x')S^{F}(x',x_2)\,,\end{aligned} \tag{3.12}$$

which can be derived using the 2PI effective action [119] on a closed time path [116].

### 3.1.2 Wigner space and the gradient expansion

By setting $t_0 \to \infty$, and using the spectral relations for $\Sigma^H$ and $S^H$, we can remove the integration boundaries from the Schwinger-Dyson equations:

$$(\mathrm{i}\partial\!\!\!/_{x_1} - M)S^{\mathcal{A}}(x_1,x_2) = \int \mathrm{d}^4x'\left(\Sigma^{H}(x_1,x')S^{\mathcal{A}}(x',x_2) + \Sigma^{\mathcal{A}}(x_1,x')S^{H}(x',x_2)\right)\,, \tag{3.13a}$$

$$\begin{aligned}(\mathrm{i}\partial\!\!\!/_{x_1} - M)S^{F}(x_1,x_2) &= \int \mathrm{d}^4x'\left(\Sigma^{H}(x_1,x')S^{F}(x',x_2) + \Sigma^{F}(x_1,x')S^{H}(x',x_2)\right)\\ &\quad + \mathrm{i}\int \mathrm{d}^4x'\left(\Sigma^{F}(x_1,x')S^{\mathcal{A}}(x',x_2) - \Sigma^{\mathcal{A}}(x_1,x')S^{F}(x',x_2)\right)\,,\end{aligned} \tag{3.13b}$$

which are now in a convenient form for the gradient expansion, as the integration limits are at $\pm\infty$. For each two-point function $G(x_1,x_2)$, we introduce the average $x = (x_1+x_2)/2$ and relative $r = (x_1 - x_2)$ coordinates. We now perform a Fourier transform with respect to the relative variable $r$.

$$G(x;k) = \int \mathrm{d}^4r\,\mathrm{e}^{\mathrm{i}kr}G(x+r/2, x-r/2)\,. \tag{3.14}$$

The products of the two point functions appearing in equations (3.13a),(3.13b) can be transformed by using the relation:

$$\int \mathrm{d}^4(x_1-x_2)\mathrm{e}^{\mathrm{i}k\cdot(x_1-x_2)}\int \mathrm{d}^4y A(x_1,y)B(y,x_1) = \mathrm{e}^{-\mathrm{i}\diamond}\{A(x;k)\}\{B(x;k)\}\,, \tag{3.15}$$

where $x = (x_1 + x_2)/2$ is the average coordinate. The diamond operator is defined as:

$$\diamond\{A\}\{B\} = \frac{1}{2}\left(\partial_x A \cdot \partial_k B - \partial_k A \cdot \partial_x B\right) . \tag{3.16}$$

This allows us to rewrite the Kadanoff-Baym equations as:

$$\left(\not{k} + \frac{\mathrm{i}}{2}\not{\partial}_x - M\right) S^{\mathcal{A}}(x;k) - \mathrm{e}^{-\mathrm{i}\diamond}\{\Sigma^H\}\{S^{\mathcal{A}}\} - \mathrm{e}^{-\mathrm{i}\diamond}\{\Sigma^{\mathcal{A}}\}\{S^H\} = 0\,, \tag{3.17a}$$

$$\begin{aligned}\left(\not{k} + \frac{\mathrm{i}}{2}\not{\partial}_x - M\right) S^F(x;k) - \mathrm{e}^{-\mathrm{i}\diamond}\{\Sigma^H\}\{S^F\} - \mathrm{e}^{-\mathrm{i}\diamond}\{\Sigma^F\}\{S^H\} &= \mathscr{C} \\ &= \mathrm{i}\left(\mathrm{e}^{-\mathrm{i}\diamond}\{\Sigma^F\}\{S^{\mathcal{A}}\} - \mathrm{e}^{-\mathrm{i}\diamond}\{\Sigma^{\mathcal{A}}\}\{S^F\}\right) ,\end{aligned} \tag{3.17b}$$

where $\mathscr{C}$ is the collision term. Assuming that the universe is both homogenous and isotropic, we may neglect all spatial derivatives, leaving us only with time derivative $\partial_{x_\mu} \to \partial_t$.

At this point, we assume a hierarchy between the variation with respect to the macroscopic scale $\partial_t$, and the microscopic scale $k$ [120, 121]. We may formally write this as:

$$\partial_t \ll k^0 . \tag{3.18}$$

This is justified both in resonant leptogenesis and leptogenesis through neutrino oscillations, as the microscopic energy scale of the heavy neutrino $k^0$ is typically much larger than the macroscopic scale, typically associated with either the equilibration process $\sim Y^2 k^0$, the Hubble expansion $H \approx \sqrt{8\pi^3 g_\star/90}T^2/m_{\mathrm{Pl}}$, or the oscillations between the heavy neutrinos $\sim \Delta M^2/k^0$. By neglecting all higher orders of the diamond operator, *i.e.* setting $\mathrm{e}^{\mathrm{i}\diamond}\{A\}\{B\} \approx AB$, the Kadanoff-Baym equations are simplified to:

$$\left(\not{k} + \frac{\mathrm{i}}{2}\not{\partial}_t - M\right) S^{\mathcal{A}} - \Sigma^H S^{\mathcal{A}} - \Sigma^{\mathcal{A}} S^H = 0\,, \tag{3.19a}$$

$$\left(\not{k} + \frac{\mathrm{i}}{2}\not{\partial}_t - M\right) S^F - \Sigma^H S^F - \Sigma^F S^H = \mathrm{i}\left(\Sigma^F S^{\mathcal{A}} - \Sigma^{\mathcal{A}} S^F\right) . \tag{3.19b}$$

We now add and subtract the equations (3.19a) and (3.19b) with their Hermitian conjugates to obtain the constraint and kinetic equations:

$$\begin{aligned}\{\mathcal{H}, \mathcal{S}^{\mathcal{A}}\} - \{\mathcal{G}^{\mathcal{A}}, \mathcal{S}^H\} &= 0\,, \\ \mathrm{i}\partial_t \mathcal{S}^{\mathcal{A}} + [\mathcal{H}, \mathcal{S}^{\mathcal{A}}] - [\mathcal{G}^{\mathcal{A}}, \mathcal{S}^H] &= 0\,,\end{aligned} \tag{3.20}$$

and

$$\{\mathcal{H}, \mathcal{S}^F\} - \{\mathcal{G}^F, \mathcal{S}^H\} = \mathrm{i}([\mathcal{G}^F, \mathcal{S}^{\mathcal{A}}] - [\mathcal{G}^{\mathcal{A}}, \mathcal{S}^F]) \tag{3.21a}$$

$$\mathrm{i}\partial_t \mathcal{S}^F + [\mathcal{H}, \mathcal{S}^F] - [\mathcal{G}^F, \mathcal{S}^H] = \mathrm{i}(\{\mathcal{G}^F, \mathcal{S}^{\mathcal{A}}\} - \{\mathcal{G}^{\mathcal{A}}, \mathcal{S}^F\}), \tag{3.21b}$$

with the shorthand notation $\mathcal{G} = \Sigma\gamma^0$, $\mathcal{H} = (\not{k} - \Sigma^H - M)\gamma^0$ and $\mathcal{S} = \gamma^0 S$. We may separate the self energies:

$$\mathcal{H} = \bar{\mathcal{H}} + \delta\mathcal{H}\,, \mathcal{G} = \bar{\mathcal{G}} + \delta\mathcal{G}\,, \tag{3.22}$$

into the contributions evaluated at local chemical equilibrium $\bar{\mathcal{H}}$, $\bar{\mathcal{G}}$, and non-equilibrium contributions $\delta\mathcal{H}$, $\delta\mathcal{G}$. The equilibrium solutions to (3.21b) are static in time by construction, and can be found by solving the algebraic equation:

$$[\bar{\mathcal{H}}, \bar{\mathcal{S}}^F] - [\bar{\mathcal{G}}^F, \bar{\mathcal{S}}^H] = \mathrm{i}(\{\bar{\mathcal{G}}^F, \bar{\mathcal{S}}^{\mathcal{A}}\} - \{\bar{\mathcal{G}}^{\mathcal{A}}, \bar{\mathcal{S}}^F\}), \tag{3.23}$$

which we obtained from (3.21b) by setting $\partial_t \bar{\mathcal{S}}^F = 0$. Assuming that the self-energies $\Sigma$ are dominated by interactions that are in equilibrium, we can safely approximate [122, 123]:

$$\mathcal{S}^{\mathcal{A}} = \bar{\mathcal{S}}^{\mathcal{A}}\,, \mathcal{S}^{\mathcal{H}} = \bar{\mathcal{S}}^{\mathcal{H}}\,, \tag{3.24}$$

and we can split the statistical propagator into the equilibrium and non-equilibrium parts:

$$\mathcal{S}^F = \bar{\mathcal{S}}^F + \delta\mathcal{S}\,. \tag{3.25}$$

The constraint and kinetic equations for the non-equilibrium part of the propagator are:

$$\{\mathcal{H}, \delta\mathcal{S}^F\} \approx -\mathrm{i}[\mathcal{G}^{\mathcal{A}}, \delta\mathcal{S}^F]\,, \tag{3.26a}$$

$$\partial_t \delta\mathcal{S} + \partial_t \bar{\mathcal{S}}^F - \mathrm{i}[\mathcal{H}, \delta\mathcal{S}] = -\{\mathcal{G}^{\mathcal{A}} + \delta\mathcal{G}^{\mathcal{A}}, \delta\mathcal{S}\} + \{\delta\mathcal{G}^F, \bar{\mathcal{S}}^{\mathcal{A}}\} - \{\delta\mathcal{G}^{\mathcal{A}}, \bar{\mathcal{S}}^F\}\,. \tag{3.26b}$$

The $\partial_t \bar{\mathcal{S}}^F$ describes the deviation from equilibrium that arises due to the expansion of the Universe. The commutator term on the left hand side of equation (3.26b) corresponds to the effective Hamiltonian that describes oscillations between different particle flavours, and the right hand side is the collision term, which describes the relaxation of the system to equilibrium.

### 3.1.3 Evolution equations for heavy neutrinos

We now proceed to solve equations (3.26a) and (3.26b) for the specific case of heavy neutrinos.

#### Solutions to the constraint equation for the heavy neutrinos

The constraint equation, as the name suggests, constrains the Dirac structure and the pole structure of the heavy neutrino propagator. We proceed by neglecting the commutator on the RHS of equation (3.26a), as it describes the finite width of the neutrino propagators:

$$\{\mathcal{H}, \delta\mathcal{S}^F\} \approx 0\,. \tag{3.27}$$

To solve the constraint equation, we may formally introduce the effective Hamiltonian $H$:

$$\mathcal{H} = k_0 - H\,, \qquad\qquad H \equiv (k_i\gamma_i + M + \Sigma^H)\gamma_0\,, \tag{3.28}$$

which allows us to write:

$$\{k_0 - H, \delta\mathcal{S}^F\} = 0\,. \tag{3.29}$$

Formally, by diagonalizing the $(4N_s) \times (4N_s)$ matrix $H(k)$, we can find the values of $k_0$ that satisfy (3.29). The factor 4 appearing in the dimensions of $H$ arises from the dimension of the Dirac matrices. The four degrees of freedom described by the Dirac matrices correspond to the two helicity, and the positive and negative energy states.

Since the early Universe is homogeneous and isotropic, the Dirac matrices appearing in the Kadanoff-Baym equations commute with the helicity operator $\hat{h} = \hat{k}_i\gamma_0\gamma_i\gamma_5$. Therefore, we can use the helicity projection operator

$$P_h = \frac{1 + h\hat{h}}{2}\,, \tag{3.30}$$

to reduce the dimensionality of equation (3.29). The two remaining Dirac degrees of freedom correspond to the positive and negative energy states.

To separate the positive and negative energy degrees of freedom, we introduce the projection operator:

$$P_s = \frac{1 + sH\Omega^{-1}}{2}\,, \tag{3.31}$$

with

$$\Omega \equiv \sqrt{H^2}\,. \tag{3.32}$$

where all the square roots are chosen such that the eigenvalues of $\Omega$ are positive. The projection operator selects the positive or negative energy solutions, depending on the sign of $s$, as:

$$P_s H = s\Omega P_s\,. \tag{3.33}$$

It is useful to split the effective Hamiltonian into the bare Hamiltonian $H_0 = (p_i\gamma_i + M)\gamma_0$, and interaction Hamiltonian $H_I = \Sigma^H\gamma^0$. We can then approximate the positive (negative) state projection operator as:

$$P_s^{(0)} \approx \frac{1 + sH_0\Omega_0^{-1}}{2}\,, \tag{3.34}$$

where $\Omega_0 = (p^2 + M^2)^{1/2}$, and $H_0 = (p_i\gamma_i + M)\gamma^0$. Using these projection operators, we write the Hamiltonian in block matrix form:

$$P_s H P_{s'} = \begin{pmatrix} \Omega_0 & 0 \\ 0 & -\Omega_0 \end{pmatrix}_{ss'} + \begin{pmatrix} H_{I\,++} & H_{I\,+-} \\ H_{I\,-+} & H_{I\,--} \end{pmatrix}_{ss'}\,, \tag{3.35}$$

where $s, s' = \pm$, and $H_{I\,ss'}$ are the block matrices of the interaction Hamiltonian. Since all energies in $\Omega_0 \sim \sqrt{M^2 + T^2}$ are larger than the interaction Hamiltonian $H_I \sim Y^2 T$, and there is no degeneracy between the positive and negative energy state blocks, we may safely neglect the block off-diagonal contributions $H_{I\,+-}$ and $H_{I\,-+}$. We proceed by neglecting all of the positive(negative) state off-diagonal entries, both in the self-energies $\mathcal{H}$, $\mathcal{G}$, and the propagators $\mathcal{S}$.

Taking the equation 3.21a and applying the helicity and postive/negative state projectors allows us to fully evaluate the Dirac trace:

$$\mathrm{Tr}_D(P_h P_s \left\{k_0 - H, \delta\mathcal{S}^F\right\}) = 0\,, \tag{3.36}$$
$$\left\{k_0 - H_{hs}, \delta\mathcal{S}^F_{hs}\right\} = 0\,,$$

where $H_{hs}$ is given by:

$$H_{hs} \equiv \mathrm{Tr}_D\left[P_h P_s H P_s\right]\,. \tag{3.37}$$

By diagonalizing the $N_s \times N_s$ matrix $H_{hs}$, and writing the flavour indices explicitly, we find the mass poles:

$$\left(k_0 - \frac{H^D_{hs\,i} + H^D_{hs\,j}}{2}\right)\delta\mathcal{S}^F_{hs\,ij} = 0 \to \delta S^F_{hs\,ij}(k) \sim \delta\left(k_0 - \frac{H^D_{hs\,i} + H^D_{hs\,j}}{2}\right)\,. \tag{3.38}$$

Which allows us to write:

$$\delta\mathcal{S}_{hs\,ij}(k) = -2\pi P_h P_s \delta\left(k_0 - \frac{H^D_{hs\,i} + H^D_{hs\,j}}{2}\right)\delta f_{hs\,ij}\,. \tag{3.39}$$

When applying to resonant leptogenesis and leptogenesis through neutrino oscillations mechanisms, it is typically sufficient to neglect the effects of the thermal masses on the position of the mass pole, and to neglect the mass differences between the heavy neutrinos:

$$\delta\mathcal{S}_{hs\,ij}(k) \approx -2\pi P_h P_s \delta\left(k_0 - s\bar{\omega}\right)\delta f_{hs\,ij}\,, \tag{3.40}$$

where $\omega = \sqrt{\vec{k}^2 + \bar{M}^2}$ is the energy evaluated at the average mass of the heavy neutrinos $\bar{M}$.

For Majorana fermions, the positive and negative energy states describe the same degrees of freedom. Since our formalism is designed to describe all types of fermions, both particle and antiparticle degrees of freedom will be present. However, through the Majorana constraint $N = N^C$, we find that the positive and negative state distribution functions are not independent:

$$\delta f_{h+\,ij}(|\vec{k}|) = \delta f_{h-\,ji}(|\vec{k}|)\,. \tag{3.41}$$

The two-point functions satisfy the relations:

$$-\int \frac{\mathrm{d}k^0}{2\pi}\,\mathrm{Tr}_D(P_h P_s \mathrm{i}\delta\mathcal{S}^F) = \delta f_{hs} \tag{3.42}$$

$$-\int \frac{\mathrm{d}k^0}{2\pi}\,\mathrm{Tr}_D(P_h P_s \mathrm{i}\bar{\mathcal{S}}^F) = [f^{\mathrm{eq}}(s\bar{\omega}) - 1/2] \tag{3.43}$$

$$-\int \frac{\mathrm{d}k^0}{2\pi}\,\mathrm{Tr}_D(P_h P_s \mathrm{i}\mathcal{S}^{\mathcal{A}}) = -\frac{\mathrm{i}}{2} \tag{3.44}$$

Similarly, we can also relate the trace of the active lepton propagator with its number density:

$$-\int \frac{\mathrm{d}^4k}{(2\pi)^4}\mathrm{i}\mathcal{S}^F_\alpha = q_\alpha \approx \frac{T^2\mu_\alpha}{6}\,. \tag{3.45}$$

## 3.2 Quantum Boltzmann equations for heavy neutrinos

In order to arrive at quantum Boltzmann equations for the heavy neutrinos, we have to transform the equations for the propagators (3.21b) to describe the distribution functions, as suggested by equations (3.42). We proceed by applying the helicity and positive(negative) state projectors to equation (3.26b), and we neglect all terms mixing the positive and negative energy states. We then integrate over the zeroth component of the momentum, to obtain the equations for the distribution functions:

$$\begin{aligned}\partial_t \delta f_{hs} + \partial_t f^{\mathrm{eq}} = -\mathrm{i}\left[H_{hs}, \delta f_{hs}\right] - \frac{1}{2}\left\{\Gamma_{hs}, \delta f_{hs}\right\} \\ - \frac{1}{2}\left\{\sum_\alpha \frac{\mu_\alpha}{T}\delta\Gamma^\alpha_{hs} + \frac{\mu_\phi}{T}\delta\Gamma^\phi_{hs}, \delta f_{hs}\right\} + \sum_\alpha \frac{\mu_\alpha + \mu_\phi}{T} f^{\mathrm{eq}}(1-f^{\mathrm{eq}})\tilde{\Gamma}^\alpha_{hs}\,.\end{aligned} \tag{3.46}$$

The effective Hamiltonian can again be decomposed into a vacuum and interaction term with

$$H_{hs} = H_{0\,hs} + H_{I\,hs}\,, \tag{3.47a}$$

$$\begin{aligned}H_{0\,hs} &= s\sqrt{|\vec{k}|^2 + M^2}\,, \\ H_{I\,hs} &= \frac{s}{2}\left[T\,\mathfrak{h}^{\mathrm{th}}_{+}\mathrm{Y}_{+hs} + T\,\mathfrak{h}^{\mathrm{th}}_{-}\mathrm{Y}_{-hs} + T\,\mathfrak{h}^{\mathrm{EV}}\frac{\mathrm{Y}_{+}+\mathrm{Y}_{-}}{2}\right]\,,\end{aligned} \tag{3.47b}$$

where $M$ is the vacuum mass of the heavy neutrinos, $\mathfrak{h}^{\mathrm{th}}_{\pm}$ are contributions from the hermitian self-energy of the heavy neutrino, and $\mathfrak{h}^{\mathrm{EV}}$ is the contribution arising due to a non-vanishing Higgs expectation value during the electroweak crossover. To determine the flavour structure of the self-energies we use the decomposition described in appendix E. The terms that describe the relaxation of the heavy neutrinos towards equilibrium are similarly given by

$$\Gamma_{hs} = T\,\left[\gamma_{+}\mathrm{Y}_{+hs} + \gamma_{-}\mathrm{Y}_{-hs}\right]\,, \tag{3.48a}$$

$$\delta\Gamma^\alpha_{hs} = T\,\left[\delta\gamma_{+}\mathrm{Y}^\alpha_{+hs} + \delta\gamma_{-}\mathrm{Y}^\alpha_{-hs}\right]\,, \tag{3.48b}$$

$$\delta\Gamma^\phi_{hs} = T\,\left[\delta\gamma^\phi_{+}\mathrm{Y}_{+hs} + \delta\gamma^\phi_{-}\mathrm{Y}_{-hs}\right]\,, \tag{3.48c}$$

$$\delta\Gamma^{\phi\alpha}_{hs} = T\,\left[\delta\gamma^\phi_{+}\mathrm{Y}^\alpha_{+hs} + \delta\gamma^\phi_{-}\mathrm{Y}^\alpha_{-hs}\right]\,, \tag{3.48d}$$

while the back-reaction term, which describes the feedback from a finite chemical potential in the lepton doublet sector is given by

$$\tilde{\Gamma}^\alpha_{hs} = \frac{1}{2}hT\,\left[\gamma_{+}\mathrm{Y}^\alpha_{+hs} - \gamma_{-}\mathrm{Y}^\alpha_{-hs}\right]\,. \tag{3.49}$$

The equations above all assume heavy neutrinos with degenerate energies. The exact expressions for the self-energies in the various $\mathfrak{h}$ and $\gamma$ in general depend on the temperature and the heavy neutrino masses. They can be calculated through the reduced self energy:

$$\gamma_+(k) = \frac{1}{T}\frac{g_w}{k^0}\left(k+\tilde{k}\right)\cdot\hat{\Sigma}_N^{\mathcal{A}}\,, \tag{3.50}$$

$$\gamma_-(k) = \frac{1}{T}\frac{g_w}{k^0}\left(k-\tilde{k}\right)\cdot\hat{\Sigma}_N^{\mathcal{A}}\,. \tag{3.51}$$

For the Hermitian part we find

$$\mathfrak{h}_+^{\mathrm{th}}(k) = \frac{1}{T}\frac{g_w}{k^0}\left(k+\tilde{k}\right)\cdot\hat{\Sigma}_N^{H}\,, \tag{3.52}$$

$$\mathfrak{h}_-^{\mathrm{th}}(k) = \frac{1}{T}\frac{g_w}{k^0}\left(k-\tilde{k}\right)\cdot\hat{\Sigma}_N^{H}\,, \tag{3.53}$$

whereas the term accounting for the expectation value of the Higgs field is given by

$$\mathfrak{h}^{\mathrm{EV}}(k) = \frac{2v^2(t)}{Tk^0}\,. \tag{3.54}$$

At present we will leave them in the general form and discuss them in more detail in the chapters discussing the specific leptogenesis scenarios.

## 3.3 Boltzmann equations for active leptons

Following a similar procedure, we may write the equation for the doublet neutrinos, this time integrating over the full 4-momentum, as they are assumed to be in kinetic equilibrium due to the fast interactions with the rest of the standard model plasma:

$$\begin{aligned}\partial_t q_{\ell\alpha} &= -\int\frac{d^4p}{(2\pi)^4}\,\mathrm{Tr}_D\left[\left\{\mathcal{G}_{\ell\alpha}^{F}(p),\mathcal{S}_{\ell\alpha}^{\mathcal{A}}(p)\right\}-\left\{\mathcal{G}_{\ell\alpha}^{\mathcal{A}}(p),\mathcal{S}_{\ell\alpha}^{F}(p)\right\}\right]\,, \\ &= \mathrm{i}\int\frac{d^4p}{(2\pi)^4}\,\mathrm{Tr}_D\left[\mathcal{G}_{\ell\alpha}^{<}(p)\mathcal{S}_{\ell\alpha}^{>}(p)-\mathcal{G}_{\ell\alpha}^{>}(p)\mathcal{S}_{\ell\alpha}^{<}(p)\right]\,,\end{aligned} \tag{3.55}$$

in appendix E we show how the active lepton collision term is related to the collision term of the heavy neutrinos, which allows us to write

$$\begin{aligned}\partial_t q_{\ell\alpha} &= \frac{\mathrm{i}}{2g_w}\int\frac{\mathrm{d}^4k}{(2\pi)^4}\,\mathrm{Tr}\left[\{\mathcal{G}^{>}_{N\alpha}(k),\mathcal{S}^{<}_{N}(k)\} - \{\mathcal{G}^{>}_{N\alpha}(k),\mathcal{S}^{<}_{N}(k)\}\right] , \\ &= \frac{1}{g_w}\int\frac{\mathrm{d}^4k}{(2\pi)^4}\,\mathrm{Tr}\left[\{\mathcal{G}^{F}_{N\alpha}(k),\mathcal{S}^{A}_{N}(k)\} - \{\mathcal{G}^{A}_{N\alpha}(k),\mathcal{S}^{F}_{N}(k)\}\right] , \\ &= \frac{1}{g_w}\sum_{h,s}\int\frac{\mathrm{d}k^3}{(2\pi)^3}\left[\mathrm{Tr}\left(\Gamma^{\alpha}_{hs}\delta f_{hs}\right) - \frac{\mu_\alpha+\mu_\phi}{T}f^{\mathrm{eq}\prime}\tilde{\Gamma}^{\alpha}_{hs} + \right. \\ &\quad \left. + \frac{\mu_\alpha}{T}\,\mathrm{Tr}\left(\delta\Gamma^{\alpha}_{hs}\delta f_{hs}\right) + \frac{\mu_\phi}{T}\,\mathrm{Tr}\left(\delta\Gamma^{\phi\alpha}_{hs}\delta f_{hs}\right)\right] , \\ &\approx -W_{\alpha\alpha}\left(q_{\ell\alpha}+\frac{q_\phi}{2}\right) + S_{\alpha\alpha} ,\end{aligned} \tag{3.56}$$

where $W_{\alpha\alpha}$ is the washout term that describes the washout of lepton asymmetries due to heavy neutrinos which are in equilibrium, while the source term $S_{\alpha\alpha}$ is the source of the lepton asymmetry created by the decay of the out-of-equilibrium heavy neutrinos. Note that in the last line we have neglected the terms that are second order in deviations from equilibrium.

### 3.3.1 Spectator Processes

Spectator processes are Standard Model processes that redistribute charges during leptogenesis and they affect the final baryon asymmetry [124, 125]. The quantity

$$\Delta_\alpha = B/3 - L_\alpha \tag{3.57}$$

is conserved by all interactions except for those mediated by the Yukawa couplings $Y$ between the heavy neutrinos and lepton doublets.

**Temperatures below $T \leq 10^5$GeV** The electron, the particle with the smallest SM Yukawa couplings, reaches equilibrium below temperatures $T \leq 10^5$GeV.[2] The fast processes mediated by the SM Yukawa interactions lead to the constraints:

$$\mu_{Qi} - \mu_{ui} + \mu_\phi = 0\,, \tag{3.58a}$$
$$\mu_{Qi} - \mu_{di} - \mu_\phi = 0\,, \tag{3.58b}$$
$$\mu_{\ell i} - \mu_{ei} - \mu_\phi = 0\,. \tag{3.58c}$$

The equilibrium condition for the strong sphaleron processes give us the relation

$$g_s(\mu_{Q1} + \mu_{Q2} + \mu_{Q3}) + \mu_{\ell 1} + \mu_{\ell 2} + \mu_{\ell 3} = 0\,, \tag{3.59a}$$

where $g_s = 3$ is the factor counting the colour states, $u_i$ and $d_i$ are the right-handed electroweak singlets of flavour $i$, and $Q_i$ denote the corresponding left-handed quark doublets. The weak sphalerons relate the asymmetries in the lepton and baryon sectors with the constraint

$$g_w(\mu_{Q1} + \mu_{Q2} + \mu_{Q3}) - (\mu_{u1} + \mu_{u2} + \mu_{u3}) - (\mu_{d1} + \mu_{d2} + \mu_{d3}) = 0\,. \tag{3.60}$$

During the electroweak crossover, the electroweak sphalerons are no longer in equilibrium, which requires modifications of the above equation as described in [127]. We leave a detailed study of these effects for future work. The charge densities associated with the diagonal generators for weak and strong interactions vanish, as implied by the fact that the weak doublets and colour triplets have a common chemical potential. On the other hand, weak hypercharge neutrality leads to the condition

$$g_w Y_\phi q_\phi + \sum_{a=e,\mu,\tau} \left( g_w g_s Y_{Qa} q_{Qa} + g_w Y_{\ell a} q_{\ell a} + g_s Y_{ua} q_{ua} + g_s Y_{da} q_{da} + Y_{ea} q_{ea} \right) = 0\,. \tag{3.61}$$

[2] For an overview of the equilibration rates of the spectator processes see *e.g.* [126]

To find the relations between the asymmetries $\Delta_\alpha$ and the charges $q_{\ell\alpha}$, as well as $q_\phi$ we solve Eqs. (3.58, 3.59, 3.60, 3.61). If we write the asymmetries as vectors in flavour space, $q_\ell = (q_{\ell 1}, q_{\ell 2}, q_{\ell 3})^t$ as well as $\Delta = (\Delta_1, \Delta_2, \Delta_3)^t$, the solutions to the above equations can be written in the compact form $q_\ell = A\Delta$ and $q_\phi = C\Delta$, with the matrix $A$ and vector $C$ given by:

$$A = \frac{1}{711}\begin{pmatrix} -221 & 16 & 16 \\ 16 & -221 & 16 \\ 16 & 16 & -221 \end{pmatrix}, \quad C = -\frac{8}{79}\begin{pmatrix} 1 & 1 & 1 \end{pmatrix}.$$

The lepton and Higgs charges often appear together in the combination

$$q_{\ell\alpha} + q_\phi/2 = \chi_{\alpha\beta}\Delta_\beta\,, \qquad \chi = -\frac{1}{711}\begin{pmatrix} 257 & 20 & 20 \\ 20 & 257 & 20 \\ 20 & 20 & 257 \end{pmatrix}. \tag{3.62}$$

The baryon asymmetry can also be expressed in terms of $\Delta$ as

$$B = D\Delta\,, \quad D = \frac{28}{79}\begin{pmatrix} 1 & 1 & 1 \end{pmatrix}, \tag{3.63}$$

which allows us to reproduce the well known relation [128] $B = \frac{28}{79}(B - L)$. The baryon asymmetry is also related to the asymmetry in the doublet leptons:

$$B = Eq_\ell\,, \quad E = -\frac{4}{3}\begin{pmatrix} 1 & 1 & 1 \end{pmatrix}. \tag{3.64}$$

**Temperatures above $T > 10^8\,\mathrm{GeV}$** At temperatures above $10^8\,\mathrm{GeV}$, the interactions mediated by the first-generation Yukawa couplings are out of equilibrium, while all second- and third- generation Yukawa couplings reach equilibrium. In this temperature regime, the matrices $A$ and $C$ are instead given by

$$A = \frac{1}{1074}\begin{pmatrix} -906 & 120 & 120 \\ 75 & -688 & 28 \\ 75 & 28 & -688 \end{pmatrix}, \qquad C = -\frac{1}{179}\begin{pmatrix} 37 & 52 & 52 \end{pmatrix}. \tag{3.65}$$

## 3.4 Expansion of the Universe

To describe particle dilution in the Universe, we follow the results of [129]. If we neglect Planck-scale suppressed corrections, the only effect of replacing the Minkowski metric by the Friedman-Lemaitre-Robertson-Walker one is that the particle modes become red-shifted. This effect is easily implemented by switching to the conformal coordinates where the metric

$$g_{\mu\nu} = a^2\eta_{\mu\nu} \tag{3.66}$$

is proportional to the Minkowski metric $\eta_{\mu\nu}$ up to a scale factor $a$. The conformal time $\eta$ is then related to the physical time via $\mathrm{d}\eta = \mathrm{d}t^{\mathrm{phys}}/a$, the comoving momentum $p$ is given by $p = ap^{\mathrm{phys}}$. In the comoving frame, the masses also have to be rescaled to $M \to aM$. Number densities are also rescaled, with $a^3 n = n^{\mathrm{phys}}$. In a radiation dominated universe, the scale factor is given by:

$$a(\eta) = a_{\mathrm{R}}\eta\,. \tag{3.67}$$

We use the parametrization where:

$$a_{\mathrm{R}} = m_{\mathrm{Pl}}\sqrt{45/(4g_\star\pi^3))} \equiv \frac{T^2}{H}\,, \tag{3.68}$$

the comoving time is then:

$$\eta = 1/T^{\mathrm{phys}}\,. \tag{3.69}$$

As a consequence of the expansion of the universe, the number densities scale as:

$$n^{\mathrm{com}} = a^3 n^{\mathrm{phys}}\,, \tag{3.70}$$

i.e., the physical number density gets diluted as time passes, $\mathrm{d}n^{\mathrm{com}}/\mathrm{d}\eta = a^4(\mathrm{d}n^{\mathrm{phys}}/\mathrm{d}t^{\mathrm{phys}} + 3Hn^{\mathrm{phys}})$, where the $3H$ is exactly the dilution term. If we consider particle yields instead, there is no additional dilution term required, as the dilution term cancels when we consider a ratio of a number density and entropy density:

$$Y_X \equiv n_X/s \to \frac{\mathrm{d}Y_X^{\mathrm{phys}}}{\mathrm{d}t^{\mathrm{phys}}} = a\frac{\mathrm{d}Y_X^{\mathrm{com}}}{\mathrm{d}t^{\mathrm{com}}}\,, \tag{3.71}$$

where the entropy density remains approximately constant per comoving volume. For the quantum Boltzmann equations (3.46) it is therefore sufficient to appropriately replace all physical quantities by their comoving counterparts.

| comoving | physical |
|---|---|
| $\mathrm{d}t$ | $\mathrm{d}t^{\mathrm{phys}}/a$ |
| $p$ | $ap^{\mathrm{phys}}$ |
| $M^{\mathrm{com}}$ | $aM$ |
| $T^{\mathrm{com}}$ | $aT^{\mathrm{phys}} = a_{\mathrm{R}}$ |

# Chapter 4

# Baryogenesis Through Leptogenesis

## 4.1 Vanilla Leptogenesis

Early studies of the origin of the BAU often relied on grand unified theories (GUT) for violation of the baryon number $B$. However, the BAU is not necessarily generated directly through some $B$ violating process. In the standard model, the electroweak sphalerons can convert a lepton asymmetry $L$ into a baryon asymmetry $B$. Therefore, instead of looking for the origin of the baryon asymmetry, we can look for mechanisms that produce a lepton asymmetry, known as *leptogenesis*. On its own, leptogenesis does not seem much more attractive than baryogenesis, however, there is a deep connection between leptogenesis and the origin of neutrino masses, as both can be explained by extending the standard model with heavy Majorana neutrinos.

In this section we will briefly review the "vanilla" realization of the leptogenesis mechanism discovered by Fukugita and Yanagida [15] and its limitations. In this mechanism, the lepton asymmetry is created through the decay of a heavy Majorana neutrino. The heavy neutrino $N$ does not decay into leptons $\ell$ and antileptons $\bar{\ell}$ with the same rate:

$$\Gamma_{N\to\ell\bar{\phi}} \neq \Gamma_{N\to\bar{\ell}\phi}\,. \tag{4.1}$$

For simplicity let us assume that the heavy neutrinos have hierarchical masses $M_3 \gg M_2 \gg M_1$. The difference between these two processes arises due to the loop correction from the Higgs particle:

$\Gamma_{N\to\ell\bar{\phi}} \sim$

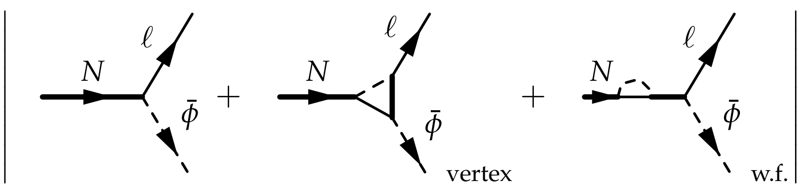


, (4.2)

where the thick lines represent the heavy neutrinos, the thin lines represent the active leptons and the dashed line corresponds to the Higgs particle. We can now calculate the decay asymmetry:

$$\epsilon_i \equiv \frac{\Gamma_{N_i\to\ell\bar{\phi}} - \Gamma_{N_i\to\bar{\ell}\phi}}{\Gamma_{N_i\to\ell\bar{\phi}} + \Gamma_{N_i\to\bar{\ell}\phi}}\,, \tag{4.3}$$

$$\approx \sum_k \frac{1}{8\pi} \frac{\mathrm{Im}\left[(YY^\dagger)^2_{ij}\right]}{(YY^\dagger)_{ii}} \left( f(M_k^2/M_i^2)\Big|_{\text{vertex}} + \frac{M_i M_k}{M_i^2 - M_k^2}\Big|_{\text{wave function}} \right), \tag{4.4}$$

which quantifies the excess of leptons produced during the decay of one heavy neutrino. We separate the result into the vertex and wave function contributions,

| | |
|---|---|
| $B$ violation | electroweak sphaleron |
| $C$ and $CP$ violation | Majorana neutrino decays |
| deviation from equilibrium | expansion of the universe |

Table 4.1: The Sakharov conditions in vanilla leptogenesis.

with $f(x) \equiv \sqrt{x}[1-(1+x)\ln[(1+x)/x]]$. On their own, these processes are not sufficient to generate the BAU. At temperatures $T \gg M_i$, the decays $N \to \ell\bar{\phi}$, $N \to \bar{\ell}\phi$ and inverse decays are in equilibrium, erasing any lepton asymmetry.

As the Universe cools down to $T < M_1$, the inverse decays become kinematically suppressed, as a lepton and a Higgs particle no longer have enough energy to produce a heavy neutrino. When the rate of inverse decays drops below the Hubble rate, the asymmetry produced by the decays is no longer washed out, and survives until the present epoch. This process can be described by the Boltzmann equations:

$$\begin{aligned} \frac{\mathrm{d}Y_{B-L}}{\mathrm{d}z} &= \epsilon_1 D(Y_{N_1} - Y_{N_1}^{\mathrm{eq}}) - WY_{B-L}\,, \\ \frac{\mathrm{d}Y_{N_1}}{\mathrm{d}z} &= -(D+S)(Y_{N_1} - Y_{N_1}^{\mathrm{eq}})\,, \end{aligned} \tag{4.5}$$

where $Y_L$ is the lepton yield, i.e. the lepton number excess divided by the entropy density, and $Y_{N_1}$ is the number density of the lightest heavy neutrino, $W$ is the lepton number washout rate, $D$ describes the heavy neutrino decays, $S$ describes the scatterings, and $z = M/T$ is the time variable.

By solving the Boltzmann equations 4.5, we can compute the final asymmetry. Through the approximations found in [78], the asymmetry can expressed as the sum of two terms:

$$Y_{B-L}(z) = Y_{B-L}^{\mathrm{init}} Exp\left[-\int_{z_i}^{z_f} W(z)\mathrm{d}z\right] - \frac{3}{4}\kappa\epsilon_1 \tag{4.6}$$

where the first term represents any initial asymmetry, and the second term describes the asymmetry generated through the decays of the lightest heavy neutrino, with $\kappa$ as the efficiency factor. Combining the expression for the decay asymmetry 4.4 with the Casas-Ibarra parametrization (2.17), a lower bound on the decay asymmetry was obtained in [75]:

$$|\epsilon_1| \lesssim \frac{3}{8\pi}\frac{M_1}{v^2}(m_3 - m_1)\,. \tag{4.7}$$

By combining this result with the numerical washout factors from [125], a lower limit on the mass of the lightest heavy neutrino [75] is obtained:

$$M_1 \gtrsim 10^9 \mathrm{GeV}\,. \tag{4.8}$$

Note that there are several loopholes that can lead to lower heavy neutrino masses. In the following, we will discuss two of them: resonant leptogenesis and leptogenesis through neutrino oscillations.

## 4.2 Evolution Equations for Leptogenesis

Both the resonant leptogenesis and leptogenesis through neutrino oscillations rely on an enhancement of the wave function diagram:

$$\epsilon_1(\text{wave function}) = \sum_k \frac{1}{8\pi} \frac{\mathrm{Im}\left[(YY^\dagger)^2_{ij}\right]}{(YY^\dagger)_{ii}} \frac{M_i M_k}{M_i^2 - M_k^2}, \tag{4.9}$$

when the masses (or energies) of the heavy neutrinos are not hierarchical. In such a scenario, the heavy neutrinos can oscillate as they propagate through the early universe, much like the light neutrinos oscillate today. As it was shown in [117], the wave function diagram can be thought of as the leading term describing oscillations of heavy neutrinos.

If the mass difference between two heavy neutrinos is small, the frequency of these oscillations can be comparable, or even smaller than rate of heavy neutrino production. This corresponds to a breakdown of the usual perturbation theory, and needs to be remedied by solving the quantum Boltzmann equations directly.

**Boltzman equations for oscillating neutrinos** To accurately describe the oscillations between the heavy neutrino flavours, it is no longer sufficient to only keep track of the number density per neutrino flavour $Y_{N_i}$. Instead, we have to take into account the states that can be in a superposition of the different mass eigenstates.

The quantity that can accurately describe this physical picture is the density matrix introduced in Chapter 3:

$$\delta f_{h\,ij} = -\mathrm{i} \int_0^\infty \frac{\mathrm{d}k^0}{2\pi} \mathrm{Tr}_D(\gamma_0 \delta S^F_{h\,ij}(k)) \tag{4.10}$$

where $i, j$ are the flavour indices, and $h = \pm 1$ is the helicity of the heavy neutrinos.

The number density of the heavy neutrinos is governed by the quantum Boltzmann equation:

$$\begin{aligned} \partial_t \delta f_h + \partial_t f^{\mathrm{eq}} = {} & -\mathrm{i}\,[H_h, \delta f_h] - \frac{1}{2}\{\Gamma_{hs}, \delta f_h\} \\ & - \frac{1}{2}\left\{\sum_\alpha \frac{\mu_\alpha}{T}\delta\Gamma^\alpha_h + \frac{\mu_\phi}{T}\delta\Gamma^\phi_h, \delta f_h\right\} + \sum_\alpha \frac{\mu_\alpha + \mu_\phi}{T} f^{\mathrm{eq}}(1 - f^{\mathrm{eq}})\tilde{\Gamma}^\alpha_{hs}, \end{aligned} \tag{4.11}$$

as introduced in Chapter 3, $H_h$ is the effective Hamiltonian, $\Gamma_h$ and $\delta\Gamma_h$ are the equilibration matrices, and $\tilde{\Gamma}_h^a$ is the backreaction term. At the same time, the lepton doublets are governed by:

$$\frac{\mathrm{d}\Delta_\alpha}{\mathrm{d}z} = -W_{\alpha\alpha}\chi_{\alpha\beta}\Delta_\beta + S_\alpha\,. \tag{4.12}$$

where $\chi$ is the susceptibility matrix relating the charges in the lepton and Higgs doublets to the asymmetries $q_{\ell\alpha} + q_\phi/2 = \chi_{\alpha\beta}\Delta_\beta$ introduced in Subsection 3.3.1. We now proceed to consider the specific leptogenesis scenarios, resonant leptogenesis, where the heavy neutrinos can be described as non-relativistic and leptogenesis through neutrino oscillations, where we assume that the heavy neutrinos have relativistic energies.

# 4.3 Resonant leptogenesis

As we have seen in Section 4.1, vanilla leptogenesis within the type-I seesaw framework requires heavy neutrinos with masses above $\sim 10^9$ GeV. This lower bound can be avoided if at least two heavy neutrinos have nearly degenerate masses, which enhances the decay asymmetry [80–86]. In order for the decay asymmetry to remain physical, the expression (4.9) has to remain finite, which is can be acheived by introducing a regulator $A_{\text{eff}}$:

$$\epsilon_1(\text{wave function}) = \sum_k \frac{1}{8\pi}\frac{\mathrm{Im}\left[(YY^\dagger)^2_{ij}\right]}{(YY^\dagger)_{ii}}\frac{M_iM_k}{M_i^2 - M_k^2 + A_{\text{eff}}^2}\,. \tag{4.13}$$

The exact form of this regulator has been discussed in the literature from several formulations of non-equilibrium QFT, the two-time formulation [130, 131], the two-momentum formulation [132] and the Wigner space formulation [133], which we discuss in the following text.

## 4.3.1 Non-Relativistic Approximations

In the non-relativistic limit, the temperature $T$ of the plasma is below the average masses of the heavy neutrino, $T \ll \bar{M}$. The four-momenta of the heavy neutrino in the plasma rest frame can be approximated as:

$$k^\mu = (k^0, \vec{k}) \approx (\pm a\bar{M}, \vec{0})\,, \tag{4.14}$$

where $a$ is the scale factor introduced in Section 3.4. The equilibration rate of a heavy neutrino is dominated by its decay process $N \to \ell\bar{\phi}$, as it is in vanilla leptogenesis. The reduced spectral self-energy of the heavy neutrino required to determine $\Gamma$ is then given by

$$\left(\hat{\Sigma}_N^{\mathcal{A}}(k)\right)^{\mu} \approx \mathrm{sgn}(k^0)\frac{k^{\mu}}{32\pi}, \tag{4.15}$$

which gives us the equilibration rates

$$\gamma_+ = \gamma_- = \frac{1}{T}\frac{g_w}{k^0}\frac{a^2\bar{M}^2}{32\pi}, \tag{4.16}$$

that we evaluate at the average mass $\bar{M}$.

Considering that the rates $\gamma_+$ and $\gamma_-$ are momentum independent, we may safely integrate over the 3-momentum to find the equations for heavy neutrino number densities

$$\bar{M}\frac{\mathrm{d}}{\mathrm{d}z}\delta n_h + \frac{ia_{\mathrm{R}}z}{2\bar{M}^2}\left[M^2, \delta n_h\right] + a_{\mathrm{R}}z\frac{g_w}{32\pi}\left\{\mathrm{Re}\, YY^{\dagger}, \delta n_h\right\} + \bar{M}\frac{\mathrm{d}}{\mathrm{d}z}n^{\mathrm{eq}} = 0, \tag{4.17}$$

where the heavy neutrino number density is given by

$$\delta n_h = \int \frac{\mathrm{d}^3k}{(2\pi)^3}\delta f_h(k). \tag{4.18}$$

It is interesting to notice that the comoving density and equations of motion are helicity independent in the non-relativistic limit, *i.e.* $\delta n_+(z) = \delta n_-(z)$. The heavy neutrino equilibrium number density is given by

$$n^{\mathrm{eq}} = \frac{z^2\mathcal{K}_2(z)}{2\pi^2}\,\mathrm{diag}(1,1) \approx \frac{z^{3/2}e^{-z}}{(2\pi)^{3/2}}\,\mathrm{diag}(1,1) \tag{4.19}$$

where $\mathcal{K}_{\nu}(z)$ are the modified Bessel functions of the second kind. In the non-relativistic limit, the evolution of the comoving SM charge densities is governed by the equation:

$$\begin{aligned} -\bar{M}\frac{\mathrm{d}}{\mathrm{d}z}\Delta_{\alpha} &= g_w S_{\alpha\alpha} - W_{\alpha\alpha}\left(q_{\ell\alpha} + \frac{1}{2}q_{\phi}\right), \\ &\equiv 4\epsilon_{\alpha\alpha}(z)\bar{M}\frac{\mathrm{d}n^{\mathrm{eq}}}{\mathrm{d}z} - W_{\alpha\alpha}\left(q_{\ell\alpha} + \frac{1}{2}q_{\phi}\right). \end{aligned} \tag{4.20}$$

The washout matrix $W$ is given by (c.f. Refs. [132, 134, 135])

$$W_{\alpha\beta} = \sum_i Y_{i\alpha}^* Y_{i\beta}\frac{3a_{\mathrm{R}}}{(2\pi)^3}z^3\mathcal{K}_1(z) \tag{4.21}$$

$$\approx \sum_i Y_{i\alpha}^* Y_{i\beta}\frac{3a_{\mathrm{R}}}{2^{\frac{7}{2}}\pi^{\frac{5}{2}}}z^{\frac{5}{2}}e^{-z}, \tag{4.22}$$

while the source term is

$$S_{\alpha\beta} = \frac{a\bar{M}}{8\pi} \sum_{ij} \delta n_{ij} \, \mathrm{i}\, \mathrm{Im}\left(Y^*_{i\alpha} Y_{j\beta}\right) \,, \tag{4.23}$$

where the helicities have been summed over, to give an overall factor two.

### 4.3.2 Strong Washout Regime

In this section we calculate the effective decay asymmetry for resonant leptogenesis in the strong washout regime. We will show that the decay asymmetry can be approximated by its late time limit in wide regions of parameter space.

Using Eq. (4.20) we can define the time-dependent flavoured effective decay asymmetry as

$$\epsilon_{\alpha\beta}(z) \equiv g_w S_{\alpha\beta}(z) \left(4\frac{\mathrm{d}n^{\mathrm{eq}}}{\mathrm{d}z}\right)^{-1} \bar{M}^{-1} \tag{4.24}$$

$$= \frac{1}{16\pi} \frac{a_{\mathrm{R}} z}{\bar{M}} \sum_{i,j} \mathrm{i}\, \mathrm{Im}[Y^*_{i\alpha} Y_{j\beta}] \delta n_{hij} \left(\frac{\mathrm{d}n^{\mathrm{eq}}}{\mathrm{d}z}\right)^{-1} \,, \tag{4.25}$$

which describes the asymmetry yield per sterile neutrino dropping out of equilibrium due to the expansion of the universe. Note that the factor 4 arises due to the two heavy neutrinos that each have two spins (helicities).

Large values of the Yukawa couplings $Y$ correspond to a strong washout of the lepton asymmetry. Simultaneously this corresponds to a fast relaxation rate for the heavy neutrinos. In Ref. [136] it was suggested that if the relaxation time of the heavy neutrinos is shorter than the freeze-out time, we can neglect the first terms of Eq. (4.17), and approximate the heavy neutrino density matrix $\delta n$ by its quasi-static limit.

We can then solve the resulting system of algebraic equations to obtain the quasi-static limits of the off-diagonal correlations entering the source term, which for $i \neq j$ gives us [133]

$$\delta n_{hij} = \frac{\mathrm{Re}[YY^\dagger]_{ij} \left[(YY^\dagger)_{ii} + (YY^\dagger)_{jj}\right]}{[YY^\dagger]_{ii}[YY^\dagger]_{jj}} \tag{4.26}$$

$$\times \frac{\frac{\bar{M}^2}{8\pi}\left[(YY^\dagger)_{ii} + (YY^\dagger)_{jj}\right] - i(M_i^2 - M_j^2)}{(M_i^2 - M_j^2)^2 + A_{\mathrm{eff}}^2} \frac{\bar{M}^3}{a_{\mathrm{R}} z} \frac{\mathrm{d}}{\mathrm{d}z} n^{\mathrm{eq}} \,. \tag{4.27}$$

We can insert the result (4.27) into the definition of the decay asymmetry to obtain the late-time effective decay asymmetry:

$$\epsilon^{\text{eff}}_{\alpha\beta} \;=\; -i(Y^*_{1\alpha}Y_{2\beta} - Y^*_{2\alpha}Y_{1\beta})\,\frac{\text{Re}[YY^\dagger]_{12}[(YY^\dagger)_{11} + (YY^\dagger)_{22}]}{16\pi(YY^\dagger)_{11}(YY^\dagger)_{22}}\,\frac{\bar{M}^2(M_2^2 - M_1^2)}{(M_1^2 - M_2^2)^2 + A_{\text{eff}}^2}\,, \tag{4.28}$$

with the regulator

$$A_{\text{eff}} \;=\; \frac{\bar{M}^2}{8\pi}[(YY^\dagger)_{11} + (YY^\dagger)_{22}]\left(1 - \frac{[\text{Re}(YY^\dagger)_{12}]^2}{(YY^\dagger)_{11}(YY^\dagger)_{22}}\right)^{1/2}. \tag{4.29}$$

### 4.3.3 Applicability of approximations

The key ingredient for the validity of the strong washout approximation introduce above is that all elements of the density matrix $\delta n_h$ relax to their quasi-static limit. To quantify this criterion, we calculate the eigenvalues of the system of differential equations (4.17) and compare to the Hubble rate. To simplify the discussion, we will first consider a toy model with a single lepton flavour.

In the single flavour approximation, we can write the effective decay asymmetry as

$$\epsilon^{\text{eff}} \;=\; \frac{1}{2}\,\frac{X\sin(2\varphi)}{X^2 + \sin^2(\varphi)}\,, \tag{4.30}$$

where $\varphi = \arg(Y_2/Y_1)$ is the phase between the Yukawa couplings, and $X$ is the dimensionless parameter quantifying the ratio of the mass difference to the decay widths

$$X \;=\; 8\pi\,\frac{M_1^2 - M_2^2}{\bar{M}^2\left(|Y_1|^2 + |Y_2|^2\right)}\,. \tag{4.31}$$

The smallest eigenvalue of the system of equations (4.17) is given by

$$\kappa \;=\; z\left[\bar{K} - \text{Re}\sqrt{K_1^2 + K_2^2 - 2i(K_1^2 - K_2^2)X - (K_1 + K_2)^2X^2 + 2K_1K_2\cos 2\varphi}\right], \tag{4.32}$$

where we introduced the usual washout parameters [78] $K_i = |Y_i|^2\bar{M}/(8\pi H)|_{T=\bar{M}}$ and $\bar{K} = (K_1 + K_2)/2$. In the democratic scenario, where $|Y_1| = |Y_2|$, the smallest eigenvalue is given by

$$\kappa \;=\; \bar{\kappa}\left[1 - \theta(\cos^2\varphi - X^2)\sqrt{\cos^2\varphi - X^2}\right], \tag{4.33}$$

with $\bar{\kappa} = z\bar{K}$, where $\theta$ is the Heaviside step function. The condition for the validity of the strong washout approximation, is that the slowest eigenmode is faster than the Hubble expansion, *i.e.* $\kappa \gg 1$ at the time of freeze-out $z = z_f \sim 10$. We can translate this condition to find the minimal washout strength required for the strong washout approximation to hold

$$\bar{K} \gg (1/z_f)(\bar{\kappa}/\kappa) . \tag{4.34}$$

To further test the limits of applicability of the strong washout approximation, we fix the phase $\varphi$ to the value that maximizes the asymmetry

$$\varphi_M = \arctan \frac{X}{\sqrt{1+X^2}} . \tag{4.35}$$

Inserting into the decay asymmetry, we find

$$|\epsilon| = \frac{1}{2\sqrt{1+X^2}} , \tag{4.36}$$

which is bounded by $|\epsilon| \leq 1/2$. The limit $|\epsilon| \to 1/2$ is corresponds $X \to 0$, and $\varphi_M \to 0$. This limit is, however, not realizable in practice. The ratio of the eigenvalues $\kappa/\bar{\kappa} \to 0$, which means that the off-diagonal modes responsible for the $CP$ asymmetry would require an infinite time to build up.

Large values of the effective decay asymmetry are therefore associated with small values of the eigenvalue $\kappa$.

For a fixed value of the decay asymmetry, the maximal value of $\kappa/\bar{\kappa}$ is obtained when $\varphi = \varphi_M$, which gives us the relation

$$\frac{\kappa}{\bar{\kappa}} \leq 1 - \theta\left[\epsilon^2 - \frac{1}{4}\left(2-\sqrt{2}\right)\right]\sqrt{\frac{[\epsilon^2 - \frac{1}{4}(2-\sqrt{2})][\epsilon^2 - \frac{1}{4}(2+\sqrt{2})]}{\epsilon^2(\epsilon^2 - 1/2)}} , \tag{4.37}$$

presented in Fig. 4.1.

The comparison between the analytical results obtained by using the late-time effective decay asymmetry and the numerical solutions to the differential equations Eq. (4.17) and (4.20) are shown in Fig. 4.2. To simplify the comparison, we take $q_\ell = -\Delta$ and neglect the charges in the Higgs field $q_\phi = 0$. We present results for two values of the washout strength $\bar{K}$, where the larger washout marginally complies with the criterion (4.34) and the smaller washout violates it.

From the plot it is visible that the time-dependent effective decay asymmetry approaches its late time limit around $z_f = \mathcal{O}(10)$.

Using the effective decay asymmetry at early times leads to a large discrepancy for the resulting lepton yield for both choices of washout strengths. The discrepancy however decreases around the time of freeze-out $z_f = \mathcal{O}(10)$, to a factor four

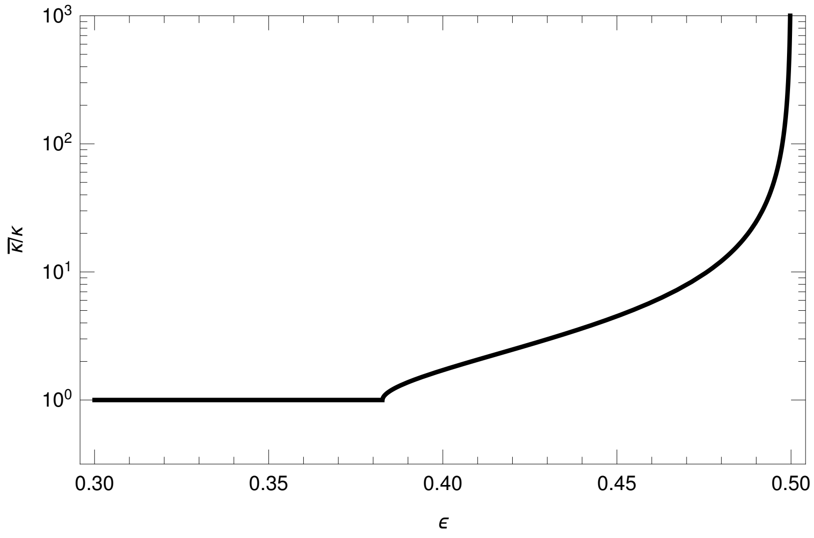


Figure 4.1: The relation between the decay asymmetry $\epsilon$ and the minimal ratio $\bar{\kappa}/\kappa$ of the smallest relaxation rate. The washout strength has to satisfy relation (4.34) for the applicability of the strong washout approximation. For $|\epsilon| \to 1/2$, the minimal values of $\bar{\kappa}/\kappa$ are larger, which means that the off-diagonal correlations take more time to build up. Therefore, larger values of the effective decay asymmetry also require a stronger washout for the approximations to be valid. Figure taken from [137].

for the smaller washout and leads to only 20% error in the case of the stronger washout which satisfies the relation (4.34).

Let us now consider a flavoured model with two heavy neutrinos and three doublet lepton flavours. We parametrize the Yukawa couplings using the Casas-Ibarra parametrization from [92] introduced in Section 2.1.1.

Since the dependence on the PMNS parameters cancels in the matrix $\mathrm{Re}[YY^\dagger]$ that appears in Eq. (4.17), we can use the Casas-Ibarra parametrization to find a lower bound on the ratio of eigenvalues to zeroth order in the mass splitting $M_2 - M_1$

$$(\kappa/\bar{\kappa})^{\mathrm{CI,NO}} = \frac{m_2 + m_3 \pm (m_3 - m_2)\mathrm{sech}(2\mathrm{Im}\omega)}{m_2 + m_3}, \tag{4.38}$$

$$(\kappa/\bar{\kappa})^{\mathrm{CI,IO}} = \frac{m_1 + m_2 \pm (m_2 - m_1)\mathrm{sech}(2\mathrm{Im}\omega)}{m_1 + m_2}, \tag{4.39}$$

where the superscripts (NO) and (IO) indicate normal or inverted hierarchy, and $m_1$, $m_2$ and $m_3$ are the masses of the active neutrinos. Taking the best fit values for the active neutrino masses, we find the limits on the ratio of eigenvalues to

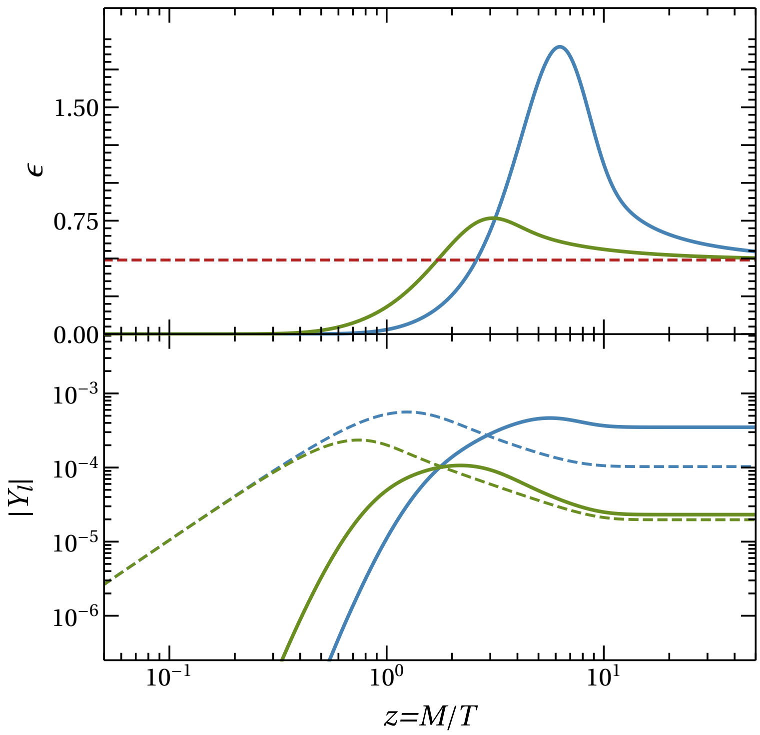


Figure 4.2: Upper panel: The evolution of the time-dependent decay asymmetry $\epsilon(z)$ as defined in (4.25) towards its the late-time limit $\epsilon = 0.49$ (red, dotted) for different values of the washout strength $\bar{K} = 5$ (blue) and $\bar{K} = 20$ (green). Lower panel: Comparison between the time dependence of the lepton yield $|Y_L| = |n_L|/s$ obtained using the time-dependent decay asymmetry for different values of the washout strength $\bar{K} = 5$ (blue, solid), and $\bar{K} = 20$ (green, solid), with the result obtained when using the late time limit (blue, dashed) and (green, dashed). Figure taken from [137].

be $(\kappa/\bar{\kappa}) \gtrsim 0.29$ for normal ordering (NO) and $(\kappa/\bar{\kappa}) \gtrsim 0.99$ for inverted ordering (IO). Combining these results with the criterion (4.34), we find that using the quasi-static limit for $\delta n_h$ is a valid approximation throughout the strong washout regime. Furthermore, using the Casas-Ibarra parametrization we find that the washout strength

$$\bar{K} = \left.\frac{\bar{M}\mathrm{tr}YY^\dagger}{16\pi H}\right|_{T=\bar{M}} \approx \begin{cases} \mathcal{O}(30)\cosh(2\mathrm{Im}\omega)\,, & \text{for NO}\,, \\ \mathcal{O}(50)\cosh(2\mathrm{Im}\omega)\,, & \text{for IO}\,, \end{cases} \tag{4.40}$$

always satisfies $\bar{K} \gg 1$, which means that the washout is always strong in the scenario with two heavy neutrinos.

In Fig. 4.3 we present a comparison between time-dependent and time-independent decay asymmetries for a scenario with realistic Yukawa couplings. In spite of the discrepancy in the asymmetries at early times, close to the freeze-out we find a $\mathcal{O}(1\%)$ agreement between the asymmetries calculated with time-dependent and time-independent effective decay asymmetries.

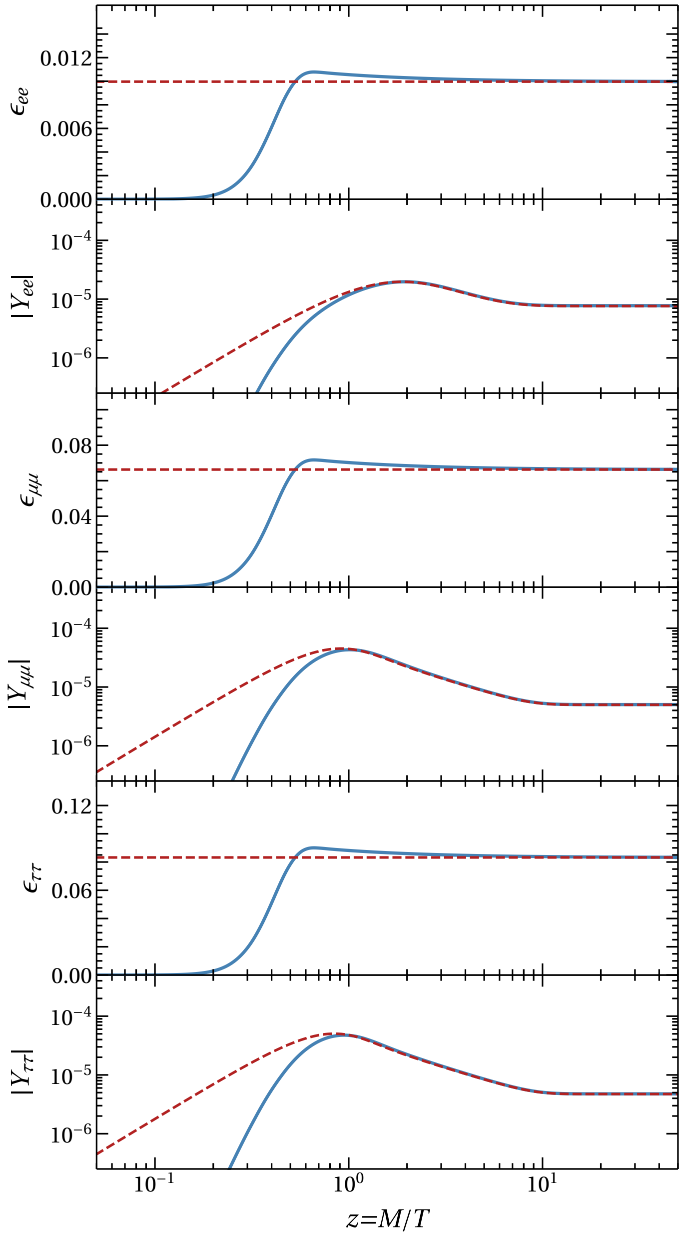


Figure 4.3: Comparison between the time-dependent decay asymmetries $\epsilon_{\alpha\alpha}(z)$ (solid) from Eq. (4.25) and their late-time limits $\epsilon_{\alpha\alpha}$ (dashed) from Eq. (4.28) for all three active lepton flavours $e$, $\mu$ and $\tau$. The parameters used are $\delta = 0$, $\alpha = 0$, $\omega = \pi/4 + 0.2i$, $\Delta M/\bar{M}^2 = -4 \times 10^{-17}$ GeV. We also compare the individual baryon-minus-lepton asymmetry yields $Y_{\alpha\alpha} = \Delta_{\alpha\alpha}/s$ obtained using the time-dependent decay asymmetry and the late-time limits. Figure taken from [137].

## 4.4 Leptogenesis Through Neutrino Oscillations

In this section we will discuss leptogenesis through neutrino oscillations, originally proposed by Akhmedov, Rubakov and Smirnov, which is why it is also known as ARS leptogenesis [88]. In contrast to the usual leptogenesis mechanism, where the BAU is produced during the freeze-out of the heavy neutrinos, in this mechanism the asymmetry is generated during the equilibration of the heavy neutrinos. The heavy neutrinos are produced through Yukawa interactions with the SM leptons and the Higgs boson. Since this interaction basis does not necessarily coincide with their mass basis, the heavy neutrinos begin to oscillate. These oscillations act as a source of lepton number and lepton flavour asymmetries. In the original treatment by Akhmedov, Rubakov and Smirnov, the washout of the lepton flavour asymmetries was neglected, and it appeared that three heavy neutrinos $n_s = 3$ were necessary to generate a total lepton asymmetry. In the work by Asaka and Shaposhnikov [71] it was pointed out that the washout of lepton flavour asymmetries can give rise to a net lepton asymmetry, making the mechanism viable even for $n_s = 2$. In the following, we focus our attention on this minimal scenario, with $n_s = 2$.

### 4.4.1 Ultra-Relativistic Approximations

In Chapter 3 we derived the evolution equations for heavy and active neutrinos with general coefficients. In leptogenesis through neutrino oscillations, the heavy neutrinos have masses at the GeV scale, however, as leptogenesis has to occur at temperatures $T > T_{\mathrm{EW}}$, where the sphaleron processes are active, this implies that the heavy neutrino will have energies much larger than its mass $T \gg M$. In contrast to the resonant regime, where we assumed the heavy neutrinos to be non-relativistic, in this scenario we consider the exactly opposite case, where the heavy neutrinos should be considered as ultra-relativistic.

For this reason, we depend crucially on thermal corrections to the neutrino self-energy. Instead of the decays that dominate the collision term in the non-relativistic case, here, the collision term is dominated by $2 \to 2$ scatterings.

The rates for these processes have been studied by various authors [117, 138–147, 147–152][1].

The thermal contributions to the self-energy are momentum dependent, which in principle means that we should keep track of each of the momentum modes in the equation (4.11). Such an approach would prove to be a considerable complication for both numerical and analytic calculations. We therefore take the standard

[1]See [153] for a recent review.

approach [71, 73, 88] of replacing the momentum-dependent equations for distribution functions by rate equations for number densities

$$\frac{\mathrm{d}}{\mathrm{d}z}\delta n_h = -\mathrm{i}[\langle H_N^{\mathrm{th}}\rangle + z^2\langle H_N^{\mathrm{vac}}\rangle, \delta n_h] - \frac{1}{2}\{\langle \Gamma_N\rangle, \delta n_h\} + \sum_{a,b=e,\mu,\tau} \langle \tilde{\Gamma}_N^{\alpha}\rangle \chi_{\alpha\beta}\Delta_\beta\,, \tag{4.41}$$

$$\frac{\mathrm{d}}{\mathrm{d}z}\Delta_\alpha = \left(\langle\gamma_+\rangle^{(1)} + \langle\gamma_-\rangle^{(1)}\right)\frac{a_{\mathrm{R}}}{T_{\mathrm{ref}}}\,\mathrm{Tr}\,\mathrm{Y}_+^{\alpha}\,\chi_{\alpha\beta}\Delta_\beta - g_w\frac{S_\alpha(\delta n_{hij})}{T_{\mathrm{ref}}}\,, \tag{4.42}$$

where the source term is given by

$$S_\alpha = S_{\alpha\alpha} = \sum_h h\frac{a_{\mathrm{R}}}{g_w}\left[\langle\gamma_+\rangle \mathrm{Tr}\left(\mathrm{Y}_{+h}^{\alpha}\delta n_h\right) - \langle\gamma_-\rangle \mathrm{Tr}\left(\mathrm{Y}_{-h}^{\alpha}\delta n_h\right)\right]\,. \tag{4.43}$$

After momentum averaging, we find the rates

$$\langle H_N^{\mathrm{vac}}\rangle = \frac{1}{2}\left\langle\frac{1}{k}\right\rangle\frac{a_{\mathrm{R}}^2}{T_{\mathrm{ref}}^3}\left(\mathrm{Re}[M^\dagger M] + \mathrm{i}h\,\mathrm{Im}[M^\dagger M]\right)\,, \tag{4.44}$$

$$\langle H_N^{\mathrm{th}}\rangle = \frac{1}{2}\frac{a_{\mathrm{R}}}{T_{\mathrm{ref}}}\left(\langle\mathfrak{h}_+^{\mathrm{th}}\rangle\mathrm{Y}_{+h} + \langle\mathfrak{h}_-^{\mathrm{th}}\rangle\mathrm{Y}_{-h}\right) + \frac{1}{2}\langle\mathfrak{h}^{\mathrm{EV}}\rangle\frac{a_{\mathrm{R}}}{T_{\mathrm{ref}}}\frac{\mathrm{Y}_+ + \mathrm{Y}_-}{2}\,, \tag{4.45}$$

$$\langle\Gamma_N\rangle = \frac{a_{\mathrm{R}}}{T_{\mathrm{ref}}}\left(\langle\gamma_+\rangle\mathrm{Y}_{+h} + \langle\gamma_-\rangle\mathrm{Y}_{-h}\right)\,, \tag{4.46}$$

$$\langle\tilde{\Gamma}_N^{\alpha}\rangle = h\frac{1}{2}\frac{a_{\mathrm{R}}}{T_{\mathrm{ref}}}\left(\langle\gamma_+\rangle^{(1)}\mathrm{Y}_{+h}^{\alpha} - \langle\gamma_-\rangle^{(1)}\mathrm{Y}_{-h}^{\alpha}\right)\,. \tag{4.47}$$

We summarize the coefficients in table 4.2. The averaging integrals for $\langle X\rangle$ and $\langle X\rangle^{(1)}$ are given by

$$\langle X\rangle\delta n \equiv \int\frac{\mathrm{d}^3k}{(2\pi)^2}X(k)\delta f(k) \tag{4.48a}$$

$$\approx \frac{\delta n}{n^{\mathrm{eq}}}\int\frac{\mathrm{d}^3k}{(2\pi)^2}X(k)f^{\mathrm{eq}}(k)\,.$$

$$\langle X\rangle^{(1)} \equiv \int\frac{\mathrm{d}^3k}{(2\pi)^2}X(k)f^{\mathrm{eq}}(k)[1-f^{\mathrm{eq}}(k)]\,, \tag{4.48b}$$

To simplify the integral in (4.48a), we assumed that the deviation from equilibrium remains proportional to the Fermi distribution throughout the evolution of the system. This approximation fails if $\gamma(k)$ is highly momentum dependent, as this causes different momentum modes to equilibrate at different times. This is the case with $\gamma_-(k)$, which is IR enhanced. Therefore, to have a reasonable estimate of the equilibration time for a mode that is populated through $\gamma_-(k)$, we consider the average momentum mode instead and use

$$\langle\gamma_-(k)\rangle \to \gamma_-(\langle k\rangle)\,. \tag{4.49}$$

| | LNC rate $X_+$ | LNV rate $X_-$ |
|---|---|---|
| Spectral | $\langle\gamma_+\rangle \approx 0.012$<br>$\langle\gamma_+\rangle^{(1)} \approx 0.012$ | $\langle\gamma_-\rangle \approx 9.7\times10^{-4}\frac{z^2\bar{M}^2}{T^2}$<br>$\langle\gamma_-\rangle^{(1)} \approx 0.019\frac{z^2\bar{M}^2}{T^2}$ |
| Hermitian | $\langle\mathfrak{h}_+\rangle \approx 0.23$<br>$\mathfrak{h}^{\rm EV} \approx \frac{2\pi^2}{18\zeta(3)}\frac{z^2v^2(z)}{T^2}$ | $\langle\mathfrak{h}_-\rangle \approx c(z)\times z^2\frac{\bar{M}^2}{T_{\rm ref}^2}$ |
| $\langle k\rangle = \frac{1}{a_{\rm R}}\frac{\pi^2}{18\zeta(3)}$ | | |

Table 4.2: The various averages appearing in the evolution equations (4.41) and (4.42). The momentum averages are calculated as described in (4.48), with two exceptions. In the calculation of $\langle\gamma_+\rangle^{(1)}$ we neglect the term $f^{\rm eq2}$, so that it is equal to $\langle\gamma_+\rangle$. On the other hand, the LNV rate $\langle\gamma_-\rangle$ is evaluated at the average momentum $\langle k\rangle$. The reason for using such an approximation is that the rate is highly IR enhanced. If we use the momentum averaging strategy described in (4.48a), we end up over representing the soft momentum modes that equilibrate early. We can see this discrepancy, as the rate $\langle\gamma_-\rangle^{(1)}$ is more than an order of magnitude bigger. The function $c(z)$ contains logarithmic contributions, and is given by $c(z) = \left[3.50 - 0.47\log\left(z^2\frac{\bar{M}^2}{T_{\rm ref}^2}\right) + 3.47\log^2\left(z\frac{\bar{M}}{T_{\rm ref}}\right)\right]\times10^{-2}$.

Note that all the terms containing $X_-$ appear with a suppression factor $z^2\bar{M}^2/T^2$. We will identify the terms $X_+$ as lepton number conserving, and $X_-$ as lepton number violating, where we assign a lepton number to the heavy neutrinos based on their helicity as previously mentioned in Section 2.2.

### Approximate Lepton Number Conservation

Relativistic heavy neutrinos in the early universe can be assigned a lepton number that corresponds to their helicity. We will call this lepton number $\tilde{L}$, with the charge assignment:

| Spinor | Lepton number |
|---|---|
| $P_+N$ | $+1$ |
| $P_-N$ | $-1$ |

To see the lepton number conservation in effect, we calculate the time derivative of $\tilde{L}$:

$$\frac{\mathrm{d}}{\mathrm{d}z}\Delta\tilde{L} = \frac{\mathrm{d}}{\mathrm{d}z}\left(-\sum_{\alpha}\Delta_\alpha + q_N\right), \tag{4.50}$$

where $q_N \equiv \mathrm{Tr}[\delta n_+] - \mathrm{Tr}[\delta n_-]$, and insert the equations (4.41) and (4.42) to find

$$\frac{\mathrm{d}\Delta\tilde{L}}{\mathrm{d}z} = -2\frac{a_\mathrm{R}}{T_\mathrm{ref}}\left(\langle\gamma_-\rangle^{(1)}\,\mathrm{Tr}\,\mathrm{Y}_+^\alpha\chi_{\alpha\beta}\Delta_\beta + \langle\gamma_-\rangle\,\mathrm{Tr}[\mathrm{Y}_-\delta n_+ - \mathrm{Y}_+\delta n_-]\right), \tag{4.51}$$

which vanishes in the limit $\gamma_- \to 0$. This implies, that the lepton number $\Delta\tilde{L}$ is conserved in the absence of $\gamma_-$. Therefore, we may call $\gamma_+$ lepton number conserving (LNC) terms, and $\gamma_-$ lepton number violating (LNV).

**Separation of the Equations Into Helicity Even and Odd Parts** For $n_s = 2$ heavy neutrinos, the equations (4.41) can become significantly simpler, if we separate the equations into helicity odd and even parts. As the lepton charge $\tilde{L}$ in the heavy neutrinos is defined through the trace, we can define the even and odd distributions

$$\delta n_e \equiv \frac{\delta n_+ + V\delta n_- V^\dagger}{2}, \qquad \delta n_o \equiv \frac{\delta n_+ - V\delta n_- V^\dagger}{2}, \tag{4.52}$$

which satisfies $2\,\mathrm{Tr}\,\delta n_o = q_N$ for any unitary matrix $V$. The equations for the helicity odd and even density matrices are given by

$$\begin{aligned}\frac{\mathrm{d}}{\mathrm{d}z}\delta n_{e,o} = &-\mathrm{i}[\langle H_e^\mathrm{th}\rangle + z^2\langle H_e^\mathrm{vac}\rangle, \delta n_{e,o}] - \frac{1}{2}\{\langle\Gamma_e\rangle, \delta n_{e,o}\} + \sum_{a,b=e,\mu,\tau}\langle\tilde{\Gamma}_{e,o}^\alpha\rangle\chi_{\alpha\beta}\Delta_\beta \\ &- \mathrm{i}[\langle H_o^\mathrm{th}\rangle + z^2\langle H_o^\mathrm{vac}\rangle, \delta n_{o,e}] - \frac{1}{2}\{\langle\Gamma_o\rangle, \delta n_{o,e}\},\end{aligned} \tag{4.53}$$

where we have supressed the index $N$. The helicity odd and even matrices $X_{e,o}$ are defined as

$$X_{e,o} = \frac{X_+ \pm VX_-V^\dagger}{2}. \tag{4.54}$$

It appears that we have achieved exactly the opposite of our goal, we have generated two extra terms, coupling the helicity even and odd parts of the density matrix. However, as we will see, with a convenient choice of $V$, these extra terms can be made small, or even vanish. In order for both $\Gamma_o$, and $H_o$ to vanish, there has to be a matrix $V$ that satisfies:

$$\Gamma_+ = (VG)\Gamma_+^t(VG)^\dagger \quad \text{and} \qquad H_+^\mathrm{th} + z^2 H_+^\mathrm{vac} = (VG)(H_+^{\mathrm{th}t} + z^2 H_+^{\mathrm{vac}t})(VG)^\dagger, \tag{4.55}$$

where $G$ is the matrix that tracks the Majorana condition introduced in E. We can verify the existence of such a matrix by calculating traces of the commutator [154]

$$\mathrm{Tr}\left[\Gamma_+\,, H_+^{\mathrm{th}} + z^2 H_+^{\mathrm{vac}}\right]^r\,, \tag{4.56}$$

for odd values of $r$. If all the traces vanish, there exists a matrix $V$ that satisfies the required relation. This relation is trivially satisfied for $n_s = 2$, and we can always find a choice of $V$ where both terms $H_o$ and $\Gamma_o$ will vanish. Note that while this holds at any given $z$, the matrices $\Gamma_+$ and $H_+^{\mathrm{th}} + z^2 H_+^{\mathrm{vac}}$ change in time, which leads to $\Gamma_o\,, H_o \sim \mathcal{O}(\mathrm{d}V/\mathrm{d}z)$. Furthermore, the term $\tilde{\Gamma}_o$ remains non-zero. In the $\tilde{L}$ number conserving limit we have $\gamma_- = \mathfrak{h}_- = 0$, which means that the matrices $H_\pm^{\mathrm{th}} \sim \Gamma_\pm$ commute, and it is sufficient to consider the commutator $[\Gamma_+\,, H_+^{\mathrm{vac}}]$.

A particularly convenient basis choice for illustrating these effects is given in the $\bar{L}$ - conserving basis introduced in Section 2.2. We find that the matrices, $\mathrm{Y}_\pm$, and $M^2$ take the form

$$\mathrm{Y}_+^\alpha = \begin{pmatrix} |F_\alpha|^2 & F_\alpha \epsilon_\alpha^* \\ F_\alpha^* \epsilon_\alpha & |\epsilon_\alpha|^2 \end{pmatrix}\,, \qquad \mathrm{Y}_-^\alpha = \begin{pmatrix} |\epsilon_\alpha|^2 & F_\alpha \epsilon_\alpha^* \\ F_\alpha^* \epsilon_\alpha & |F_\alpha|^2 \end{pmatrix}\,, \tag{4.57}$$
$$M^2 = \bar{M}^2 \begin{pmatrix} 1+\mu^2 & 2\mu \\ 2\mu & 1+\mu^2 \end{pmatrix}\,,$$

with the matrix $V$ in the limit $\mathfrak{h}_- = \gamma_- = 0$ given by

$$V \approx \begin{pmatrix} 0 & 1 \\ 1 & 0 \end{pmatrix}\,. \tag{4.58}$$

In this basis, all matrices, $\Gamma_o$, $H_o^{\mathrm{th}}$, $H_o^{\mathrm{vac}}$, as well as $\tilde{\Gamma}_o^\alpha$, vanish at zeroth order in $\epsilon$, $\gamma_-$ and $\mathfrak{h}_-$. This means that the helicity even distributions $\delta n_e$ approximately decouple from the rest of the system, only entering through the source term which is $\epsilon$ suppressed. In the following we adopt such a basis unless stated otherwise, which allows us to always neglect the $\epsilon$-suppressed backreaction terms $\Gamma_e$ of the helicity even distributions.

### 4.4.2 Analytic Expansions for Leptogenesis Through Neutrino Oscillations

In this section we will discuss regimes in which we can find useful approximations to the leptogenesis approximations. For simplicity, we will neglect the effects coming from LNV terms, which we discuss in more detail in Subsection 4.4.3.

Leptogenesis via neutrino oscillations relies on two physical processes, oscillations between the heavy neutrino flavours, that arises from the effective Hamiltonian $H$, and equilibration (production) of the heavy neutrinos which is governed by the matrix $\Gamma$.

Oscillations happen due to a misalignment between the basis in which the heavy neutrinos are produced$\sim\,\Gamma$, and their mass basis$\sim\,H$. The mass basis itself contains two terms, the thermal $H^{\rm th}$, and vacuum parts $H^{\rm vac}$. The thermal contribution typically commutes with the equilibration matrix, and therefore does not initiate oscillations. An exception to this is possible when one includes $\tilde{L}NV$ terms, which we will discuss in more detail in Subsection 4.4.3.

As the oscillations happen between two mass eigenstates, for $n_s$ heavy neutrinos we find $n_s(n_s-1)/2$ different oscillation frequencies. At the same time, the $n_s$ eigenvalues of the equilibration matrix $\Gamma_N$ correspond to $n_s$ different equilibration time scales.

In the minimal model with $n_s = 2$ heavy neutrinos, this corresponds to a single oscillation time scale. If we neglect thermal corrections $H^{\rm th}$, this time scale would be determined by the differences between the heavy neutrino masses

$$z_{\rm vac} = (a_{\rm R}|M_i^2 - M_j^2|)^{-1/3} T_{\rm ref}\,, \tag{4.59}$$

which corresponds to $z_{\rm vac}^3 \Delta H^{\rm vac} = \mathcal{O}(1)$, where $\Delta H$ signifies the difference between the eigenvalues. At early times, the thermal part of the effective Hamiltonian dominates, and can prevents neutrino oscillations. To identify the time scale when the vacuum part of the Hamiltonian begins to dominate over the thermal part, we introduce the time scale of *vacuum mass dominance*

$$z_{\rm vmd} = \sqrt{\frac{\Delta H^{\rm th}}{\Delta H^{\rm vac}}} \approx \sqrt{\frac{T_{\rm ref}^2 \mathfrak{h}_+^{\rm th}\,{\rm Tr}[YY^\dagger]}{M_2^2 - M_1^2}} = z_{\rm vac}\sqrt{\frac{z_{\rm vac}}{z_{\rm th}}}\,, \tag{4.60}$$

where we identified the difference between the eigenvalues of $YY^\dagger$ with the trace, as the smaller of the two eigenvalues is negligible compared to the large one. Finally, we have the time scale of the potential thermal oscillations which is close to the equilibration time scale

$$z_{\rm th} = \frac{1}{\Delta H^{\rm th}} = \frac{T_{\rm ref}}{a_{\rm R}\mathfrak{h}_+^{\rm th}\,{\rm Tr}[YY^\dagger]}\,, \qquad z_{\rm eq} = \frac{1}{{\rm Tr}[\Gamma]} = \frac{T_{\rm ref}}{a_{\rm R}\gamma_+\,{\rm Tr}[YY^\dagger]}\,. \tag{4.61}$$

The relations between these time scales determines how leptogenesis is realized in a specific scenario.

To identify where these regimes lie in parameter space, in Fig. 4.4, we identify the line that corresponds to $z_{eq} = z_{vac}$. This is the boundary between the *oscillatory* regime, where vacuum oscillations dominate, and the *overdamped* regime, where equilibration (of at least one heavy neutrino flavour) is fast.

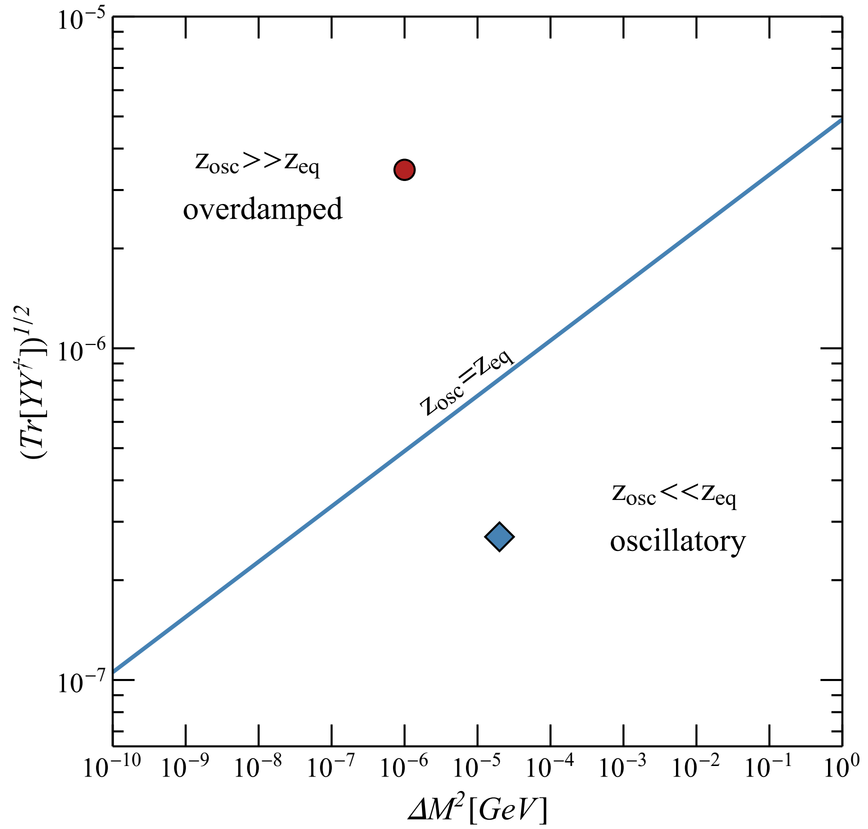


Figure 4.4: The regions in parameter space corresponding to oscillatory or overdamped regimes. We identify the line where the two time-scales, $z_{\rm vac}$ and $z_{\rm eq}$ are equal. The red circle and the blue diamond correspond to the benchmark scenarios described in Table 4.3. Note that the larger values of the Yukawa coupling correspond to larger mixing angles.

| | | overdamped | oscillatory |
|---|---|---|---|
| $M = 1\,\text{GeV}$ | $\text{Re}\,\omega = 3\pi/4$ | $\Delta M^2 = 10^{-6} M^2$ | $\Delta M^2 = 2 \times 10^{-5} M^2$ |
| $\delta = 3\pi/2$ | $\alpha_1 = 0$ | $\text{Im}\,\omega = 4.71$ | $\text{Im}\,\omega = 2.16$ |
| $\alpha_2 = -2\pi$ | | $U^2 = 3.6 \times 10^{-7}$ | $U^2 = 2.2 \times 10^{-9}$ |

Table 4.3: The parameters corresponding to the benchmark points for each of the regimes. Normal ordering is assumed in both cases.

### Oscillatory Regime

We now focus on the *oscillatory regime*. We characterize the oscillatory regime by the vacuum oscillations between the heavy neutrinos being much faster than their relaxation time

$$z_{\rm vac} \ll z_{\rm eq} \,. \tag{4.62}$$

The difference between the scales $z_{\rm vac}$ and $z_{\rm eq}$ allows us to separate the oscillation and equilibration processes.

To describe the fast oscillations, we switch to the interaction picture through the transformation

$$\delta n_{e\,I} = \exp\left(\mathrm{i}\frac{z^3}{3}H_e^{\rm vac}\right)\delta n_e \exp\left(-\mathrm{i}\frac{z^3}{3}H_e^{\rm vac}\right) \,, \tag{4.63}$$

which should also be applied to the matrices $\Gamma$ and $H^{\rm th}$. The evolution equations can then be written as

$$\frac{\mathrm{d}}{\mathrm{d}z}\delta n_{e,o\,,I} = -\mathrm{i}\left[\langle H^{\rm th}_{e,I}\rangle, \delta n_{e,o\,I}\right] - \frac{1}{2}\left\{\langle \Gamma_{e\,I}\rangle, \delta n_{e,o\,I}\right\} - \frac{1}{2}\left\{\langle \Gamma_{o\,I}\rangle, \delta n_{o,e\,I}\right\} + \mathcal{O}(\mu_\alpha) \,. \tag{4.64}$$

Since we are considering times $z \ll z_{\rm eq}$, we may use a perturbative expansion in $\Gamma$ and $H^{\rm th}$. At zeroth order we find:

$$\delta n^{(0)}_{e\,ij} = -n^{\rm eq}\delta_{ij} \,, \qquad\qquad \delta n^{(0)}_{o} = 0 \,. \tag{4.65}$$

By inserting this term into the right hand side of equation (4.63), we find the first order terms

$$\delta n^{(1)}_{e\,,o\,ij} = -\exp[\mathrm{i}(H^{\rm vac}_{e\,i} - H^{\rm vac}_{e\,j})z^3/3]\int_0^z \mathrm{d}z' \exp[-\mathrm{i}(H^{\rm vac}_{e\,i} - H^{\rm vac}_{e\,j})z'^3/3] n^{\rm eq}\Gamma_{e,o\,ij} \tag{4.66}$$

$$= -n^{\rm eq}\Gamma_{e,o\,ij}\mathcal{F}_{ij}(z) \,,$$

$$\mathcal{F}_{ij} = \left[C_{ij} - \frac{z}{3}E_{2/3}\left(-\frac{\mathrm{i}}{3}\Omega_{ij}z^3\right)\right]\exp\left(-\frac{\mathrm{i}}{3}\Omega_{ij}z^3\right) \,, \tag{4.67}$$

where $\Omega_{ij}$ is

$$\Omega_{ij} = \frac{a_{\rm R}}{T^3_{\rm ref}}\frac{\pi^2}{36\zeta(3)}(M^2_{ii} - M^2_{jj}) \,, \tag{4.68}$$

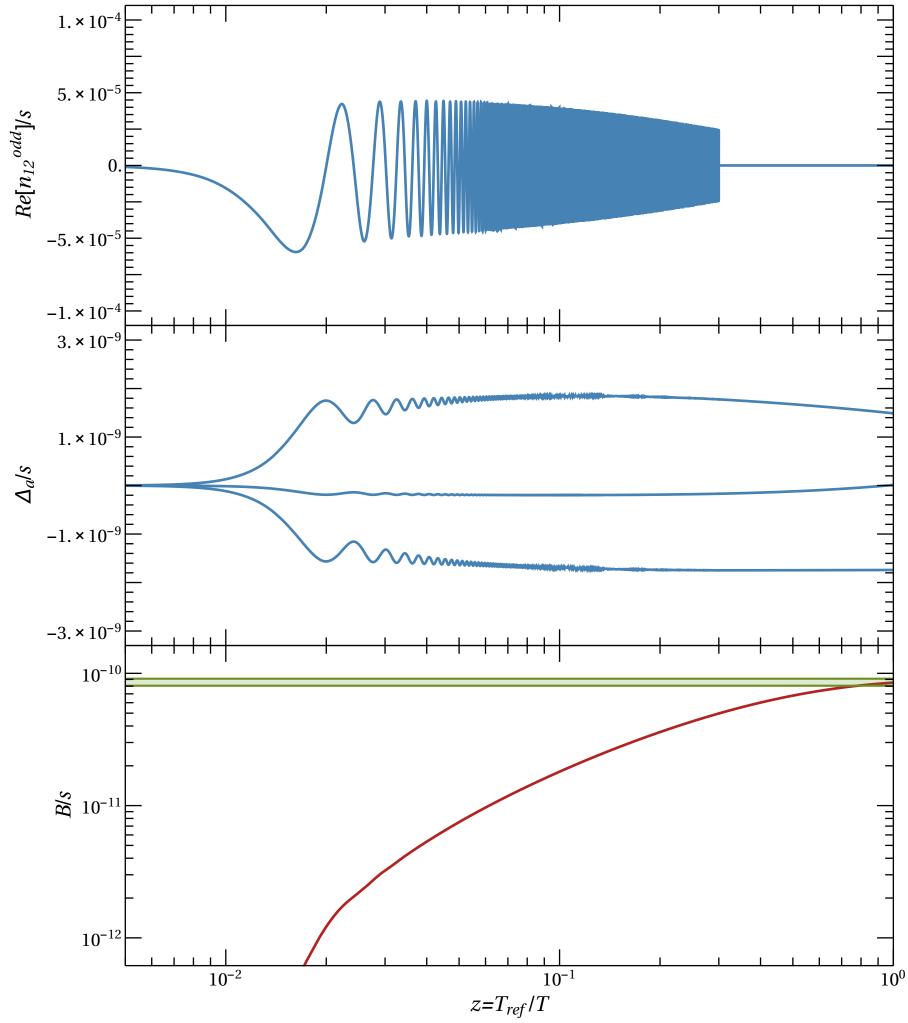


Figure 4.5: In the upper panel we present the oscillations of the heavy neutrinos in the *oscillatory* regime. The $CP$-violating correlations, that act as a source for the doublet asymmetries are characterised by the helicity odd off-diagonal flavour correlations in their mass basis. As the oscillations become increasingly fast, their contribution to the asymmetry decreases, and it becomes safe to cut them off, as indicated in the plot. In the middle panel we present the asymmetries generated in the individual SM flavours. The total lepton asymmetry is only generated when the washout begins, as can be seen in the plot. In the lowest panel we show the baryon asymmetry generated through this process. The error bars of the observed value are indicated by the green band. Parameters used for this figure correspond to the *oscillatory* benchmark point from table 4.3. Figure taken from [118].

$C_{ij}$ is an integration constant which we determine to be

$$C_{ij} = \lim_{z\to 0}\left[\frac{z}{3}E_{2/3}\left(-\frac{\mathrm{i}}{3}\Omega_{ij}z^3\right)\right] = \frac{\Gamma\left(\frac{1}{3}\right)}{3^{\frac{2}{3}}(-\mathrm{i}\Omega_{ij})^{\frac{1}{3}}}\,, \tag{4.69}$$

and

$$E_n(x) = \int_1^\infty \mathrm{d}t\,\frac{\mathrm{e}^{-xt}}{t^n}\,. \tag{4.70}$$

is the exponential integral function. In the mass basis, with the choice of $V = 1$, we find the following expression for the equilibration matrices

$$\Gamma_e = \langle\gamma_+\rangle\frac{a_\mathrm{R}}{T_\mathrm{ref}}\,\mathrm{Re}[YY^\dagger]_{ij}\,, \qquad \Gamma_o = \langle\gamma_+\rangle\frac{a_\mathrm{R}}{T_\mathrm{ref}}\mathrm{i}\,\mathrm{Im}[YY^\dagger]_{ij}\,. \tag{4.71}$$

**Initial Asymmetries in the Doublet Leptons** Due to the separation of the equilibration time scales, we may separate the initial production of the asymmetries and the washout of lepton doublet asymmetries. Therefore, at early times $z \ll z_\mathrm{eq}$, we find that the flavoured asymmetries are given by

$$\Delta_\alpha(z) = -g_w\int_0^z\frac{\mathrm{d}z'}{T_\mathrm{ref}}S_\alpha(z')\,. \tag{4.72}$$

We substitute the solutions (4.66) for the helicity even and odd densities $\delta n_{e,o}$ to obtain the source term, which is proportional to the integral

$$\int_0^z \mathrm{d}z'\;\mathrm{Im}\left[\mathcal{F}_{ij}(z')\right] = \frac{z^2}{2}\,\mathrm{Im}\;{}_2F_2\left(\left\{\frac{2}{3},1\right\};\left\{\frac{4}{3},\frac{5}{3}\right\};-\frac{\mathrm{i}}{3}|\Omega_{ij}|z^3\right)\;\mathrm{sgn}(M_{ii}^2 - M_{jj}^2)\,, \tag{4.73}$$

where the hypergeometric function $F$ is defined as

$${}_pF_q(\{a_1,\ldots,a_p\};\{b_1,\ldots,b_q\};w) = \sum_{k=0}^\infty\prod_{i=1}^p\frac{\Gamma(k+a_i)}{\Gamma(a_i)}\prod_{j=1}^q\frac{\Gamma(b_j)}{\Gamma(k+b_j)}\frac{w^k}{k!}\,, \tag{4.74}$$

for $p, q \in \mathbb{N}_0$ and $w \in \mathbb{C}$, where $\Gamma(x)$ is the Gamma function. After the first few oscillations, the asymmetries quickly saturate close to their asymptotic values. For times $z_\mathrm{vac}\mathcal{O}(1) < z \ll z_\mathrm{eq}$ we can approximate the doublet asymmetries as

$$\Delta_\alpha(z) = -g_w\int_0^z\frac{\mathrm{d}z'}{T_\mathrm{ref}}S_\alpha \approx -g_w\int_0^\infty\frac{\mathrm{d}z'}{T_\mathrm{ref}}S_a \equiv \Delta_a^\mathrm{sat}\,. \tag{4.75}$$

This integral is obtained by taking the limit of the hypergeometric function

$$\int_0^\infty \mathrm{d}z \ \mathrm{Im}\left[\mathcal{F}_{ij}(z)\right] = -\frac{\pi^{\frac{1}{2}}\Gamma(\frac{1}{6})}{2^{\frac{2}{3}}3^{\frac{4}{3}}|\Omega_{ij}|^{\frac{2}{3}}} \ \mathrm{sgn}(M_{ii}^2 - M_{jj}^2)\,. \tag{4.76}$$

Inserting this integral into $\Delta_\alpha^{\mathrm{sat}}$, and dividing by $s = 2\pi^2 g_\star a_{\mathrm{R}}^3/45$ to obtain the asymmetry yield per flavour, we find

$$\begin{aligned}\frac{\Delta_\alpha^{\mathrm{sat}}}{s} &= \frac{\mathrm{i}}{g_\star^{\frac{5}{3}}} \frac{3^{\frac{13}{3}}5^{\frac{5}{3}}\Gamma(\frac{1}{6})\zeta(3)^{\frac{5}{3}}}{2^{\frac{8}{3}}\pi^{\frac{41}{6}}} \sum_{\substack{i,j,\gamma \\ i\neq j}} \frac{Y^\dagger_{\alpha i}Y_{i\gamma}Y^\dagger_{\gamma j}Y_{j\alpha}}{\mathrm{sgn}(M_{ii}^2 - M_{jj}^2)} \left(\frac{m_{\mathrm{Pl}}^2}{|M_{ii}^2 - M_{jj}^2|}\right)^{\frac{2}{3}} \langle\gamma_+\rangle^2 \\ &\approx -\sum_{\substack{i,j,\gamma \\ i\neq j}} \frac{\mathrm{Im}[Y^\dagger_{\alpha i}Y_{i\gamma}Y^\dagger_{\gamma j}Y_{j\alpha}]}{\mathrm{sgn}(M_{ii}^2 - M_{jj}^2)} \left(\frac{m_{\mathrm{Pl}}^2}{|M_{ii}^2 - M_{jj}^2|}\right)^{\frac{2}{3}} \times 3.4\times 10^{-4}\langle\gamma_+\rangle^2\,. \end{aligned} \tag{4.77}$$

The comparison between the analytic solutions for $\delta n_o$ and $\Delta_\alpha$ with the numerical results is presented in Fig. 4.6. The approximations are quite accurate at early times, but a discrepancy is generated at later times due to the higher order washout and backreaction effects we neglected.

**Washout of the Doublet Asymmetry** At time scales corresponding to the equilibration scale $z = z_{\mathrm{eq}}$, the oscillations between the heavy neutrino flavours have become fast enough that we can average them out, and neglect the off-diagonal correlations $\delta n_{ij}|_{i\neq j} \approx 0$. If we neglect the off-diagonal correlations, we can reduce the density matrix equations to a system of rate equations that governs the evolutions of the doublet and heavy neutrino charges

$$\frac{\mathrm{d}\Delta_\alpha}{\mathrm{d}z} = \langle\gamma_+\rangle \frac{a_{\mathrm{R}}}{T_{\mathrm{ref}}} \sum_i |Y_{i\alpha}|^2 \left(\sum_\beta \chi_{\alpha\beta}\Delta_\beta - q_{Ni}\right)\,, \tag{4.78a}$$

$$\frac{\mathrm{d}q_{Ni}}{\mathrm{d}z} = -\langle\gamma_+\rangle \frac{a_{\mathrm{R}}}{T_{\mathrm{ref}}} \sum_\alpha |Y_{i\alpha}|^2 \left(q_{Ni} - \sum_\beta \chi_{\alpha\beta}\Delta_\beta\right)\,, \tag{4.78b}$$

where the $q_{Ni}$ are the charges per heavy neutrino with mass $M_i$. Assuming that the oscillations have saturated $z \gg z_{\mathrm{vac}}$, for the initial conditions we can take the values $\Delta_\alpha^{\mathrm{sat}}$ for the doublet charges, and $q_{Ni} = 0$ for the heavy neutrino charges. The $(3 + n_s)$ coupled differential equations all appear with constant coefficients, which we can represent as a differential equation for a vector of the charges $V_{\Delta N} =$

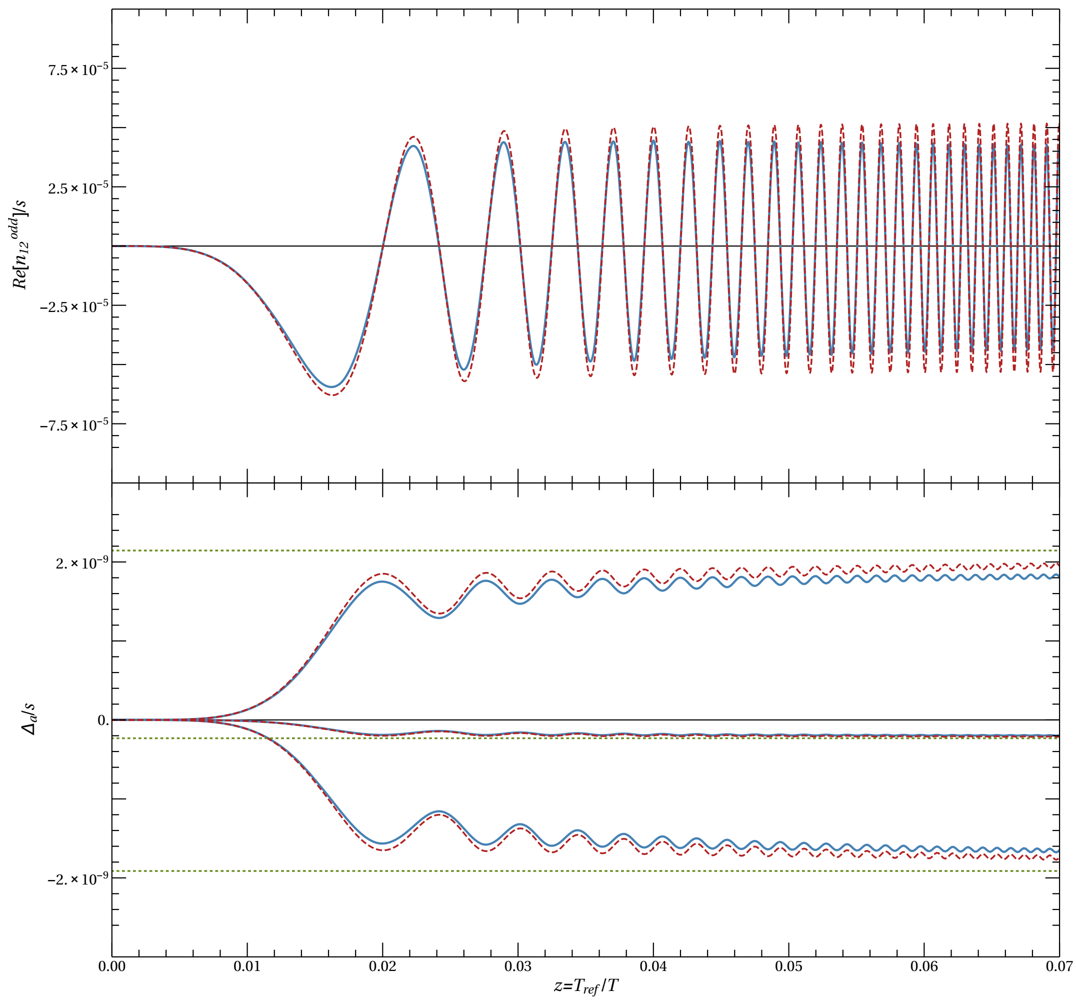


Figure 4.6: The comparison between the analytic results (red, dashed) to the numerical solutions (blue, solid) for the time evolution of the $CP$-violating correlation of the heavy neutrinos $\mathrm{Re}[\delta n_{o\,12}]$ (upper panel), as well as for the individual asymmetries in the doublet neutrino $\Delta_\alpha$ (lower panel). For comparison, we also show the saturated values $\Delta_\alpha^{\mathrm{sat}}$ from Eq. (4.77) in (dotted, green). Note that the approximate asymmetries approach a constant value, as the washout effects have been neglected. In the minimal scenario with two heavy neutrinos, the initial lepton asymmetry vanishes $\sum_\alpha \Delta_\alpha = 0$. Figure taken from [118].

$(\Delta^t, q_N^t)^t$

$$\frac{\mathrm{d}}{\mathrm{d}z} V_{\Delta N} = \frac{a_\mathrm{R}}{T_\mathrm{ref}} \gamma_\mathrm{av} K V_{\Delta N}\,, \qquad K = \begin{pmatrix} K^{\Delta\Delta} & K^{\Delta N} \\ K^{N\Delta} & K^{NN} \end{pmatrix}, \tag{4.79}$$

where the block matrix elements $K^{\Delta\Delta}, K^{\Delta N}, K^{N\Delta}$ and $K^{NN}$ read

$$\begin{aligned} K^{\Delta\Delta}_{\alpha\beta} &= \sum_{k=1}^{n_s} |Y_{k\alpha}|^2 \chi_{\alpha\beta}\,, \qquad & K^{\Delta N}_{\alpha j} &= -|Y_{j\alpha}|^2\,, \\ K^{N\Delta}_{ib} &= \sum_{\delta=1}^{3} |Y_{i\delta}|^2 \chi_{\delta\beta}\,, & K^{NN}_{ij} &= -\sum_{\delta=1}^{3} |Y_{i\delta}| \delta_{ij}\,, \end{aligned} \tag{4.80}$$

the latin indices $i, j = 1, 2, \ldots, n_s$ correspond to the heavy neutrino and $\alpha, \beta = 1, 2, 3$ to the doublet neutrino flavours. If we diagonalize the matrix $K$

$$K^\mathrm{diag} = \mathrm{T}^{-1} K \mathrm{T}\,, \tag{4.81}$$

with T as a transformation matrix and with the eigenvectors of $K$ as column vectors, we can write the formal solution

$$\begin{pmatrix} \Delta(z) \\ q_N(z) \end{pmatrix} = \mathrm{T} \exp\left( \frac{a_\mathrm{R}}{T_\mathrm{ref}} \gamma_\mathrm{av} K^\mathrm{diag}\, z \right) \mathrm{T}^{-1} \begin{pmatrix} \Delta^\mathrm{in} \\ q_N^\mathrm{in} \end{pmatrix}. \tag{4.82}$$

The baryon charge $Y_B$ freezes in at the sphaeron freeze out temperature $T_\mathrm{sph}$, which in our case corresponds to $T_\mathrm{ref}$ with $z = 1$. Following the relation (3.63), the BAU can be expressed as

$$Y_B = \frac{28}{79} \frac{1}{s} [\Delta_1(z) + \Delta_2(z) + \Delta_3(z)]_{z=1}\,. \tag{4.83}$$

We present a comparison of the analytic results for the evolution of the baryon asymmetry with the numerical solution in Fig. 4.7.

**Overdamped Regime**

We now consider the *overdamped* regime, where the equilibration rate of at least one heavy neutrino is faster than the vacuum oscillations $z_\mathrm{eq} \gg z_\mathrm{vac}$, *i.e.* at least one of the heavy neutrino flavours equilibrates before a single oscillation is complete. An example of such an evolution is presented in Fig. 4.8. This region of parameter space is interesting for two reasons, first, it corresponds to large mixing angles, which means it will be accessible to future experiments sooner, and second, it corresponds to small mass differences between the heavy neutrinos which are typically found in the approximately $\bar{L}$-conserving scenarios. In this scenario we

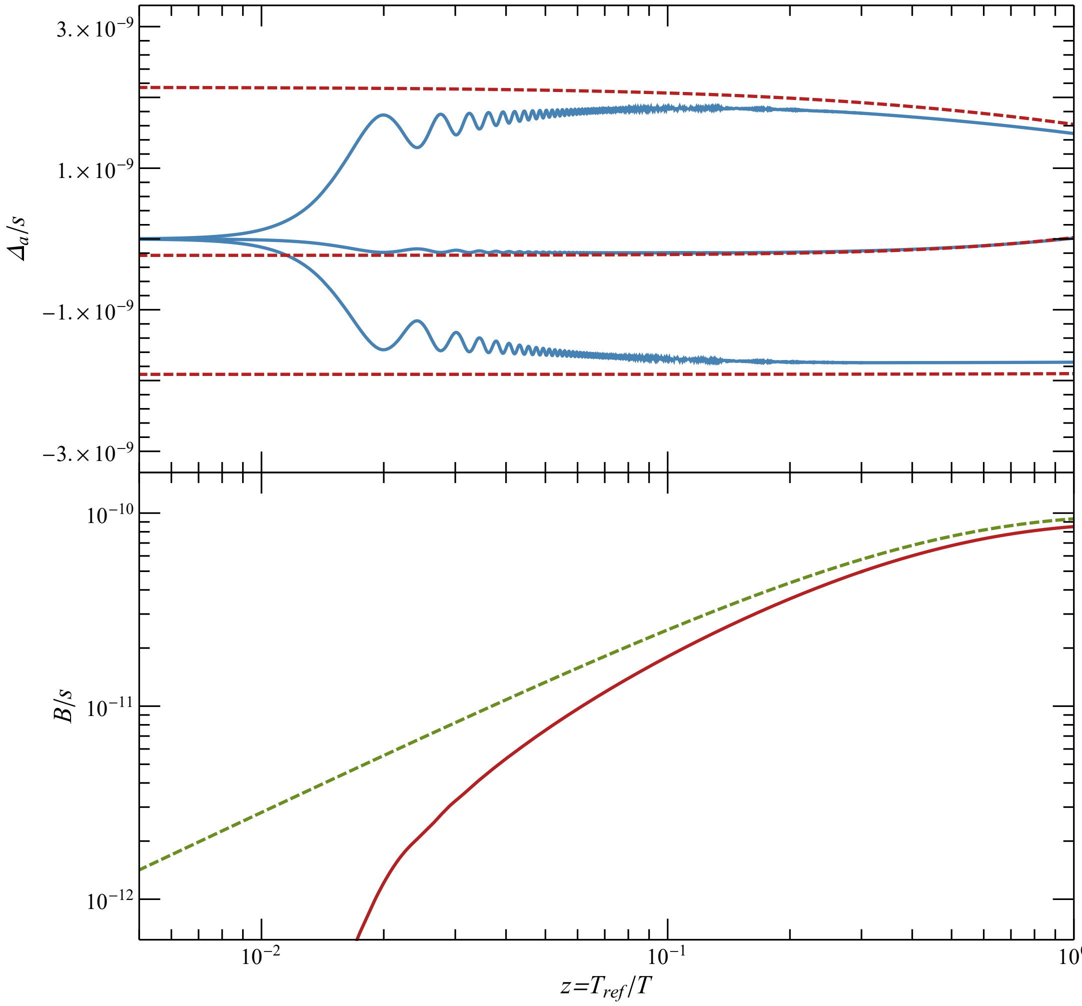


Figure 4.7: The comparison between the numerical solution, and the analytic results for the baryon asymmetry. In the upper panel we present the evolution of the individual flavour asymmetries (thick, blue), compared with the results obtained with the analytic results obtained by using the saturated values $\Delta_\alpha^{\rm sat}$ as their initial values (red, dashed). In the lower panel we see the results for the evolution of the baryon asymmetry. In the analytical approximation (green, dashed) we assume that all of the asymmetry is produced instantaneously, therefore it yields a significantly larger BAU for early times compared to the numerical results (thick, red). At later times $z > z_{\rm vac}$ this discrepancy decreases down to an $\mathcal{O}(10\%)$ difference. Figure taken from [118].

find that one of the eigenvalues of $Y_\pm$ can be several orders of magnitude smaller compared to the other one, as can be seen from (4.57). This means that the two interaction eigenstates behave very differently in the plasma. The eigenstate that corresponds to the larger eigenvalue of $\Gamma_e$ interacts rapidly, and it quickly reaches equilibrium. On the other hand, the eigenstate corresponding to the smaller eigenvalue interacts feebly with the plasma, and it remains out of equilibrium until the neutrinos start to oscillate. In this scenario, the thermal masses of the heavy neutrinos dominate the effective Hamiltonian at early times, which means that the interaction eigenstates also correspond to the mass eigenstates. The oscillations of the weakly coupled eigenstate therefore only happen only when the temperature drops low enough that the vacuum mass differences become comparable to those induced by the thermal masses. This corresponds to the times scale of *vacuum mass dominance* $z_{\mathrm{vmd}}$. As we are now considering time scales $z > z_{\mathrm{eq}}$, we can no longer use the same perturbative expansion in Yukawa couplings that we have used in the oscillatory regime.

Instead we use an approach similar to the one from 4.3.2, which is suitable for scenarios where the equilibration is fast.

**Evolution of the Heavy Neutrino Number Densities** To find analytic approximations for the evolution of the heavy neutrino number densities, we use the basis where $Y_+$ is diagonal, where we can clearly associate the weakly and strongly interacting eigenstates with the couplings $F_\alpha$ and $\epsilon_\alpha$ respectively. In this basis, the heavy neutrino thermal mass and equilibration matrices take the form

$$\langle \Gamma_{N,e} \rangle \approx \langle \gamma_+ \rangle \frac{a_{\mathrm{R}}}{T_{\mathrm{ref}}} \begin{pmatrix} \sum_\alpha |F_\alpha|^2 & 0 \\ 0 & 0 \end{pmatrix} , \tag{4.84a}$$

$$\langle H_{N,e}^{\mathrm{th}} \rangle \approx \langle \mathfrak{h}_+ \rangle \frac{a_{\mathrm{R}}}{T_{\mathrm{ref}}} \begin{pmatrix} \sum_\alpha |F_\alpha|^2 & 0 \\ 0 & 0 \end{pmatrix} , \tag{4.84b}$$

$$\text{for} \qquad V = \begin{pmatrix} 0 & 1 \\ 1 & 0 \end{pmatrix} . \tag{4.84c}$$

where we neglected all terms of $\mathcal{O}(\epsilon)^2$. It can be shown that the terms $\Gamma_o$, as well as $H_o^{\mathrm{th}}$ also vanish to leading order in $\epsilon$. The helicity-even part of the vacuum Hamiltonian is given by

$$H_N^{\mathrm{vac}} = \frac{\pi^2}{36\zeta(3)} \frac{a_{\mathrm{R}}}{T_{\mathrm{ref}}^3} \bar{M}^2 \begin{pmatrix} 1+\mu^2 & 2\mu \\ 2\mu & 1+\mu^2 \end{pmatrix} + \mathcal{O}(\mu\epsilon) . \tag{4.85}$$

To keep the results more general, in the following we only assume that $\langle \Gamma_{N\,e} \rangle_{11}$ and $\langle H_{N\,e}^{\mathrm{th}} \rangle_{11}$ are the only non-vanishing entries of the equilibration and thermal mass

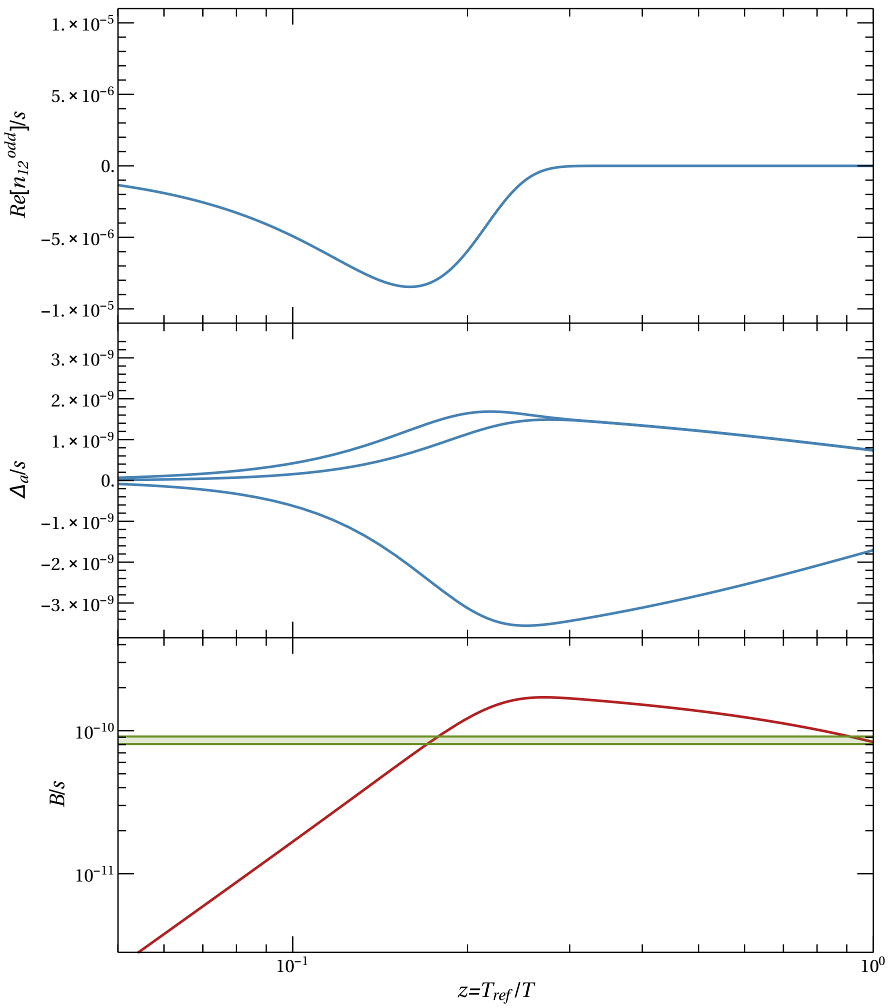


Figure 4.8: The production of the BAU in the overdamped regime. In the top panel we present the evolution of the off-diagonal element of the heavy neutrino density matrix that acts as a source of the individual lepton asymmetries. In contrast to the oscillatory regime, the off-diagonal correlation does not oscillate, but instead grows and relaxes to equilibrium. In the middle panel we present the evolution of the individual lepton asymmetries. Since the asymmetry is being produced after the equilibration time scale, the flavoured washout is already efficient at redistributing the flavour asymmetries into a total lepton (baryon) asymmetry. In the bottom panel we show the evolution of the baryon asymmetry. The observed value of the BAU is indicated by the green bands. Figure taken from [118].

matrices. Inserting these expressions into the evolution equations (4.53), we find the equations for the degrees of freedom that experience the equilibration directly

$$\frac{\mathrm{d}\delta n_{e\,11}}{\mathrm{d}z} = -\langle\Gamma_{N\,e}\rangle_{11}\delta n_{e\,11} - \mathrm{i}\,z^2\left[\langle H^{\mathrm{vac}}_{N\,e}\rangle_{12}\delta n_{e\,21} - \langle H^{\mathrm{vac}}_{N\,e}\rangle^*_{12}\delta n_{e\,12}\right], \tag{4.86a}$$

$$\frac{\mathrm{d}\delta n_{e\,12}}{\mathrm{d}z} = -\frac{\langle\Gamma_{N\,e}\rangle_{11}}{2}\delta n_{e\,12} - \mathrm{i}\langle H^{\mathrm{th}}_{N\,e}\rangle_{11}\delta n_{e\,12} - \mathrm{i}\,z^2\sum_k\left[\langle H^{\mathrm{vac}}_{N\,e}\rangle_{1k}\delta n_{e\,k2} - \delta n_{e\,1k}\langle H^{\mathrm{vac}}_{N\,e}\rangle_{k2}\right], \tag{4.86b}$$

and the ones that equilibrate indirectly, through the mixing with the directly equilibrated elements

$$\frac{\mathrm{d}\delta n_{e\,22}}{\mathrm{d}z} = -\mathrm{i}z^2\left[\langle H^{\mathrm{vac}}_{N\,e}\rangle^*_{12}\delta n_{e\,12} - \langle H^{\mathrm{vac}}_{N\,e}\rangle_{12}\delta n_{e\,21}\right]. \tag{4.87}$$

For times $z \gg z_{\mathrm{eq}}$, we may safely assume that the degrees of freedom in (4.86) have reached the quasi-static limit, where

$$\mathrm{d}\delta n_{e\,11}/\mathrm{d}z \;=\; \mathrm{d}\delta n_{e\,12}/\mathrm{d}z \;=\; \mathrm{d}\delta n_{e\,21}/\mathrm{d}z \;\approx 0\,. \tag{4.88}$$

Which means that each of the terms on the right hand side of equation (4.86) is much larger than the derivatives on the left hand side. This approximation allows us to express the densities $\delta n_{e\,11}$, $\delta n_{e\,12}$ and $\delta n_{e\,21}$ in terms of the weakly coupled density $\delta n_{e\,22}$

$$\delta n_{e\,11} = \frac{z^4|\langle H^{\mathrm{vac}}_{N\,e}\rangle_{12}|^2}{\langle\Gamma_{N\,e}\rangle^2_{11}/4 + \langle H^{\mathrm{th}}_{N\,e}\rangle^2_{11} + z^2 2\langle H^{\mathrm{th}}_{N\,e}\rangle_{11}\left[\langle H^{\mathrm{vac}}_{N\,e}\rangle_{11} - \langle H^{\mathrm{vac}}_{N\,e}\rangle_{22}\right] + z^4\tilde{H}^2_N}\delta n_{e\,22}, \tag{4.89a}$$

$$\delta n_{e\,12} = -\frac{z^2\langle H^{\mathrm{vac}}_{N\,e}\rangle_{12}\left\{\mathrm{i}\langle\Gamma_{N\,e}\rangle_{11}/2 + \langle H^{\mathrm{th}}_{N\,e}\rangle_{11} + z^2\left[\langle H^{\mathrm{vac}}_{N\,e}\rangle_{11} - \langle H^{\mathrm{vac}}_{N\,e}\rangle_{22}\right]\right\}}{\langle\Gamma_{N\,e}\rangle^2_{11}/4 + \langle H^{\mathrm{th}}_{N\,e}\rangle^2_{11} + z^2 2\langle H^{\mathrm{th}}_{N\,e}\rangle_{11}\left[\langle H^{\mathrm{vac}}_{N\,e}\rangle_{11} - \langle H^{\mathrm{vac}}_{N\,e}\rangle_{22}\right] + z^4\tilde{H}^2_N}\delta n_{e\,22}, \tag{4.89b}$$

with the shorthand notation

$$\tilde{H}^2_N \equiv |\langle H^{\mathrm{vac}}_{N\,e}\rangle_{12}|^2 + \left[\langle H^{\mathrm{vac}}_{N\,e}\rangle_{11} - \langle H^{\mathrm{vac}}_{N\,e}\rangle_{22}\right]^2.$$

To determine the evolution of the weakly coupled state, we insert the above solutions into (4.87)

$$\begin{aligned}\frac{\mathrm{d}\delta n_{22}}{\mathrm{d}z} &= -\frac{z^4|\langle H^{\mathrm{vac}}_{N\,e}\rangle_{12}|^2\langle\Gamma_{N\,e}\rangle_{11}}{\langle\Gamma_{N\,e}\rangle^2_{11}/4 + \langle H^{\mathrm{th}}_{N\,e}\rangle^2_{11} + z^2 2\langle H^{\mathrm{th}}_{N\,e}\rangle_{11}\left[\langle H^{\mathrm{vac}}_{N\,e}\rangle_{11} - \langle H^{\mathrm{vac}}_{N\,e}\rangle_{22}\right] + z^4\tilde{H}^2}\delta n_{22} \\ &= -\langle\Gamma_{N\,e}\rangle_{11}\frac{|\langle H^{\mathrm{vac}}_{N\,e}\rangle_{12}|^2}{\tilde{H}^2_N}\frac{z^4}{(z^2+z_c^2)(z^2+z_c^{*2})}\delta n_{22}, \end{aligned} \tag{4.90}$$

where we introduce the complex parameter

$$z_c = \sqrt{\frac{\langle H_N^{\mathrm{th}}\rangle_{11}}{\tilde{H}_N}\left[\frac{\langle H_N^{\mathrm{vac}}\rangle_{11} - \langle H_N^{\mathrm{vac}}\rangle_{22}}{\tilde{H}_N} + \mathrm{i}\sqrt{\frac{|\langle H_N^{\mathrm{vac}}\rangle_{12}|^2}{\tilde{H}^2} + \frac{\langle \gamma_+\rangle^2}{\langle \mathfrak{h}_+^{\mathrm{th}}\rangle^2}}\right]}\,. \tag{4.91}$$

If we take the vacuum part of the Hamiltonian from (4.85), and neglect the ratio $(\langle\gamma_+\rangle/\langle\mathfrak{h}_+^{\mathrm{th}}\rangle)^2$, we find that the absolute value of the parameter $|z_c|$ corresponds to the time at which the vacuum masses become comparable to the thermal masses, *i.e.*

$$|z_c| \approx z_{\mathrm{vmd}} = z_{\mathrm{vac}}\sqrt{\frac{z_{\mathrm{vac}}}{z_{\mathrm{th}}}} \gg z_{\mathrm{vac}}\,. \tag{4.92}$$

We can now analytically solve Eq. (4.90) to find

$$\delta n_{22} = \delta n_{22}(0)\exp\left\{-\langle\Gamma_N\rangle_{11}\frac{|\langle H_N^{\mathrm{vac}}\rangle_{12}|^2}{\tilde{H}_N^2}\left[z - \frac{\mathrm{Im}\left(z_c^3\arctan\frac{z}{z_c}\right)}{\mathrm{Im}\, z_c^2}\right]\right\}\,. \tag{4.93}$$

At times before the vacuum mass dominance, $z \lesssim |z_c|$, we can safely approximate

$$\delta n_{22} \approx \delta n_{22}(0)\exp\left(-\langle\Gamma_{Ne}\rangle_{11}\frac{|\langle H_{Ne}^{\mathrm{vac}}\rangle_{12}|^2}{\tilde{H}_N^2}\frac{z^5}{5|z_c|^4}\right)\,. \tag{4.94}$$

From equation (4.94), we can calculate the equilibration time for the weakly coupled state

$$z_{\mathrm{w}}^{\mathrm{eq}} = |z_c|\sqrt[5]{\frac{5z_{\mathrm{eq}}}{|z_c|}\frac{\tilde{H}_N^2}{|\langle H_N^{\mathrm{vac}}\rangle_{12}|^2}}\,. \tag{4.95}$$

Considering that the equilibration time scale is by construction much shorter than $|z_c| \sim z_{\mathrm{vmd}}$, we find that it is justified to use Eq. (4.94) to describe the equilibration of $\delta n_{22}$, as long as $|\langle H_N^{\mathrm{vac}}\rangle_{12}|^2 \gg |\langle H_N^{\mathrm{vac}}\rangle_{22} - \langle H_N^{\mathrm{vac}}\rangle_{11}|^2$, which is the case in the $\bar{L}$-conserving limit. In the $\bar{L}$-conserving limit we can express the equilibration time scale for the weakly coupled state as

$$z_{\mathrm{w}}^{\mathrm{eq}} = \sqrt[5]{\frac{405\zeta^2(3)\langle\mathfrak{h}_+\rangle^2}{\pi^2\langle\gamma_+\rangle}\frac{T_{\mathrm{ref}}^5\sum_\alpha|F_\alpha|^2}{a_{\mathrm{R}}\bar{M}^2\mu^2}}\,. \tag{4.96}$$

We can now insert the solution (4.94) into the equations for the off-diagonal terms that act as a source for the asymmetry

$$\mathrm{i}\,\mathrm{Im}[\delta n_{e\,12}] = -\frac{z^2\mathrm{i}\langle H_{Ne}^{\mathrm{vac}}\rangle_{12}\langle\Gamma_{Ne}\rangle_{11}}{2\tilde{H}_N^2|z^2+z_c^2|^2}\delta n_{22}(z)\,. \tag{4.97}$$

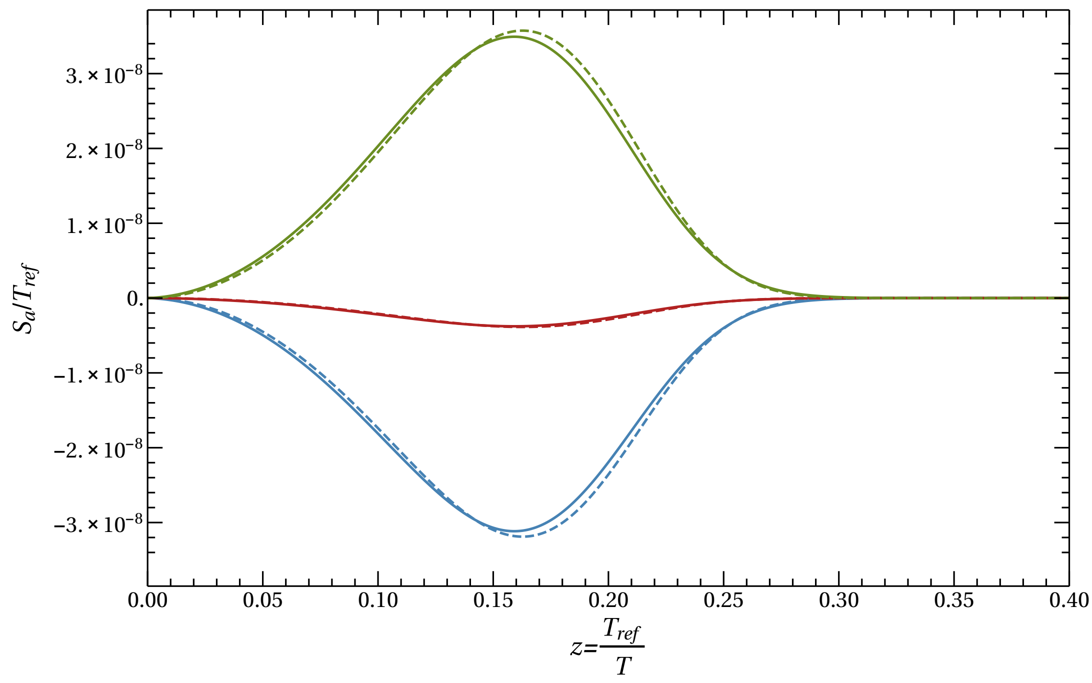


Figure 4.9: Comparison between the numerical (solid) and the analytic (dashed) results for the source of the lepton asymmetries for the three SM flavours. Figure taken from [118].

Inserting into the source term we find

$$
\begin{aligned}
S_a &= a_{\mathrm{R}} \frac{\langle \gamma_+ \rangle}{g_w} \operatorname{Tr}[\operatorname{Im}(\mathrm{Y}^{\alpha}_{+})\delta n_e] \\
&= 4 \frac{\langle \gamma_+ \rangle^2 a_{\mathrm{R}}^2}{g_w T_{\mathrm{ref}}} \frac{\sum_\beta |F_\beta|^2}{\tilde{H}_N^2} \frac{z^2}{|z^2 + z_c^2|^2} \operatorname{Im}\left[F^*_\alpha \epsilon_\alpha\right] \langle H^{\mathrm{vac}}_{N\,e} \rangle_{12} \delta n_{22}(z)
\end{aligned}
\tag{4.98}
$$

We find that the leading order of the source term is non-vanishing in the smaller Yukawa couplings $\epsilon_\alpha$. In Fig. 4.9 we present the time evolution of the source term.

The unflavoured source term $S = \sum_\alpha S_\alpha$ vanishes as a $\Gamma_o = \sum \Gamma^\alpha_o = 0$ imposes $\sum_\alpha F_\alpha \epsilon^*_\alpha = 0$. In the $B - \bar{L}$-conserving limit, where $\mu \ll \bar{M}$, we can further simplify the source term to:

$$\begin{aligned}\frac{S_\alpha}{s\,T_{\mathrm{ref}}} &\approx -\frac{45\sqrt{5}}{g_\star^{3/2} g_w 4\pi^{7/2}} \frac{\langle\gamma_+\rangle^2}{\langle\mathfrak{h}_+^{\mathrm{th}}\rangle^2} \frac{m_{\mathrm{Pl}}\bar{M}\mu}{T_{\mathrm{ref}}^3} \frac{\mathrm{Im}[F_\alpha^* \epsilon_\alpha]}{\sum_\beta |F_\beta|^2} z^2 \exp\left(-\frac{z^5}{z_{\mathrm{w}}^{\mathrm{eq}\,5}}\right) \\ &= -5.65\times 10^{-7} \times \frac{m_{\mathrm{Pl}}\bar{M}\mu}{T_{\mathrm{ref}}^3} \frac{\mathrm{Im}[F_\alpha^* \epsilon_\alpha]}{\sum_\beta |F_\beta|^2} z^2 \exp\left(-\frac{z^5}{z_{\mathrm{w}}^{\mathrm{eq}\,5}}\right). \end{aligned} \tag{4.99}$$

**Applicability of the approximations** For the approximations we made to be valid, the derivatives of the overdamped degrees of freedom $\delta n_{11}$ and $\delta n_{12}$ have to be small compared to the individual entries on the right-hand side of equations (4.86). In particular, we are interested if the approximations are valid after the strongly coupled state reaches equilibrium, and before the weakly coupled state fully equilibrates, *i.e.* for times $z_{\mathrm{eq}} \ll z_{\mathrm{w}}^{\mathrm{eq}}$. If we use the approximate form of the overdamped densities

$$\delta n_{e\,11} = \frac{|(H_N^{\mathrm{vac}})_{12}|^2}{(\tilde{H}_N^{\mathrm{vac}})^2} \frac{z^4}{|z_c|^4} \delta n_{e\,22}\,, \tag{4.100a}$$

$$\delta n_{e\,12} = -\frac{(H_N^{\mathrm{vac}})_{12}}{(\tilde{H}_N^{\mathrm{vac}})^2} \frac{z^2}{|z_c|^4} \left[(H_N^{\mathrm{th}})_{11} + \mathrm{i}(\Gamma_N)_{11}\right] \delta n_{e\,22}\,, \tag{4.100b}$$

we find that their derivatives are approximately given by

$$\delta n_{e\,11} = \frac{|\langle H_{N\,e}^{\mathrm{vac}}\rangle_{12}|^2}{\tilde{H}_N^2} \frac{z^4}{|z_c|^4} \delta n_{e\,22}\,, \tag{4.101a}$$

$$\delta n_{e\,12} = -\frac{\langle H_{N\,e}^{\mathrm{vac}}\rangle_{12}}{\tilde{H}_N^2} \frac{z^2}{|z_c|^4} \left[\langle H_{N\,e}^{\mathrm{th}}\rangle_{11} + \mathrm{i}\langle\Gamma_{N\,e}\rangle_{11}\right] \delta n_{e\,22}\,. \tag{4.101b}$$

which means that we may safely use the quasi-static limit for the overdamped of freedom, as long as the derivative of $\delta n_{22}$ remains small, which is true for $z < |z_c|$.

**Evolution of the Asymmetries in the Overdamped Regime** In contrast to the oscillatory regime, the time scale of the washout of the active charges are faster, or comparable to the time scales at which the individual lepton asymmetries are being produced.

As a consequence of this, it is not possible to treat the production and washout of the lepton asymmetries as separate processes. However, if we separate the equations into the helicity-even and odd parts, we can first solve the helicity-even part, as we have done above, and use it as an input (source) for the coupled system of helicity-odd equations, *i.e.* the coupled equations of $\delta n_o$ and the asymmetries $\Delta_\alpha$.

This procedure can be seen as keeping all the large Yukawa couplings $F_\alpha$ in the equations, but treating the smaller set of Yukawa couplings $\epsilon_\alpha$ as a small expansion parameter. Separating the sets of equations is therefore equivalent to solving the equations to zeroth order in $\epsilon$, and using them as an input for the equations that are first order in $\epsilon$.

**Suppression due to Backreaction** To describe the effects of backreaction on the heavy neutrinos we consider the equations for the helicity-odd heavy neutrino densities (4.53), which are coupled to the asymmetries in the doublet leptons (4.42). The backreaction term, that describes the feedback of the asymmetries in the doublet leptons onto the heavy neutrinos is given by

$$\langle \tilde{\Gamma}^{\alpha}_{N\,e} \rangle = \frac{1}{2} \langle \gamma_+ \rangle^{(1)} \frac{a_{\mathrm{R}}}{T_{\mathrm{ref}}} \begin{pmatrix} |F_\alpha|^2 & 0 \\ 0 & 0 \end{pmatrix} + \mathcal{O}(\epsilon)\,, \tag{4.102}$$

*i.e.* it dominantly couples to the overdamped degree of freedom $\delta n_{o\,11}$. As in the previous section, we apply the quasi-static approximation for the overdamped degrees of freedom $\delta n_{o\,11}$, $\delta n_{o\,12}$ and $\delta n_{o\,21}$, which gives us the density

$$\begin{aligned} \delta n_{o\,11} \approx& \sum_{\beta,\gamma} \frac{|F_\beta|^2}{2\sum_\delta |F_\delta|^2} \chi_{\beta\gamma} \Delta_\gamma \left( 1 - \frac{\langle H^{\mathrm{vac}}_{N\,e} \rangle_{12}|^2}{\tilde{H}^2_N} \frac{z^4}{|z^2 + z_c^2|^2} \right) \\ &+ \frac{|\langle H^{\mathrm{vac}}_{N\,e} \rangle_{12}|^2}{\tilde{H}^2_N} \frac{z^4}{|z^2 + z_c^2|^2} \delta n_{o\,22}\,. \end{aligned} \tag{4.103}$$

To find the evolution equations for the slowly evolving degrees of freedom, we insert the above equations into the equations for the weakly coupled state $\delta n_{o\,22}$ as well as the equations for the lepton doublets to find

$$\begin{aligned} \frac{\mathrm{d}\Delta_a}{\mathrm{d}z} =& \tilde{W}_{\alpha\beta} \Delta_\beta - g_w \frac{S_a(z)}{T_{\mathrm{ref}}} \qquad\qquad (4.104\mathrm{a}) \\ &+ \frac{a_{\mathrm{R}}}{T_{\mathrm{ref}}} \langle \gamma_+ \rangle |F_\alpha|^2 \frac{|\langle H^{\mathrm{vac}}_{N\,e} \rangle_{12}|^2}{\tilde{H}^2_N} \frac{z^4}{|z^2 + z_c^2|^2} \left( 2\delta n_{o\,22} - \sum_{\beta,\gamma} \frac{|F_\beta|^2}{\sum_\delta |F_\delta|^2} \chi_{\beta\gamma} \Delta_\gamma \right) \\ \frac{\mathrm{d}\delta n_{o\,22}}{\mathrm{d}z} =& -\langle \Gamma_{N\,e} \rangle_{11} \frac{|\langle H^{\mathrm{vac}}_{N\,e} \rangle_{12}|^2}{\tilde{H}^2_N} \frac{z^4}{|z^2 + z_c^2|^2} \frac{1}{2} \left( 2\delta n_{o\,22} - \sum_{\beta,\gamma} \frac{|F_\beta|^2}{\sum_\delta |F_\delta|^2} \chi_{\beta\gamma} \Delta_\gamma \right)\,, \\ &\qquad\qquad (4.104\mathrm{b}) \end{aligned}$$

where we introduced the effective washout matrix

$$\tilde{W}_{\alpha\beta} = \frac{a_{\mathrm{R}}}{T_{\mathrm{ref}}} \langle \gamma_+ \rangle |F_\alpha|^2 \sum_\gamma \left( \delta_{\alpha\gamma} - \frac{|F_\gamma|^2}{\sum_\delta |F_\delta|^2} \right) A_{\gamma\beta}\,. \tag{4.105}$$

We can combine Eqs. (4.104a) and (4.104b) to simplify the expression for the active lepton densities

$$\frac{\mathrm{d}\Delta_\alpha}{\mathrm{d}z} = \sum_\beta \tilde{W}_{\alpha\beta}\Delta_\beta - g_w \frac{S_\alpha(z)}{T_{\mathrm{ref}}} - 2\frac{|F_\alpha|^2}{\sum_\delta |F_\delta|^2}\frac{\mathrm{d}\delta n_{o\,22}}{\mathrm{d}z}\,. \tag{4.106}$$

If we neglect the term proportional to the derivative of $\delta n_{o\,22}$, which remains small for $z \lesssim |z_c|$, we can formally calculate the flavoured asymmetries by calculating the integrals

$$\Delta_\alpha(z) \approx \sum_{\beta,\gamma=1,2} v^T_{\alpha\beta}\mathrm{e}^{w_\beta z}\int_0^z \mathrm{d}z'\,\mathrm{e}^{-w_\beta z'} v_{\beta\gamma} g_w \frac{S_\gamma(z')}{T_{\mathrm{ref}}}\,. \tag{4.107}$$

where $w_{1,2}$ are the two non-vanishing eigenvalues of the matrix $\tilde{W}_{\alpha\beta}$, with the corresponding flavour eigenvectors $v_{\beta\gamma}$.

Since we have neglected the derivatives $\mathrm{d}\delta n_{o\,ii}/\mathrm{d}z$, the total lepton number remains conserved. The approximate lepton number conservation is then reflected in vanishing eigenvalue of the effective washout matrix $\tilde{W}$.

To obtain a total non-vanishing lepton number, we have to include the corrections of $\mathcal{O}(\mathrm{d}\delta n_{o\,ii}/\mathrm{d}z)$. This suppression is a result that is only present due to the backreaction of the active asymmetries onto the heavy neutrinos.

We now proceed to include these corrections by calculating the density in $\delta n_{o\,22}$, which can be obtained by integrating Eq. (4.104b) with the approximate form for the doublet asymmetries from Eq. (4.107). In practice, it is sufficient to neglect it for times before the equilibration time of the weakly coupled state $z < z_{\mathrm{w}}^{\mathrm{eq}}$, and at later times replace it by the quasi static limit.

To include the violation of the lepton number $L = \sum L_\alpha$ through washout, we include the corrections of $\mathcal{O}(\mathrm{d}\Delta_\alpha/\mathrm{d}z)$ to the overdamped degree of freedom $\delta n_{e\,11}$. The BAU can then be calculated by if we integrate the sum $\sum_\alpha \mathrm{d}\Delta_\alpha/\mathrm{d}z$ by parts, which gives us

$$B(z) \approx \frac{28}{79}\left[\sum_{\alpha\beta}\Delta_\alpha(z)\chi_{\alpha\beta}\frac{|F_\beta|^2}{\sum_\delta |F_\delta|^2} + 2\delta n_{o\,22}(z)\right]\,. \tag{4.108}$$

The resulting expression is correct up to $\mathcal{O}(50\%)$ corrections for $z > |z_c|$. It is interesting that the above expression reflects the approximate $B - \tilde{L}$-conservation, as it is essentially given by

$$B(z) \approx \frac{28}{79} \times 2\,\mathrm{Tr}(\delta n_o) = \frac{28}{79}(B - L)\,. \tag{4.109}$$

The comparison between these analytic expressions and the numerical results is presented in Fig. 4.10, while a complete comparison between the analytical and numerical results is presented in Fig. 4.11.

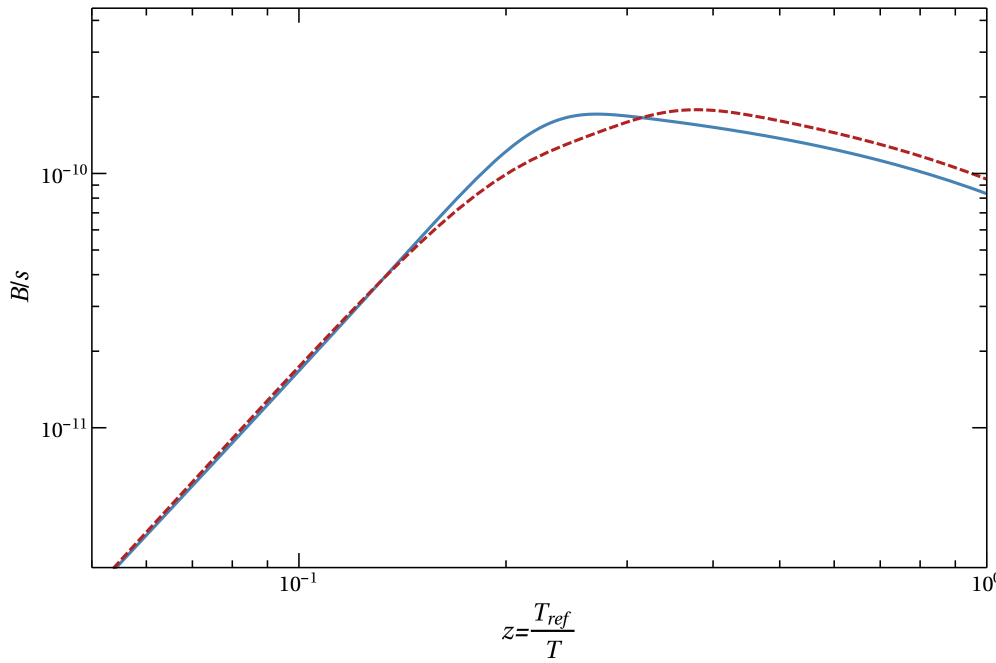


Figure 4.10: Comparison between the BAU obtained numerically (blue, full) and using the semi-analytic approximations (red, dashed). The parameters correspond to *overdamped* benchmark point from 4.3. Figure taken from [118].

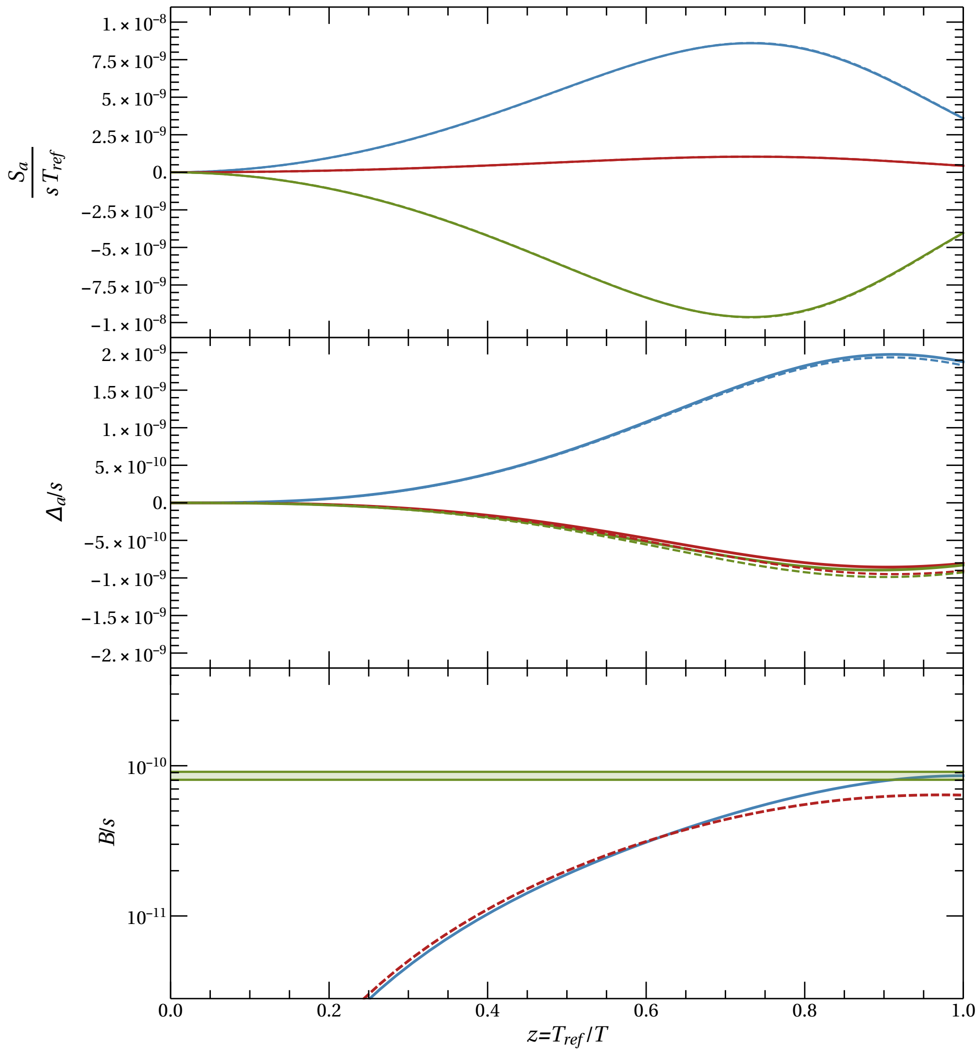


Figure 4.11: The comparison between numerical and analytic solutions for the source term, individual lepton charges and the baryon asymmetry for parameter choices that lead to maximal mixing angles for right-handed neutrino masses of $\bar{M} = 1$GeV in the case of normal hierarchy. Numerical solutions are shown with the solid lines. The analytical approximations are always presented with a dashed line, for the source term they are indistinguishable from the numerical result. The parameters used for this plot are $\Delta M^2 = 4.002 \times 10^{-8}\bar{M}^2$, $\omega = \frac{5\pi}{4} + 5.26\mathrm{i}$, $\alpha_1 = 0$, $\alpha_2 = 0$,$\delta = \pi/2$, and the discrete parameter $\xi = 1$. The small $CP$-violating parameters are $\mu = 1.001 \times 10^{-8}\bar{M}$ and $\sum_a |\epsilon_a|^2 = 3.65 \times 10^{-10} \sum_a |Y_a|^2$.

**BAU in the case of a highly flavour asymmetric washout** The largest mixing angles $U^2$ typically correspond to a large asymmetry in the washout strengths for different active neutrino flavours, *i.e.* $|F_\alpha|^2 \ll \sum_\beta |F_\beta|^2$ for some flavour $\alpha$. If the washout timescale of that flavour is longer than the timescale of the equilibration of weakly coupled heavy neutrino, and that the remaining two flavours have a strong washout, we can further simplify the equations (4.107).

The evolution of the flavour with the smallest washout $\Delta_\alpha$ can be approximated by the integral

$$\frac{\Delta_\alpha(z)}{s} = -\exp\left(-\frac{\langle\gamma_+\rangle a_\mathrm{R}}{2T_\mathrm{ref}}|F_\alpha|^2 z\right)\int_0^z \mathrm{d}z' g_w \frac{S_\alpha(z')}{sT_\mathrm{ref}} \exp\left(\frac{\langle\gamma_+\rangle a_\mathrm{R}}{2T_\mathrm{ref}}|F_\alpha|^2 z'\right)\,, \quad (4.110)$$

while the other two flavours rapidly reach their quasi-static equilibrium, with $\Delta_\beta = -\Delta_\alpha/2$.

If we completely neglect the washout of the flavour $\Delta_\alpha$ for $z \ll z_\mathrm{W}^\mathrm{eq}$, the exponential within the integral can be approximated by unity. The approximate lepton flavour asymmetry is then given by:

$$\frac{\Delta_a(z)}{s} = -\frac{405\zeta^{6/5}(3)}{60^{1/5}\,2\pi^5}\frac{\langle\gamma_+\rangle^{7/5}}{\langle\mathfrak{h}_+^\mathrm{th}\rangle^{4/5} g_\star^{6/5}}\left[\frac{m_\mathrm{Pl}^2}{\bar{M}\mu(\sum_\beta|F_\beta|^2)^2}\right]^{1/5}\times \quad (4.111a)$$

$$\times\,\mathrm{Im}[F_\alpha^*\epsilon_\alpha]\gamma\left(\frac{3}{5},\frac{z^5}{z_\mathrm{W}^{\mathrm{eq}5}}\right)\exp\left(-\frac{\langle\gamma_+\rangle a_\mathrm{R}}{2T_\mathrm{ref}}|F_\alpha|^2 z\right)$$

$$\approx -4.44\times10^{-6}\left[\frac{m_\mathrm{Pl}^2}{\bar{M}\mu(\sum_\beta|F_\beta|^2)^2}\right]^{1/5}\mathrm{Im}[F_\alpha^*\epsilon_\alpha]\gamma\left(\frac{3}{5},\frac{z^5}{z_\mathrm{W}^{\mathrm{eq}5}}\right)\exp\left(-\frac{\langle\gamma_+\rangle a_\mathrm{R}}{2T_\mathrm{ref}}|F_\alpha|^2 z\right)\,, \quad (4.111b)$$

where $\gamma(s,x)$ is the lower incomplete gamma function

$$\gamma(s,x) \equiv \int_0^x t^{s-1}\mathrm{e}^{-t}\mathrm{d}t\,. \quad (4.111c)$$

To obtain the total BAU, we insert the above expression into Eq. (4.108), and neglect the corrections of $\mathcal{O}(|F_\alpha|^2/(\sum_\beta|F_\beta|^2)$. The BAU is then given by

$$\frac{B(z)}{s} \approx \frac{1}{s}\frac{28}{79}\left(\frac{\Delta_\alpha(z)}{6} + 2\delta n_{o\,22}(z)\right) \quad (4.112a)$$

$$\approx -2.62\times10^{-7}\left[\frac{m_\mathrm{Pl}^2}{\bar{M}\mu(\sum_\beta|F_\beta|^2)^2}\right]^{1/5}\mathrm{Im}[F_\alpha^*\epsilon_\alpha]$$

$$\times\;\gamma\left(\frac{3}{5},\frac{z^5}{z_\mathrm{W}^{\mathrm{eq}5}}\right)\exp\left(-\frac{\langle\gamma_+\rangle a_\mathrm{R}}{2T_\mathrm{ref}}|F_\alpha|^2 z\right)\left[1+\theta(z-z_\mathrm{W}^\mathrm{eq})\right]\,, \quad (4.112b)$$

| | Scaling of the parameters | | | Scaling of the observables | |
|---|---|---|---|---|---|
| At the original scale | $\bar{M}$ | $\mu$ | $\mathrm{Im}\,\omega$ | $U_{ai}^2$ | $B(z=1)$ |
| Rescaled | $\zeta M$ | $\eta/\zeta\mu$ | $\mathrm{Im}\,\omega + \log(\eta/\zeta^3)/6$ | $\eta^{1/3}\zeta^{-2}U_{ai}^2$ | $B(\eta^{1/3})\zeta\eta^{-1/3}$ |

Table 4.4: The approximate relation between the mixing angles and number densities (right column) under a change of the Casas-Ibarra parameters (left column). The complex angle $\mathrm{Im}\,\omega$ can be chosen in such a way that the ratio of the equilibration and vacuum oscillation time scales remains constant. A particular solution to the evolution equations $B(z)$ can this way be related to a class of parameters through the appropriate scaling.

where we used $\Delta_\beta = -\Delta_\alpha/2$. The number density of the weakly coupled heavy state $\delta n_{o\,22}$ is completely neglected for times $z < z_{\mathrm{W}}^{\mathrm{eq}}$, and replaced by the quasi-static limit at times $z > z_{\mathrm{W}}^{\mathrm{eq}}$, which is reflected by the Heaviside theta function. Physically, before $z_{\mathrm{W}}^{\mathrm{eq}}$, the lepton asymmetry in $L$ can only be compensated by the strongly coupled state, in $\delta n_{o\,11}$, while after $z_{\mathrm{W}}^{\mathrm{eq}}$, the weakly coupled state can also carry a portion of the asymmetry. This increases the total $\tilde{L}$ asymmetry that is stored in the heavy neutrino sector, and therefore, the total $L$ asymmetry in the lepton doublets.

**Approximate scaling of the asymmetry**

In the case of large mixing angles, where we can neglect the smaller Yukawa couplings $|\varepsilon_\alpha|^2 \sim \epsilon|F_\alpha|^2 \approx 0$, there are only three independent physically relevant time scales in the problem, the vacuum oscillation rate, and the equilibration rate, and the temperature of the sphaleron freezeout, which we approximate to the temperature of the electroweak crossover $T_{\mathrm{EW}}$. If we keep the ratios of the vacuum Hamiltonian, and the equilibration rates fixed, we can relate different solutions to the evolution equations of the heavy neutrino, and doublet lepton densities. The size of the equilibration rate, as well as the vacuum Hamiltonian are connected to the mass splitting $\mu$ and to the complex angle $\mathrm{Im}\,\omega$. The scaling of the variables is presented table 4.4 from [118]. Note that this scaling cannot be use in the presence of $\tilde{L}NV$ processes, they introduce a new timescale to the problem.

### 4.4.3 The Role of Lepton Number Violating Processes

So far we have completely neglected the effects from to the $\tilde{L}NV$ processes. The $\tilde{L}$ charge is defined by the helicity of the heavy neutrinos, and will therefore be violated by their Majorana mass $M$. As the heavy neutrinos below the $W$-boson mass are predominantly produced as relativistic, the effect from $\tilde{L}NV$ will be sup-

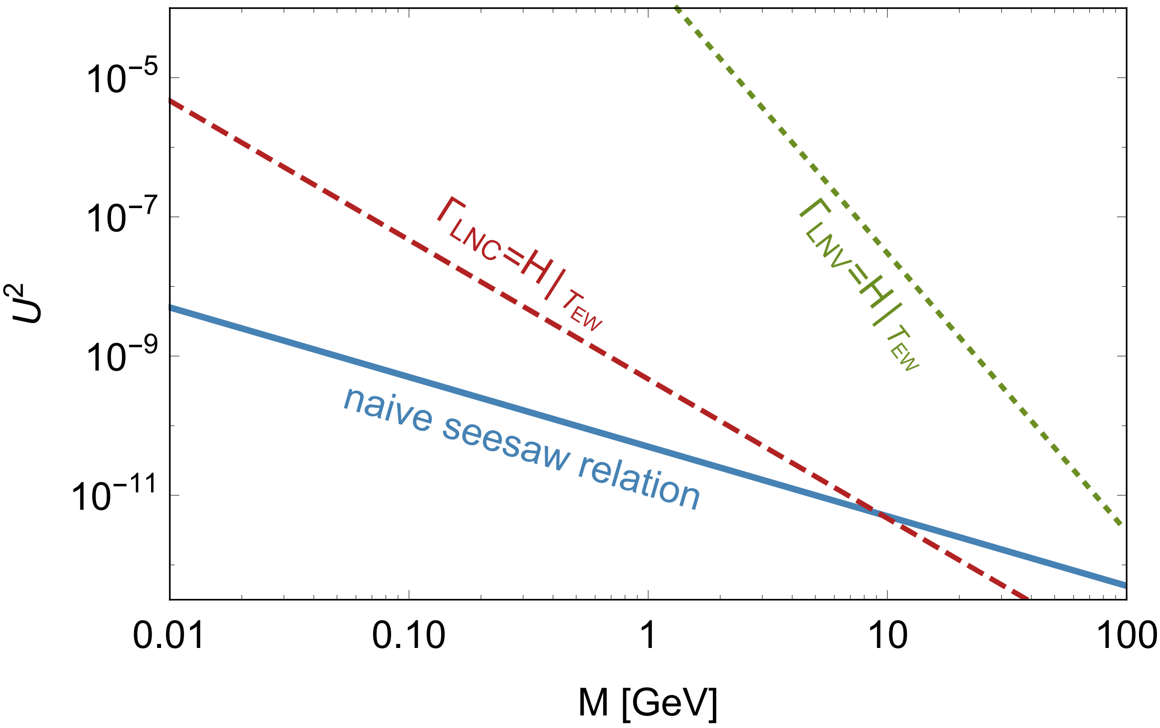


Figure 4.12: The different equilibration scales in leptogenesis through neutrino oscillations. The naive seesaw relation is presented in (blue, solid), and roughly corresponds to the minimal size of the mixing $U^2$ consistent with the measured neutrino masses. The coupling that is required to bring the heavy neutrinos into equilibrium through the $\tilde{L}NC$ interactions by the electroweak temperature $T_{\text{EW}}$ is represented in (red, dashed). On the other hand, the LNV interactions are suppressed by another factor $M^2/T^2$, and only reach equilibrium for couplings above the (green, dotted) line.

pressed by $M^2/T^2$. These effects have been neglected in most previous studies of the leptogenesis through neutrino oscillations parameter space.

In the following we discuss several important effects arising due to the $\tilde{L}$ number violating processes.

- direct production of the lepton asymmetry, $\sum_\alpha S_\alpha \neq 0$
- equilibration of the weakly coupled state $\nu_{R_w}$
- washout of the lepton asymmetry $\tilde{L}$
- generation of the asymmetry in the degenerate limit $\mu \to 0$

**Direct Production of the Lepton Asymmetry** In the usual ARS leptogenesis scenario [71, 88], the lepton flavour asymmetry is generated through the $CP$-violating oscillations among the heavy neutrinos. The total lepton asymmetry initially vanishes, and is only produced through the washout of the flavoured asymmetries $\Delta_\alpha$. For parameters close to the seesaw scale, we can estimate the produced lepton asymmetry to be suppressed by Yukawa couplings of $\mathcal{O}(Y^6)$, *cf.* ref. [155] for a pedagogical discussion. This can intuitively be understood if we combine Eq. (4.77) with (4.78) to first order in the Yukawa couplings. As the total $\tilde{L}$ number is conserved, a lepton asymmetry can only be produced once the asymmetry is redistributed from $L_\alpha$ to the heavy neutrinos through washout (or backreaction).

In contrast to this scenario, in the presence of $\tilde{L}$-number violating processes, the BAU can be produced already at $\mathcal{O}(Y^4 M^2/T^2)$. The corrections from $\tilde{L}$-number violating processes, are dominated by the Higgs decays in the symmetric phase [97], or by the mixing between heavy and light states in the broken phase [98, 152], and give rise to the additional suppression factor $\mathcal{O}(M^2/T^2)$.[2] To see which one of these effects dominates, we have to compare the two suppression factors, $|Y_{i\alpha}|^2$ and $M^2/T^2$, where $T$ corresponds to the temperature at which the asymmetry is being produced. For $|Y_{i\alpha}| \sim Y_0$, this implies that the temperature $T$ at which the asymmetry is produced has to be $T \lesssim \mathcal{O}(v\sqrt{\bar{M}/m_\alpha}$. Note that any asymmetry produced this way is protected form the $\tilde{L}$-conserving washout, and could therefore be the dominant contribution to the BAU even for $|Y_{i\alpha}| \gg Y_0$.

**Equilibration of the Weakly Coupled States** In the symmetry protected limit, where $\sum_\alpha |\epsilon_\alpha|^2 \ll \sum_\alpha |F_\alpha|^2$, the two interaction eigenstates have vastly different equilibration time scales. In Section 4.4.2 we have seen that the weakly coupled state only reaches equilibrium through the mixing with the strongly coupled one. However, in the presence of $\tilde{L}$-number violating processes, the weakly coupled states can also be produced directly. To illustrate this, let us consider the equilibration matrix for the heavy neutrinos in the interaction basis

$$\Gamma_{N+} = \sum_\alpha \frac{a_\mathrm{R}}{T_\mathrm{ref}} \begin{pmatrix} \langle\gamma_+\rangle|F_\alpha|^2 & 0 \\ 0 & \langle\gamma_-\rangle|F_\alpha|^2 \end{pmatrix} + \mathcal{O}(\epsilon)\,. \tag{4.113}$$

The weakly coupled state, which corresponds to $\delta n_{22}$ which is not produced in the absence of the $\tilde{L}NV$ processes, now also gets a contribution, however, suppressed by the factor $\langle\gamma_-\rangle \sim M^2/T^2$.

Without these processes, it would in principle be possible to postpone the equilibration of the weakly coupled state arbitrarily, by adjusting $\mu$ and therefore $z_\mathrm{w}^\mathrm{eq}$. However, as we see in the equation above, the $\tilde{L}NV$ processes cause equilibration

[2] For an earlier discussion see ref. [79].

on their own, with the time scale

$$z^{\text{eq}}_{LNV} = \sqrt[3]{\frac{3\,T^3_{\text{ref}}}{9.7\times 10^{-4} a_{\text{R}} \bar{M}^2 \sum_\alpha |F_\alpha|^2}} = 181.8 \left(\frac{\sum_\alpha |F_\alpha|^2}{Y_0^2}\right)^{-1/3} \left(\frac{\bar{M}}{1\,\text{GeV}}\right)^{-1/3}, \tag{4.114}$$

where we have used the values from table 4.2, and $Y_0$ is the size of the Yukawa couplings in the naive seesaw limit 2.15. In Fig. 4.12 we present the size of mixing angle $U^2$ necessary for the $\tilde{L}NV$ interactions to equilibrate before the electroweak temperature $T_{\text{EW}}$. As the weakly coupled state determines the deviation from equilibrium of the whole system in the overdamped regime, an enhanced equilibration rate can have dramatic consequences for the generation of the BAU. An example point where exactly this equilibration effect prevents successful leptogenesis is presented in the left panel of Fig. 4.13.

**Washout of the Lepton Asymmetry $\tilde{L}$** In Section 4.4.1, we have shown that the total asymmetry $\tilde{L}$ remains conserved if we can neglect terms $\sim \gamma_-$. The conservation of such a lepton number can be a double-edged sword, as it also limits the lepton asymmetry to be equal to the asymmetry in the heavy neutrino sector. If the washout of the heavy neutrinos is strong, the asymmetry in the heavy neutrino sector is suppressed as was discussed in 4.4.2. The $\tilde{L}NV$ processes can bypass this suppression, as they can delete lepton asymmetries directly, and convert lepton flavour asymmetries into a total lepton number asymmetry more efficiently. An example of a point where these processes are necessary to produce the BAU are presented in the right panel of Fig. 4.13.

**Generation of the Asymmetry in the Degenerate limit $\mu \to 0$.** It is commonly assumed that no baryon asymmetry can be produced if the two heavy neutrinos are exactly degenrate $\mu \to 0$. In this limit it appears that the equilibration matrix commutes exactly with the effective Hamiltonian of the heavy neutrinos. This would prevent any oscillations between the heavy neutrino states, and no lepton, or baryon asymmetries would be generated.

In the presence of $\tilde{L}NV$ processes it is possible that the effective Hamiltonian no longer commutes with the equilibration matrix, as they can have different dependences on flavour and helicity.

To study this scenario analytically, we constrain ourselves to the weak washout regime, where we can use the Yukawa couplings as a small expansion parameter. We proceed to iteratively solve equations Eq. 4.41, which gives us the approximate

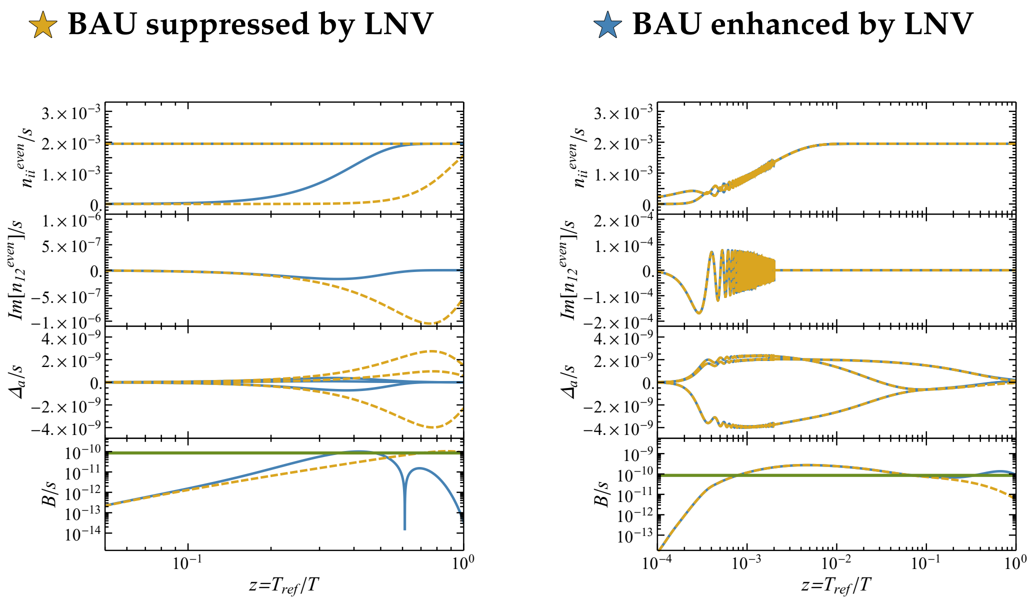


Figure 4.13: Comparison between the evolution of the heavy neutrino number densities with (blue, solid), and without (yellow, dashed) the $\tilde{L}NV$ processes. In the left panel we show the evolution of the neutrino number densities and lepton asymmetries for a point where the $\tilde{L}$-number violation supresses the final BAU. Without the $\tilde{L}NV$ processes, we can postpone the equilibration of the weakly coupled state by adjusting the mass splitting $\mu$ between the heavy neutrinos. When $\tilde{L}NV$ processes are included, the weakly coupled state can equilibrate on its own, before a significant mixing with the strong state. This can reduce the size of the source term, and completely prevent the generation of the BAU. In the right panel we show an example of a point where the $\tilde{L}NV$ processes enhance the BAU. At early times the $\tilde{L}NV$ processes can be neglected, which yields an identical evolution of the flavoured lepton asymmetries. Approximate $\tilde{L}$ conservation can suppress the total lepton asymmetry. If $\tilde{L}$-number is violated at late times, this suppression is no longer efficient, which allows for a larger final BAU. Figure taken from [46].

solutions

$$\delta n_h(z) = -n^{\rm eq} + n^{\rm eq}\frac{a_{\rm R}}{T_{\rm ref}}\int_0^z {\rm d}z' \left(\langle\gamma_+(z')\rangle {\rm Y}_{+h} + \langle\gamma_-(z')\rangle {\rm Y}_{-h}\right) \tag{4.115}$$
$$- n^{\rm eq}\left(\frac{a_{\rm R}}{T_{\rm ref}}\right)^2 \frac{\rm i}{2}\left[{\rm Y}_{+h}, {\rm Y}_{-h}\right]\int_0^z {\rm d}z' \int_0^{z'} {\rm d}z'' \left(\langle\mathfrak{h}_+(z')\rangle\langle\gamma_-(z'')\rangle - \langle\mathfrak{h}_-(z')\rangle\langle\gamma_+(z'')\rangle\right) .$$

We can insert the above solutions into the source term:

$$S_\alpha = \frac{a_{\rm R}}{g_w}\left[\sum_h h\langle\gamma_+\rangle {\rm Tr}\left({\rm Y}^\alpha_{+h}\delta n_h\right) - h\langle\gamma_-\rangle {\rm Tr}\left({\rm Y}^\alpha_{-h}\delta n_h\right)\right] \tag{4.116}$$
$$\sim {\rm iTr}\left({\rm Y}^\alpha_+\left[{\rm Y}_+, {\rm Y}_-\right]\right)\int_0^z {\rm d}z' \int_0^{z'} {\rm d}z'' \left(\langle\mathfrak{h}_+(z')\rangle\langle\gamma_-(z'')\rangle - \langle\mathfrak{h}_-(z')\rangle\langle\gamma_+(z'')\rangle\right) \neq 0\,,$$

to find a non-vanishing result.

It is interesting that the unflavoured source vanishes as $S = \sum_\alpha S_\alpha \sim {\rm i}\,{\rm Tr}({\rm Y}_+\left[{\rm Y}_+, {\rm Y}_-\right]) = 0$. In spite of the $\tilde{L}NV$ processes, one still has to rely on washout to generate a total lepton asymmetry.

In the usual ARS scenario, this source vanishes as only one helicity interacts with the medium, which gives us vanishing coefficients $\langle\gamma_-\rangle = \langle\mathfrak{h}_-\rangle = 0$. In the standard leptogenesis scenario we find the same result, as the helicity effects are neglected, and $\langle\gamma_-\rangle \approx \langle\gamma_+\rangle$, as well as $\langle\mathfrak{h}_-\rangle = \langle\mathfrak{h}_+\rangle$, which leads to a vanishing integral in Eq. (4.116).

# Chapter 5

# Testing the Low-scale Seesaw and Leptogenesis

In this chapter we discuss the possibility of testing the low-scale seesaw and leptogenesis mechanisms at existing and near-future experiments.

We first discuss the allowed parameter space for low-scale leptogenesis, and present two studies, with and without the $\widetilde{LNV}$ processes. For heavy neutrinos with masses around $\sim \mathcal{O}(1)$GeV, we neglect the $\widetilde{LNV}$ processes by setting $\mathfrak{h}_-, \gamma_- \to 0$. This allows us to use the analytic approximations from Section 4.4.2.

In the following study we include the $\widetilde{LNV}$ processes in the symmetric phase $\mathfrak{h}_-, \gamma_- \neq 0$, as well as the effect on $\mathfrak{h}_-$ during the crossover. This approach is appropriate for larger masses $\sim \mathcal{O}(10)$GeV. For an average heavy neutrino mass of $\bar{M} = 30$GeV, we also present a comparison between the allowed regions in parameter space, to emphasize the importance of including the $\widetilde{LNV}$ processes for larger masses.

The quantities that determine whether heavy neutrinos can be produced and detected at future experiments are the masses of the heavy neutrinos, $M_i$, and their mixing angles to the active leptons $U^2_{\alpha i}$. From an experimental perspective, it is therefore interesting to determine the allowed range of masses and mixing angles that are consistent with both the seesaw mechanism and leptogenesis.

We compare the range of heavy neutrino mixing angles and masses consistent with the BAU with the expected sensitivities of current and future experiments such as NA62, SHiP, FCC-ee, ILC and the CEPC. The potential of future experiments to test leptogenesis is commonly estimated by comparing the projections of the leptogenesis parameter space onto the $M_i - U^2_{\alpha i}$ plane, with the projection of the experimental sensitivity. As both the leptogenesis parameter space and the experimental sensitivities depend not only on the size of the particular mixing angle $U^2_{\alpha i}$, but also on the other mixing angles, this comparison is not fully consistent.

For the displaced-vertex searches at FCC-ee, ILC and CEPC we perform a more detailed analysis, where we confront the leptogenesis parameter space with the expected numbers of events at each of these experiments. We estimate the precision of measuring the flavoured mixing angles $U^2_\alpha$ at each of these experiments.

Finally, we also discuss the potential of measuring the mass differences between the heavy neutrinos, either directly, by measuring the masses individually, or indirectly, through heavy neutrino oscillations in the laboratory [156].

## 5.1 Parameter Space in Absence of the $\widetilde{LNV}$ Processes

To determine the limits on the mixing angles of the heavy neutrinos consistent with leptogenesis in the low-mass region, $\sim 1$GeV, we rely on the analytic approximations from Section 4.4.2.

For the analytic approximations to be applicable at this point, we have to neglect the $\widetilde{LNV}$ processes, which are suppressed by a factor $M^2/T^2 \lesssim (M/T_{\rm EW})^2 \sim$

$(M/1\mathrm{GeV})^2 \times 10^{-4}$. These effects can nonetheless be important, in particular during the electroweak crossover. In the present discussion we will neglect them, and include them when we study larger heavy neutrino masses, where they can have a much bigger effect (*c.f.* Fig. 4.12).

The sensitivity of the future experiments grows with the mixing angle $U^2$, as for a bigger mixing angle, more heavy neutrinos can be produced in a collision, and a bigger fraction of them will decay within the detector. Large mixing angles require large Yukawa couplings, which in turn implies that the washout and damping rates are strong (*c.f.* Fig 4.4).

For the large mixing angles we therefore rely on the approximations that correspond to the *overdamped* regime, where the equilibration of one of the heavy neutrino states happens before the oscillations between them have started.

Since the final equations in Subsection 4.4.2 are only semianalytic, for a general choice of Yukawa couplings, we still have to solve the integrals in Eq. (4.107) numerically. Instead of numerically solving the equations for each choice of parameters, we may instead use the approximate scaling relations from 4.4.2 to obtain a family of solutions to the evolution equations.

To find the upper limits on the flavoured mixing angles we rescale the mass splitting such that the BAU is maximal at the time of freezeout,

$$\frac{\mathrm{d}B(\eta^{1/3})}{\mathrm{d}\eta} = 0\,, \tag{5.1}$$

and then change the absolute mass scale to get agreement with the observed BAU,

$$\zeta = \frac{\eta^{1/3} B_{\mathrm{observed}}}{B(\eta^{1/3})}\,. \tag{5.2}$$

Having fixed the imaginary part of the complex angle $\mathrm{Im}\,\omega$, the average mass $\bar{M}$ and the mass splitting $\mu$, we may now scan over the remaining parameters, the Majorana phases $\alpha_{1,2}$, the Dirac $CP$ phase, $\mathrm{Re}\,\omega$ and the discrete parameter $\xi$. We choose each of those parameters randomly between 0 and $2\pi$ ($4\pi$ for the Majorana phases), and between 1 and $-1$ for $\xi$.

The points in parameter space corresponding to the minimal values of the mixing angles $U_\alpha^2$ correspond to small values of the Yukawa couplings, and hence to late equilibration of the heavy neutrinos. At the same time, the small size of the Yukawa couplings leads to a smaller lepton asymmetries, which are suppressed by $Y^4$. We can compensate for this suppression if we choose a sufficiently small mass splitting parameter μ. However, the oscillations between the heavy neutrinos have to occur before the sphaleron freezeout $z_{\mathrm{vac}} < T_{\mathrm{ref}}/T_{\mathrm{sph}} \approx 1$, which gives us a

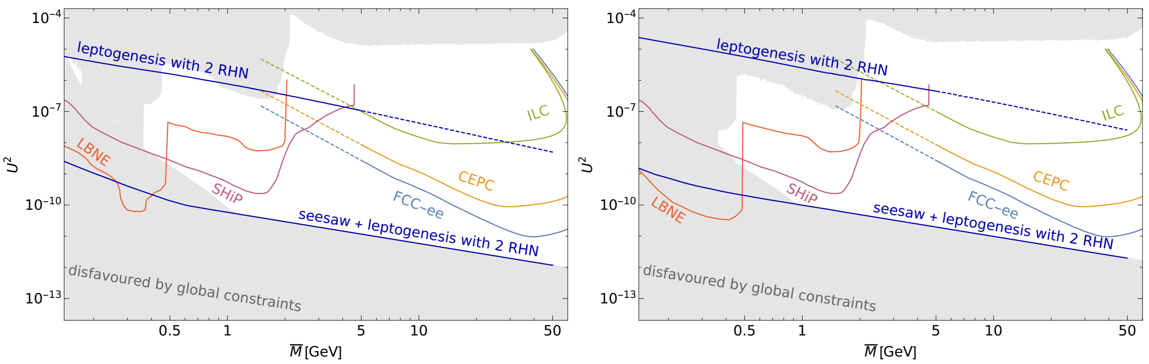


(a) Normal ordering. (b) Inverted ordering.

Figure 5.1: The range of masses $\bar{M} = (M_1 + M_2)/2$ and mixing angles $U^2$ consistent with the seesaw mechanism and leptogenesis for normal (top panel) and inverted (lower panel) ordering. The grey area indicates the region of parameter space disfavoured by the combined constraints. The region where the mixing angle $U^2$ is consistent with both neutrino oscillation data and leptogenesis is indicated by the dark blue lines. The upper bounds presented here are used beyond the masses for which it is safe to neglect the $\tilde{L}NV$ processes, which we indicate by the dashed dark blue line. For comparison we also present the estimated sensitivities of future experiments. The purple line corresponds to the SHiP experiment with 90% c.l. upper limits assuming 0.1 background events in $2 \times 10^{20}$ proton target collisions for a ratio of $U_e^2 : U_\mu^2 : U_\tau^2 \sim 52 : 1 : 1$ [157, 158]. The orange line corresponds to the LBNE/DUNE sensitivity with an assumed exposure of $5 \times 10^{21}$ protons on target for a detector length of 30 m [159]. The sensitivities of FCC-ee (light blue), the CEPC (yellow) and ILC (green) lines each correspond to the Z pole run for a centre of mass energy $m_{\rm cms} = m_Z$ [46]. Note that the sensitivity estimates of these experiments are no longer reliable below $\bar{M} < 5$GeV, which we indicate by the dashed lines. We will discuss these sensitivities in more detail in Section 5.2.1.

lower limit on the mass splitting

$$\bar{M}^2 \mu \gtrsim \frac{27\, T_{\rm sph}^3 \zeta(3)}{2\pi^2 a_{\rm R}} \approx 5.3 \times 10^{-12}\,\mathrm{GeV}^2\,. \tag{5.3}$$

Note that this limit can be bypassed if one includes the corrections from $\mathfrak{h}^{\rm EV} \neq 0$. As the oscillation, equilibration and sphaleron freezeout time scales can all coincide, these points in parameter space do not clearly correspond to either of the approximate regimes. We therefore rely on fully numerical solutions to the evolution equations, to find the lower bounds in figures 5.1-5.4.

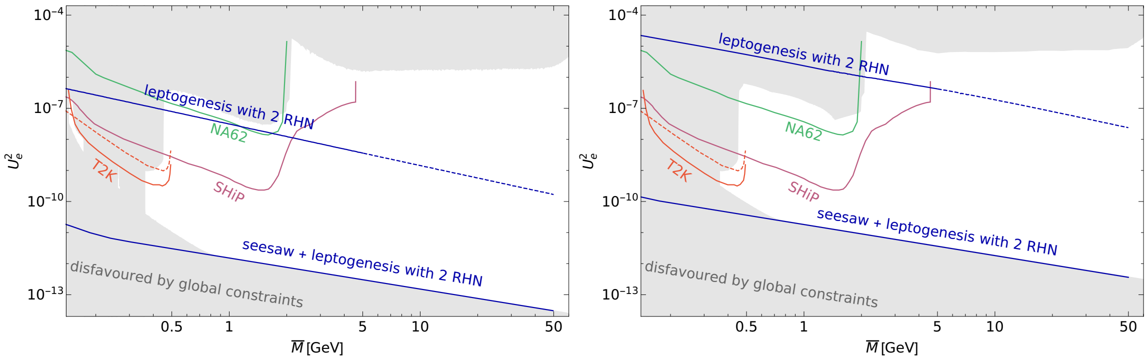


(a) Normal ordering. (b) Inverted ordering.

Figure 5.2: The range of masses $\bar{M} = (M_1 + M_2)/2$ and mixing angles $U_e^2$ consistent with the seesaw mechanism and leptogenesis for normal (top panel) and inverted (lower panel) ordering. The grey area indicates the region of parameter space disfavoured by the combined constraints. The region where the mixing angle $U_e^2$ is consistent with both neutrino oscillation data and leptogenesis is indicated by the dark blue lines. The upper bounds presented here are used beyond the masses for which it is safe to neglect the $\tilde{L}NV$ processes, which we indicate by the dashed dark blue line. For comparison we also present the estimated sensitivities of future experiments. The purple line corresponds to the SHiP experiment with 90% c.l. upper limits assuming 0.1 background events in $2 \times 10^{20}$ proton target collisions for a ratio of $U_e^2 : U_\mu^2 : U_\tau^2 \sim 52 : 1 : 1$ [157, 158]. The light blue line corresponds to the LBNE/DUNE sensitivity with an assumed exposure of $5 \times 10^{21}$ protons on target for a detector length of 30 m [159]. The T2K sensitivity has been estimated in ref. [160] for $10^{21}$ protons on target at 90% c.l. with full volume for both the $K^+ \to e^+ N \to e^+ e^- \pi^+$ two-body decays (red, solid) and the $K^+ \to e^+ N \to e^+ e^- e^+ \nu_e$ three-body decays (red, dashed) [160]. The expected sensitivity of NA62 to $U_e^2$ is given by the turquoise line with $2 \times 10^{18}$ 400 GeV protons on target [17]. The sensitivity estimates for FCC-ee, CEPC, and ILC will be discussed in more detail in Section 5.2.1.

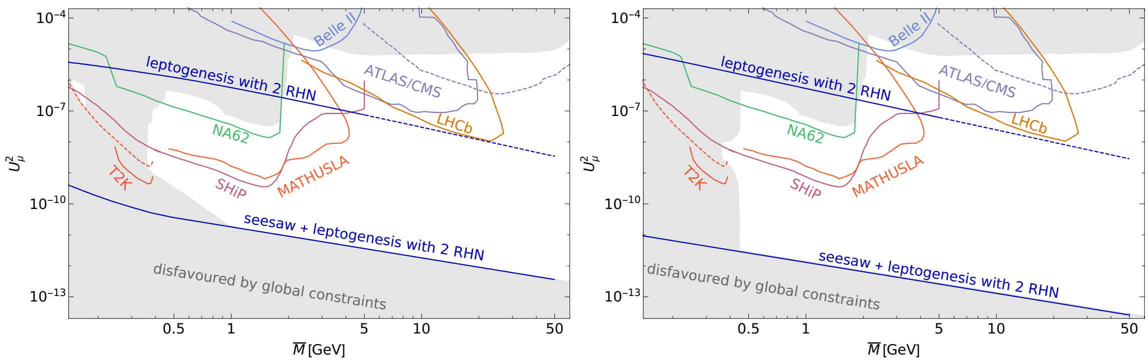


(a) Normal ordering.

(b) Inverted ordering.

Figure 5.3: The range of masses $\bar{M} = (M_1 + M_2)/2$ and mixing angles $U_\mu^2$ consistent with the seesaw mechanism and leptogenesis for normal (top panel) and inverted (lower panel) ordering. The grey area indicates the region of parameter space disfavoured by the combined constraints. The region where the mixing angle $U_\mu^2$ is consistent with both neutrino oscillation data and leptogenesis is indicated by the dark blue lines. The upper bounds presented here are used beyond the masses for which it is safe to neglect the $\tilde{L}NV$ processes, which we indicate by the dashed dark blue line. For comparison we also present the estimated sensitivities of future experiments. The purple line corresponds to the SHiP experiment with 90% c.l. upper limits assuming 0.1 background events in $2 \times 10^{20}$ proton target collisions for a ratio of $U_e^2 : U_\mu^2 : U_\tau^2 \sim 1 : 16 : 3.8$ [157, 158]. The expected sensitivity of NA62 to $U_\mu^2$ is given by the turquoise line with $2 \times 10^{18}$ 400 GeV protons on target. The T2K sensitivity (red) has been estimated in ref. [160] for $10^{21}$ protons on target at 90% c.l. with full volume for both the $K^+ \to \mu^+ N \to \mu^+ \mu^- \pi^+$ two-body decays (red, solid) and the $K^+ \to \mu^+ N \to \mu^+ \mu^- e^+ \nu_e$ three-body decays (red, dashed) [160]. The blue line indicates the limits on $U_\mu^2$ that can be obtained from LNV decays of $5 \times 10^{10}$ $B^+$ mesons at Belle II. The ATLAS/CMS limits on $U_\mu^2$ with $\sqrt{s} = 13$TeV and 300 fb$^{-1}$ are indicated by the violet lines, for displaced lepton jet (solid) and prompt trilepton (dashed) searches [30], while the yellow line corresponds to the LHCb sensitivity to $U_\mu^2$ [161]. The sensitivity of the proposed MATHUSLA experiment is represented by the orange line [37]. The sensitivity estimates for FCC-ee, CEPC, and ILC will be discussed in more detail in Section 5.2.1.

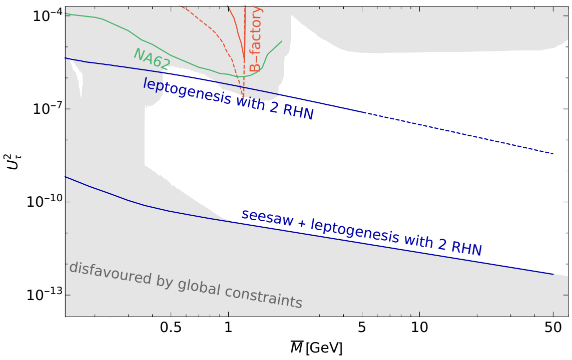


(a) Normal ordering.

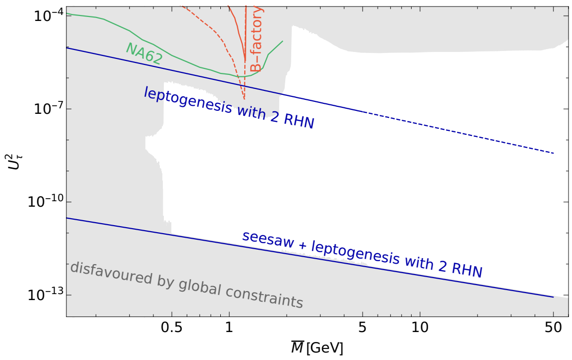


(b) Inverted ordering.

Figure 5.4: The range of masses $\bar{M} = (M_1 + M_2)/2$ and mixing angles $U_e^2$ consistent with the seesaw mechanism and leptogenesis for normal (top panel) and inverted (lower panel) ordering. The grey area indicates the region of parameter space disfavoured by the combined constraints. The region where the mixing angle $U^2$ is consistent with both neutrino oscillation data and leptogenesis is indicated by the dark blue lines. The upper bounds presented here are used beyond the masses for which it is safe to neglect the $\tilde{L}NV$ processes, which we indicate by the dashed dark blue line. For comparison we also present the estimated sensitivities of future experiments. The expected sensitivity of NA62 to $U_\tau^2$ is given by the turquoise line with $2 \times 10^{18}$ 400 GeV protons on target. The 95% c.l. limits on $U_\tau^2$ are shown for a kinematic analysis of $10^6$ $\tau^- \to \nu\pi^-\pi^+\pi^-$ decays at B-factories, indicated by (red, solid) for the conservative and most optimistic (red, dashed) estimates [162]. The mixing $U_\tau^2$ can also be probed by SHiP [157, 158] and LBNE/DUNE [157, 158], however, no experimental sensitivities have been published for benchmark scenarios that would allow a simple estimate of the sensitivity to $U_\tau^2$. The sensitivity estimates for FCC-ee, CEPC, and ILC will be discussed in more detail in Section 5.2.1.

## 5.2 Parameter Space With the $\tilde{L}NV$ Processes

In this section we discuss the parameter space for leptogenesis when the $\tilde{L}NV$ processes from 4.4.3 are included. We constrain our analysis to heavy neutrino masses between 5 and 50GeV. For masses above 5GeV we assume that the dominant contribution to the $\tilde{L}NV$ rate is from the processes that are also present in the symmetric phase of the electroweak theory, and we neglect the "indirect" contribution to the $\tilde{L}NV$ rate [98, 152] that arises from the mixing between the doublet and singlet neutrinos in the broken phase.

The analytic approximations from 4.4.2 cannot be used without modifications in this regime. Therefore we resort to solve the evolution equations for the heavy neutrinos numerically.

To find the points in parameter space consistent with the observed BAU, we use the Metropolis-Hastings algorithm B, with the log-likelihood function

$$\log \mathscr{L} = -\frac{1}{2}\frac{(Y_B - Y_B^{\mathrm{obs}})^2}{\sigma_{\mathrm{obs}}^2}, \tag{5.4}$$

where $Y_B$ is the BAU obtained by numerically solving equations (4.53) and (4.42), and the observed value $Y_B^{\mathrm{obs}}$ of the BAU, and its variance $\sigma_{\mathrm{obs}}$ are given in Eq. (1.1). Note that we do use the Metropolis-Hastings algorithm here only as a parameter scan algorithm, without assigning a probabilistic interpretation to the densities of produced points. The reason for this approach is that the Casas-Ibarra parametrization used here is a bottom-up parametrization, and there is no objective way to assign a prior for the parameters that enter it. Further following this logic, instead of using one Markov-chain to scan over the whole parameter space, we fix the average mass $\bar{M}$ and the imaginary part of the angle $\mathrm{Im}\,\omega \sim \log U^2$, and apply the Metropolis-Hastings algorithm to the remaining parameters. We summarize the proposal distributions in table 5.1. After the points are generated, we only keep points with $Y_B$ within $5\sigma_{\mathrm{obs}}$ of the observed value. Finally, to explore the "extreme" leptogenesis scenarios, we perform a targeted scan where we choose $\alpha$ and $\delta$ in a way that extremizes the ratios $U_\alpha^2/U^2$. These points can give us the largest mixing angles $U^2$, as they have a highly flavour asymmetric washout, which can preserve the BAU even in the presence of a strong washout.

### 5.2.1 Measurement of Leptogenesis Parameters at Future Lepton Colliders

In this section we discuss the potential of the future lepton colliders to measure the heavy neutrino parameters. One of the most important properties of the heavy neutrinos are the flavour mixing ratios $U_\alpha^2/U^2$. By measuring these ratios we can

| variable | proposal distribution |
|---|---|
| $\bar{M}$ | constant |
| $\mathrm{Im}\,\omega$ | constant |
| $\mu$ | log-normal |
| $\mathrm{Re}\,\omega$ | normal |
| $\alpha$ | normal |
| $\delta$ | normal |

Table 5.1: Proposal distributions used in the Metropolis-Hastings algorithm. Note that the average mass $\bar{M}$ and $\mathrm{Im}\,\omega$ remain fixed after the initial choice. For the remaining parameters we generate proposal points using a normal distribution, with the exception of the mass splitting $\mu$, which we vary on a logarithmic scale in order to capture the resonant enhancement for small values of $\mu$. We fix the remaining parameters entering $U_{\mathrm{PMNS}}$ to their best fit values.

determine whether the heavy neutrinos are consistent with the low-scale seesaw mechanism and leptogenesis.

Heavy neutrinos with masses between a few GeV and the $W$ boson mass can have long lifetimes, ranging from picoseconds to nanoseconds [163]. The distance between the point where the heavy neutrinos are produced, and where they decay in the detector can therefore be macroscopic, which appears as a displaced vertex *c.f.* Fig. 5.5. This type of exotic signature is especially promising for heavy-neutrino masses below the $W$-boson mass, in particular at future lepton colliders with high integrated luminosities, see *e.g.* ref. [39, 43].

The large mixing angles that can be accessed by collider experiments corresponds to the symmetry protected scenario from Section 2.2, in particular when combined with the small mass splittings required for leptogenesis [40, 105, 118].

For the phenomenology of the heavy neutrinos we may neglect the small $LNV$ parameters, and set $\mu = \epsilon = 0$, as they have negligible impact on the production and decay of the heavy neutrinos.[1] Therefore it is sufficient to discuss the displaced vertex searches in the symmetric limit and use the results from ref. [43].

We will discuss the following future lepton colliders with these specific physics programs:

- FCC-ee: The Future Circular Collider in the electron positron mode with its envisaged high integrated luminosity of $\mathcal{L} = 10\,\mathrm{ab}^{-1}$ for the $Z$ pole run[2].

[1] Note that this is not entirely correct, as a finite mass splitting $\mu$ can give rise to oscillations between heavy neutrino "particle" and antiparticle states as discussed in [156, 165]. This effect does not impact our analysis since we do not distinguish between neutrinos and antineutrinos.

[2] It also features a physics run at 240 GeV centre-of-mass energy with an integrated luminosity of $\mathcal{L} = 5\,\mathrm{ab}^{-1}$ same as the CEPC however the $Z$ pole run is more competitive at the FCC-ee.

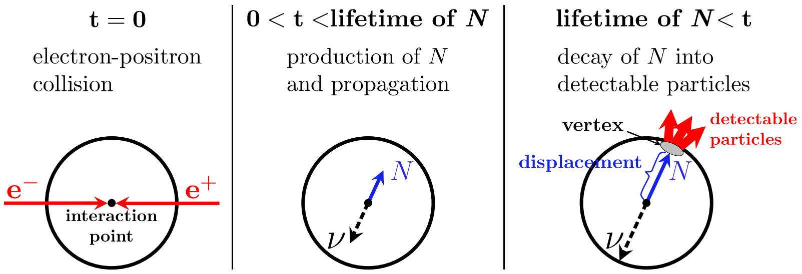


Figure 5.5: Long lived heavy neutrinos can give rise to a displaced vertex, which is a macroscopic displacement between the interaction point and the vertex. This signature becomes even more pronounced for tiny mixing angles, which yield a longer heavy neutrino lifetime. For a discussion of such signatures in other theoretical frameworks see *e.g.* [164]. Figure taken from [46].

- CEPC: The Circular Electron Positron Collider running at the $Z$ pole and 240 GeV centre-of-mass energy with an integrated luminosity $\mathcal{L} = 0.1\,\mathrm{ab}^{-1}$ and $5\,\mathrm{ab}^{-1}$, respectively.

- ILC: The International Linear Collider running at the $Z$ pole and 500 GeV centre-of-mass energy with an integrated luminosity of $\mathcal{L} = 0.1\,\mathrm{ab}^{-1}$ and $\mathcal{L} = 5\,\mathrm{ab}^{-1}$, respectively.

At lepton colliders, heavy neutrinos are primarily produced through the process $e^+e^- \to \nu N$. For centre-of-mass energies of 90 GeV, this production process is dominated by the $s$-channel exchange of a $Z$ boson, whereas for 240 and 500 GeV, the dominant process is a $t$-channel exchange of a $W$-boson. At the $Z$-pole the production cross section depends on the total mixing angle $\sigma_{\nu N}(U^2)$, while for higher centre-of-mass energies it dominantly depends on the mixing to the electron $\sigma_{\nu N}(U_e^2)$.

We can classify the decays of the heavy neutrinos into four different channels: semileptonic ($N \to \ell jj$), leptonic ($N \to \ell\ell\nu$), hadronic ($N \to jj\nu$), and invisible ($N \to \nu\nu\nu$). The branching ratios are presented in Fig. 5.6, with the caveat that the parton picture used here is no longer valid for heavy neutrino masses below 5 GeV. For a discussion of heavy neutrino decays into scalar and vector mesons see *e.g.* refs. [166, 167].

The relative mixing angle to a lepton flavour $U_\alpha^2/U^2$ can be probed through the semileptonic decays of the heavy neutrino. The branching ratio of the semileptonic decays with a charged lepton $\ell_\alpha$ in the final state is approximately given by $\mathrm{Br}(N \to \ell_a jj) \simeq 0.5 \times U_a^2/U^2$.

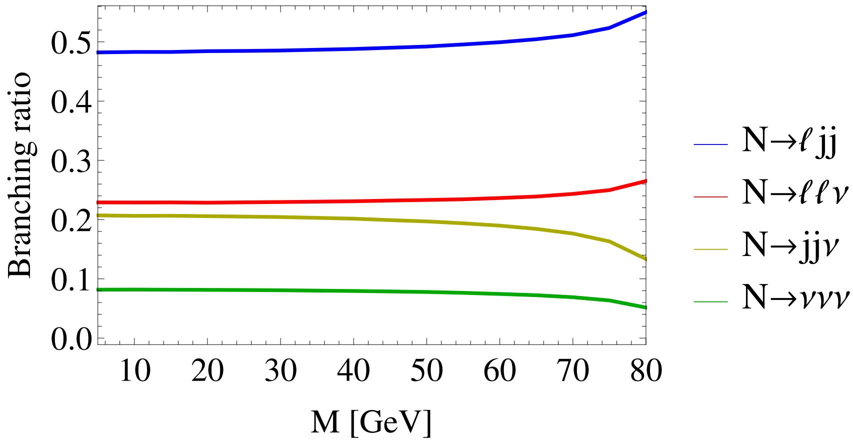


Figure 5.6: Branching ratios of heavy neutrino decays. We denote the different possible final states by colour, the semileptonic lepton-dijet ("$\ell jj$", blue line), the dilepton ("$\ell\ell\nu$", red line), the dijet ("$jj\nu$", yellow line), and the invisible decays ("$\nu\nu\nu$", green line). The semileptonic and leptonic branching ratios are summed over all lepton flavours. Figure taken from [46].

We can approximate the expected number of displaced decay events with a charged lepton of flavour $\alpha$ in the final state as

$$N_a = \sigma_{\nu N}(\sqrt{s}, \bar{M}, U_e, U_\mu, U_\tau) \times \mathrm{Br}(N \to \ell_a jj) \times \mathcal{L} \times P(x_1, x_2, \tau)\,. \tag{5.5}$$

where $P(x_1, x_2, \tau)$ is the fraction of the displaced decays of the heavy neutrino with proper lifetime $\tau$ that happen between the detector-defined boundaries $x_1$ and $x_2$, and $\mathcal{L}$ is the integrated luminosity of the experiment. The lifetime of the heavy neutrino is given by the inverse of the total decay width and is proportional to $U^2\bar{M}^5$ if we neglect the masses of the particles in the final state.

Since $P$ is the probability of a particle decay between $x_1$ and $x_2$, it follows an exponential distribution, which gives us

$$P(x_1, x_2, \tau) = \exp\left(-\frac{x_1}{\beta\gamma c\tau}\right) - \exp\left(-\frac{x_2}{\beta\gamma c\tau}\right) \tag{5.6}$$

with the relativistic $\beta = v/c$ and Lorentz factor $\gamma$. Given the boundaries of an SiD-like detector [168] with the inner region ($x_1 = 10\,\mu$m) and the outer radius of the tracker ($x_2 = 1.22\,$m), we assume that the displaced vertex signature is free from SM background (see ref. [43]).

The cross section for the different discussed performance parameters of the above mentioned colliders is calculated numerically using `WHIZARD` [169, 170] by including initial state radiation and only for the ILC by including also a (L,R) initial state polarisation of (80%,20%) and beamstrahlung effects.

We demand at least four displaced vertex events over the zero background hypothesis to establish a signal above the $2\sigma$ level. In the case of a $Z$ pole run, the total number of events is uniquely determined by $U^2$, which allows us to determine the total mixing angle $U^2$ from the total number of events. The situation is somewhat different for centre-of-mass energies above 90 GeV, as the number of events also depends on the relative electron mixing $U_e^2/U^2$. This dependence on the flavour mixing pattern means that for a fixed mixing angle $U^2$ we cannot uniquely determine the expected number of events. In the plots we therefore distinguish between the "guaranteed discovery" region, where we can expect more than four events for all points consistent with the seesaw and leptogenesis, and the "potential discovery" region, where more than four events are realized only for certain points in the parameter space.

The heavy neutrino mass $M_i$ could be measured from the invariant mass of the semileptonic final states $M_{\ell jj}$. We can assume that the precision is of the same order as the jet-mass reconstruction, which is $\sim 4\,\%$ for jet energies of $45\,\mathrm{GeV}$ with the `Pandora Particle Flow Algorithm` [171]. With a sizeable number of events, the mass can be measured even more precisely from the $\nu\mu^-\mu^+$ final states. For a displaced vertex, the momentum of the neutrino can be inferred from the requirement of pointing back to the primary vertex, which yields the invariant mass $M_{\nu\mu\mu}$.

To determine the flavour mixing ratios $U_\alpha^2/U^2$, we consider the ratios of the number of semileptonic events $N_{\mathrm{sl}} = \sum_\alpha N_\alpha$ and the number of semileptonic events with $N_\alpha$ with a charged lepton $\ell_\alpha$ in the final state.

The observable random variables are the number of semileptonic events $\hat{N}_{\mathrm{sl}}$ which is Poisson distributed with mean $N_{\mathrm{sl}}$, and the $\hat{N}_\alpha$ which follows a multinomial distribution with probability $p_a = U_a^2/U^2$. The expected number of semileptonic decays with $\ell_\alpha$ in the final state is given by $N_\alpha = N_{\mathrm{sl}} U_\alpha^2/U^2$. The error of measuring $U_\alpha^2/U^2$, expressed as $\frac{\delta(U_a^2/U^2)}{U_a^2/U^2}$ with $\delta$ being the standard deviation for $U_\alpha^2/U^2$, comes from the statistical uncertainty of the ratio $N_\alpha/N_{\mathrm{sl}}$. Since $N_\alpha$ is not independent of $N_{\mathrm{sl}}$ the precision of the flavour mixing ratio $U_\alpha^2/U^2$ is given by

$$\frac{\delta(U_\alpha^2/U^2)}{U_a^2/U^2} \approx \sqrt{\frac{1}{N_\alpha} - \frac{1}{N_{\mathrm{sl}}}}, \tag{5.7}$$

in contrast to the usual propagation of error where the uncertainties add. A more detailed discussion of this point is given in appendix F. In Section 5.2.2 we discuss the statistical precision of the flavour-dependent mixing $U_\alpha^2/U^2$ at the different lepton colliders for points consistent with leptogenesis.

### 5.2.2 Results of the Parameter Scan

**Sensitivity in the $\bar{M} - U^2$ plane**

In Fig. 5.7 we present the range of masses $\bar{M}$ and mixing angles $U^2$ consistent with baryogenesis through leptogenesis together with the expected sensitivity of future lepton colliders. The left column corresponds to normal light neutrino mass ordering (NO), while the right column corresponds to the inverted ordering (IO). The upper grey region denotes the mixing angles excluded by the constraints on $U^2$ from DELPHI [172, 173]. The requirement to reproduce the light neutrino masses through the seesaw mechanism with two right-handed neutrinos imposes a lower bound on the mixing angle $U^2$ indicated by the lower grey region. The blue line corresponds to the largest mixing angles consistent with leptogenesis. We perform the parameter scan up to masses of $\bar{M} = 50$GeV, as the estimate of the $\tilde{L}NV$ damping rate becomes unreliable for larger masses. The experimental sensitivity lines correspond to four expected events. We differentiate between the "guaranteed discovery" (dashed) and "potential discovery" (solid) lines. Above the "guaranteed discovery" lines, all generated points produce at least four expected events, while above the "potential discovery" line only a subset with a favourable flavour pattern can produce more than four events.

In the top row we present the expected sensitivity at the FCC-ee with $\sqrt{s} = 90$GeV (green), in the middle row we have ILC with $\sqrt{s} = 90$GeV (red) and $\sqrt{s} = 500$GeV (yellow), while in the lowest row we present the expected sensitivity at CEPC with $\sqrt{s} = 90$GeV (purple) and $\sqrt{s} = 240$GeV (orange).

Of the experiments considered, FCC-ee has the best prospects of finding heavy neutrinos, and covers a large region of the leptogenesis parameter space.

At ILC and CEPC we see a significant difference in sensitivity for the NO and IO cases, in particular for $\sqrt{s} > 90$GeV. The reason is twofold, for IO successful leptogenesis is possible with larger mixing angles $U^2$, but more importantly, the mixing to the electron, $U_e^2$, is suppressed compared to the other mixing angles in the case of NO. The dominant heavy neutrino production channel for $\sqrt{s} > 90$GeV is through coupling to the electron, which leads to fewer expected events for NO. As a result, for NO, there are no expected events at ILC with $\sqrt{s} = 500\,$GeV or CEPC with $\sqrt{s} = 240\,$GeV. Furthermore, for IO we present two lines, corresponding to the "potential discovery" and "guaranteed discovery" regions, indicated by the solid and dashed lines respectively.

Note that although CEPC and FCC-ee are quite similar, the main reason for the smaller reach of CEPC at $\sqrt{s} = 90\,$GeV is the much shorter planned run time. In Fig. 5.8 we present the potential improvement for a longer run time at $\sqrt{s} = 90\,$GeV.

In figures 5.9 and 5.10, we show the number of displaced vertex events that can be achieved at FCC-ee. Large numbers of events can allow for a precise measurement of the flavour mixing ratios $U_\alpha^2/U^2$, as we will discuss in Section 5.2.2.

**Constraints on the Heavy Neutrino Mixing Ratios**

The mixing ratios $U_\alpha^2/U^2$ to the different lepton flavours are already constrained by the seesaw mechanism as can be seen in figures 2.4, 2.5. For large mixing angles $U^2$ leptogenesis imposes even stronger constraints on these mixing ratios. Large mixing angles $U^2$ are associated with large Yukawa couplings, and therefore strong washout of both $L$ and $\tilde{L}$ asymmetries. The large washout of the lepton asymmetry can be avoided if the flavoured washout strengths are suppressed, *i.e.* if $(Y^\dagger Y)_{\alpha\alpha} \ll \mathrm{Tr}(Y^\dagger Y)$, which implies that $U_\alpha^2 \ll U^2$. Therefore, for the largest mixing angles $U^2$ consistent with leptogenesis we can expect a large asymmetry in the mixing ratios $U_e^2 : U_\mu^2 : U_\tau^2$. In Fig. 5.11 we present the largest mixing angles consistent with leptogenesis for a fixed choice of mixing ratios $U_e^2 : U_\mu^2 : U_\tau^2$ with a fixed benchmark mass $\bar{M} = 30\mathrm{GeV}$. The dark black line corresponds to the boundary of the region consistent with the light neutrino oscillation data. The dark blue regions correspond to large mixing angles $U^2$, while the smaller mixing angles are shown in yellow. We can see that the range of allowed mixing ratios becomes smaller for larger values of the mixing angle $U^2$, and that the largest mixing angles correspond to the edges of the triangles, where a flavour asymmetric washout is realized. For normal neutrino mass ordering this is realized when the mixing to the electron is minimal $U_e^2/U^2 \approx 0.006$, which corresponds to $\alpha_2 = -2\delta + \pi$. For inverted ordering we find the largest mixing angles when $U_\mu^2$ and $U_\tau^2$ are small compared to $U_e^2$, with $U_e^2/U^2 \approx 0.94$ and $U_\mu^2/U^2 + U_\tau^2 \leq 0.06$.

The importance of flavour asymmetric washout can also be seen in the $U_\alpha^2/U^2 - U^2$ plane in figures 5.12, where we find that the large mixing angles $U^2$ are found in “spikes” where one of the flavour ratios is extremal.

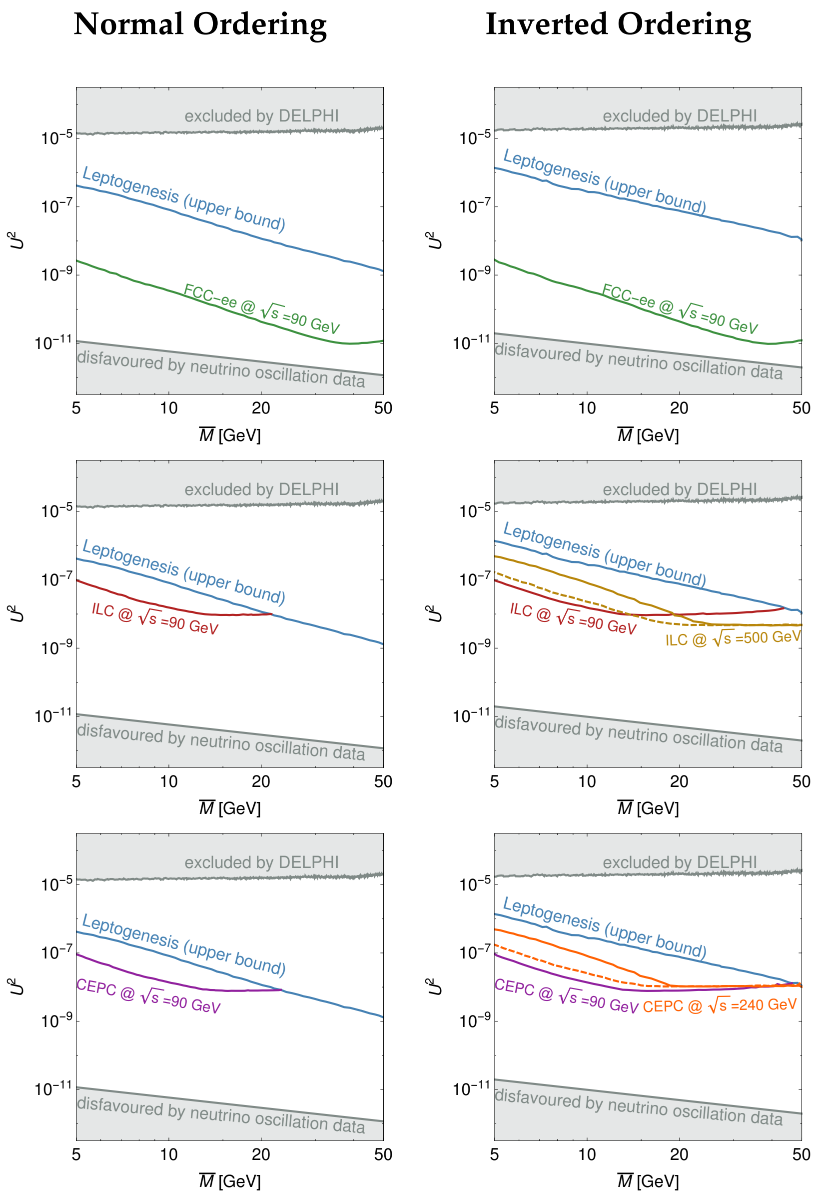


Figure 5.7: The largest possible $U^2$ for which the BAU can be generated for given $\bar{M}$ (blue, solid). The regions of the viable leptogenesis parameter space where future lepton colliders can observe at least four expected displaced vertex events are indicated by the remaining coloured lines. The upper gray region is excluded by DELPHI, while the lower gray region is disfavoured by the requirement of reproducing the light neutrino masses through the seesaw mechanism. The “guaranteed discovery area” and “potential discovery area” are indicated by the solid and dashed lines respectively. A more detailed discussion is given in the main text, *c.f.* Subsection 5.2.2 Figure taken from [46].

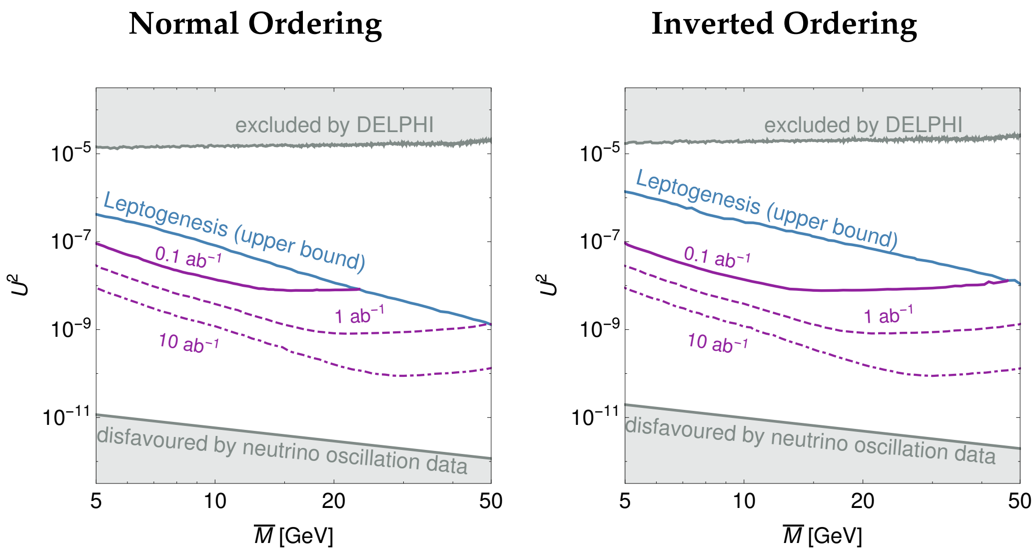


Figure 5.8: The largest possible $U^2$ for which the BAU can be generated for given $\bar{M}$ (blue, solid). The region in the leptogenesis parameter space where the CEPC experiment can observe at least four expected displaced vertex events is indicated by the purple lines. The currently planned run corresponds to the solid line, whereas the dashed line corresponds to the equal $Z$-pole running time as is currently planned by FCC-ee, and the dot-dashed line corresponds to what is possible with the crab waist technology. The upper gray region is excluded by DELPHI, while the lower gray region is disfavoured by the requirement of reproducing the light neutrino masses through the seesaw mechanism. A more detailed discussion is given in the main text, *c.f.* Subsection 5.2.2 Figure taken from [46].

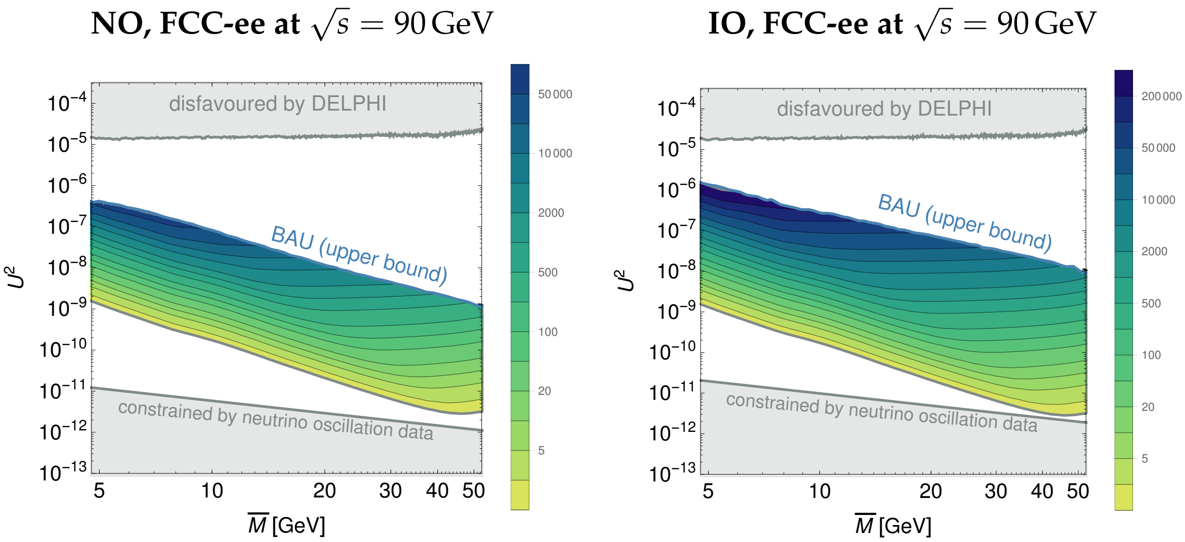


Figure 5.9: Number of expected displaced vertex events at the FCC-ee with $\sqrt{s} = 90\,\text{GeV}$ for parameter points consistent with leptogenesis. Left and right panel correspond to normal and inverted mass ordering, respectively. Figures taken from [46].

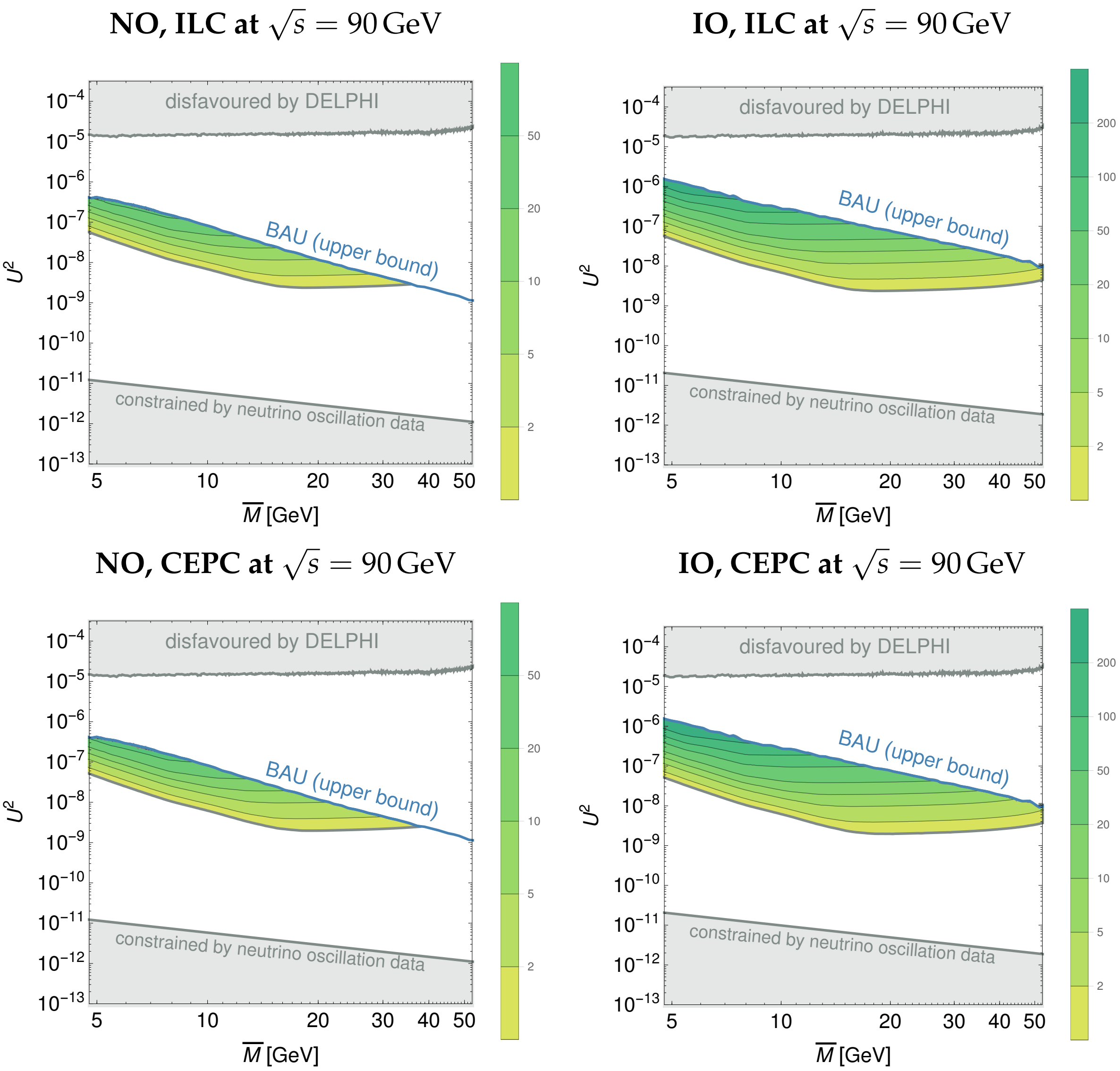


Figure 5.10: Number of expected displaced vertex events at the ILC with $\sqrt{s} = 90\,\mathrm{GeV}$ (top row) and at the CEPC with $\sqrt{s} = 90\,\mathrm{GeV}$ (bottom row) in case of both normal ordering (left column) and inverted ordering (right column) for parameter points consistent with leptogenesis. Figures taken from [46].

**Sensitivity to Measuring the Mixing Ratios at Future Experiments** The large numbers of events that can be achieved by the FCC-ee can lead to a precise determination of the mixing angles $U_\alpha^2$. When combined with the constraints from the seesaw and leptogenesis, this can be a powerful test to see whether heavy neutrinos are the origin of the light neutrino masses and the BAU. With an infinite experimental precision, we could easily determine whether the measured neutrino parameters lie within the allowed regions from Fig. 5.11. In reality, we can only expect a finite number of events, and therefore a finite precision at a future collider. In figures 5.12 we estimate the precision of measuring each of the mixing ratios from Eq. 5.7 in the $U_\alpha^2/U^2 - U^2$ plane. The solid coloured regions correspond to points in parameter space consistent with leptogenesis. The lines corresponding to the different levels of precision are indicated by the colour, from low precision (yellow), to high (dark blue).

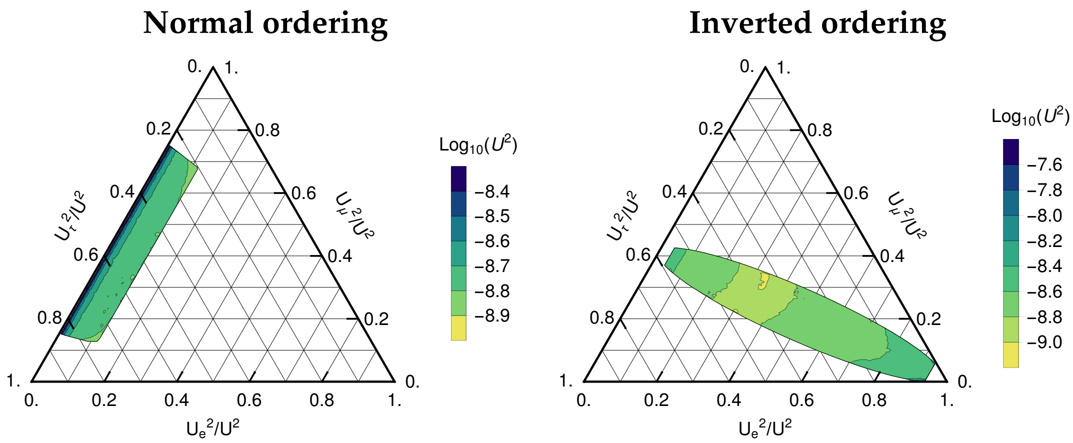


Figure 5.11: The black line indicates the region allowed by light neutrino oscillation data. The colour coding indicates the largest mixing angle $U^2$ consistent with the seesaw and leptogenesis constraints for a given choice of $U_e^2 : U_\mu^2 : U_\tau^2$, where the average heavy neutrino mass is $\bar{M} = 30\,\text{GeV}$. The panels correspond to normal (left) and inverted (right) neutrino mass orderings. The largest viable mixing angles correspond to highly flavour asymmetric flavour patterns, where $U_\alpha^2 \ll U^2$ for at least one of the flavours. Figure taken from [46].

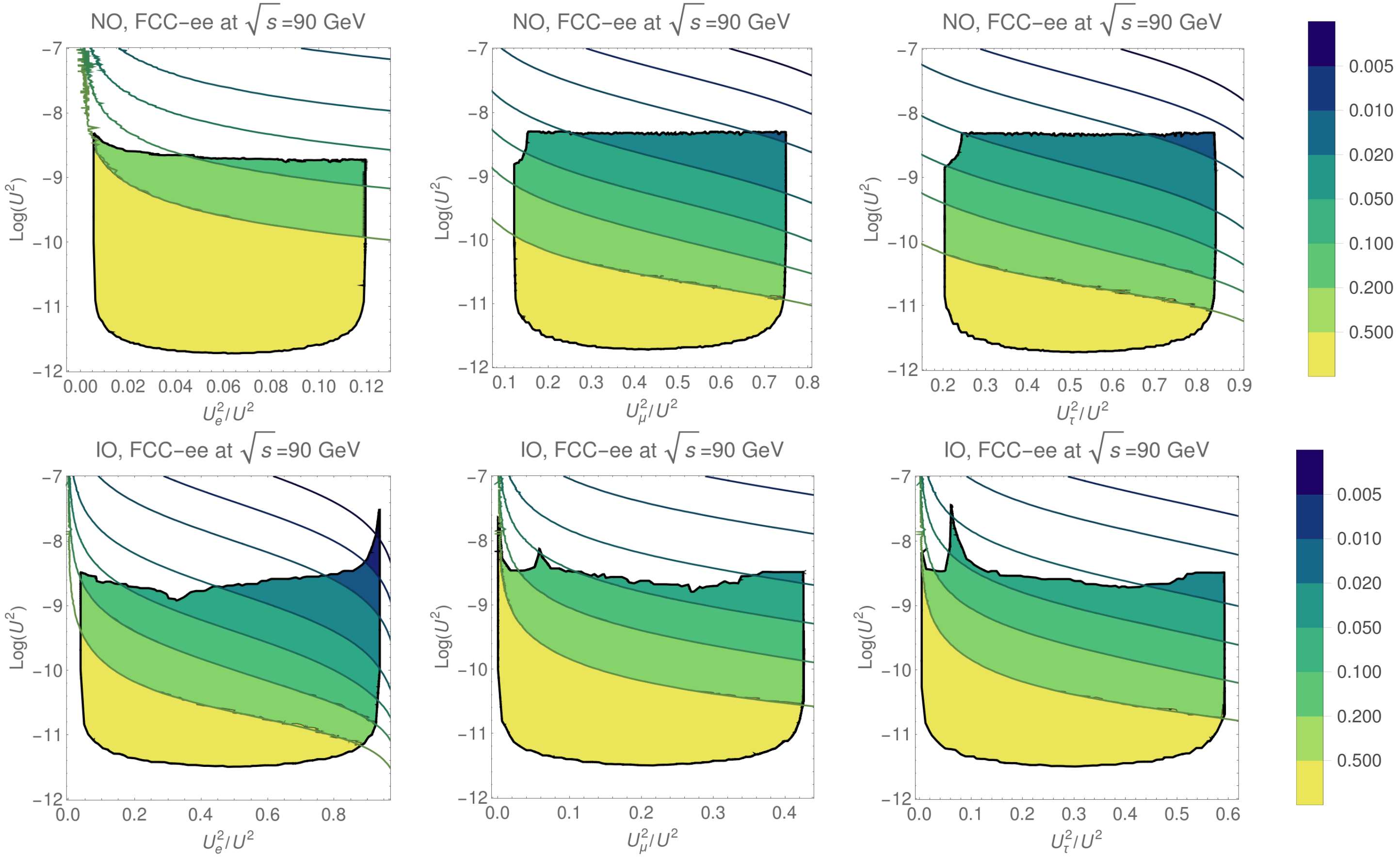


Figure 5.12: The expected precision of measuring the ratio $U_\alpha^2/U^2$ at FCC-ee with $\sqrt{s} = 90\,\text{GeV}$ for normal (left panel) and inverted (right panel) neutrino mass ordering. The precision is indicated by colour, from low precision $< 50\%$ in yellow, and high precision $> 0.5\%$ in dark blue. Solid colour indicates the region consistent with both the seesaw mechanism and leptogenesis. The two heavy neutrinos are assumed to be almost degenerate in mass at $M = 30\,\text{GeV}$. Details are given in the main text, cf. section 5.2.2. Figure from [46].

**Constraints on the Heavy Neutrino Mass Splitting $\Delta M = |M_2 - M_1|$**

The difference between the two heavy neutrino masses is another parameter crucial for low-scale leptogenesis, which can determine both the size of the lepton asymmetry through resonant enhancement, and the time when the majority of the asymmetry is produced.

In Fig. 5.13 we show the regions of the mass splitting $\Delta M$ consistent with the BAU and the light neutrino oscillation data. for an average mass of $\bar{M} = 30$ GeV.

The most direct way of measuring the mass difference is by directly measuring the masses of the two heavy neutrino mass eigenstates and their physical mass difference $\Delta M_{\text{phys}}$ as given in equation (2.12), which is different from $\Delta M$ after the EWSB.

Realistically, we can expect the precision of mass measurements to be of $\sim 4\%$ (*c.f.* Section 5.2.1), which puts the mass splitting resolution in the GeV range, where it is safe to approximate $\Delta M_{\text{phys}} \approx \Delta M$.

For very small mass differences $\mathcal{O}(10^{-}11)$ GeV, the mass splitting could be measured through a non-trivial ratio between LNV and LNC processes. Unambiguous LNV signatures could be seen at a future proton-proton or electron-proton collider, or even at the LHC [33, 156, 165, 174–176].

To find a non-trivial LNV to LNC process ratio, the mass splitting has to be comparable to the decay width of the heavy neutrino, $\Gamma \sim \Delta M$. For our benchmark mass of $\bar{M} = 30\,\text{GeV}$, the decay rate is approximately given as $\Gamma \sim 6.0 \times 10^{-6} U^2$. Even for an optimistic scenario with $U^2 \sim 10^{-9}$, a mass splitting of $\Delta M_{\text{phys}} \sim 10^{-14}$ GeV is required for a non-trivial ratio between the number of LNV and LNC processes. To obtain such a small mass splitting, a cancellation is needed between mass splitting $\Delta M$ and $\Delta M_{\theta\theta}$, which is only possible for $\cos 2\,\text{Re}\,\omega \sim 1$, and $\Delta M \sim \Delta M_{\theta\theta}$, where $\Delta M_{\theta\theta} \sim$. For larger mass differences, the ratio of LNV and LNC processes approaches 1, as is expected for pure Majorana fermions, and no more information can be extracted about the mass difference $\Delta M_{\text{phys}}$.

However, it could still be possible to extract information about the heavy neutrino mass splitting by observing oscillations between mass eigenstates. Even if the total ratios of LNV and LNC processes are close to 1, it could be possible to see an oscillation pattern between LNV and LNC processes as a function of the vertex displacement if the oscillation length is macroscopic [156, 177]. The oscillation time is directly proportional to the physical mass splitting $\Delta M_{\text{phys}}$, which would allow us to extract information on the relation between the $\text{Re}\,\omega$ and $\Delta M$. In the linear seesaw limit $\Delta M / \Delta M_{\theta\theta} \to 0$, this yields a macroscopic oscillation pattern. It is interesting that even for larger mass differences, where $\Delta M \approx \Delta M_{\text{phys}}$, the oscillations could be resolved given a sufficient relativistic boost factor.

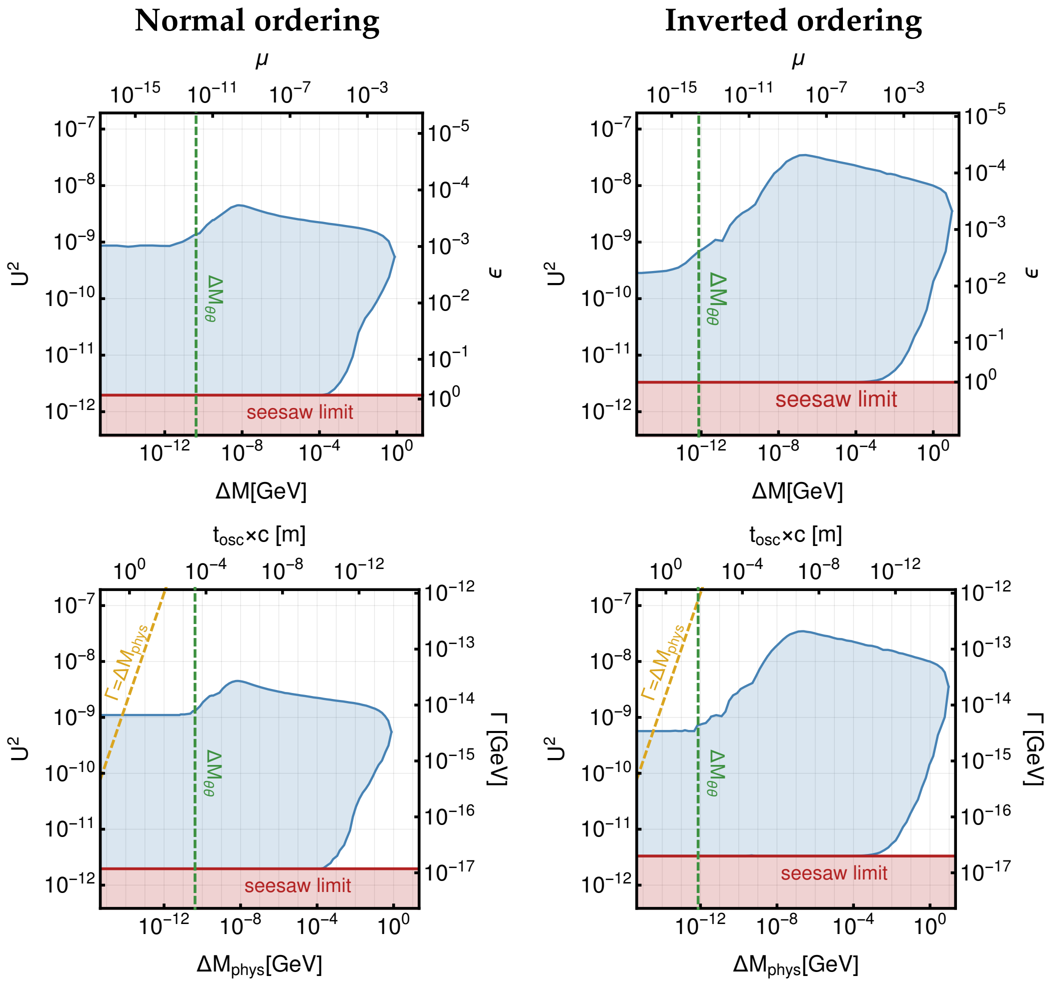


Figure 5.13: The region of parameter space (blue) in the $U^2 - \Delta M$ (upper row) and $U^2 - \Delta M_{\text{phys}}$ (lower row) projections, where the average heavy neutrino mass is fixed to $\bar{M} = 30\,\text{GeV}$. Normal and inverted orderings are shown in the left and right columns respectively. The lower limit on the mixing angle $U^2$ allowed by the light neutrino oscillation data is shown by the red line. The mass difference induced by the Higgs field VEV, $\Delta M_{\theta\theta}$ from (2.12) is shown by the vertical, dashed green line. The physical mass splitting $\Delta M_{\text{phys}}$ is related to the Lagrangian mass difference $\Delta M$ through relation (2.12). It is interesting that leptogenesis is allowed even for $\Delta M = 0$ as $\Delta M_{\theta\theta} \neq 0$ during the electroweak crossover. In addition to the mixing angle $U^2$ and mass splittings, we also show the oscillation time (lower row, upper frame labels), and decay widths (lower row, right frame label), as well as the small parameters $\mu$ (upper row, upper frame label), and $\epsilon$ (upper row, right frame label). The yellow line corresponds $\Gamma = \Delta M_{\text{phys}}$, where we can expect a non-trivial ratio between LNV and LNC processes. Figure taken from [46].

**Importance of $\tilde{L}NV$ Processes for $\Delta M$** It is interesting that although the $\tilde{L}NV$ processes have a quite dramatic effect for individual parameter points (*c.f.* 4.13, the allowed region in the $\bar{M} - U^2$ projection remains quite similar in the studies of parameter space with and without the $\tilde{L}NV$ effects (*c.f.* figures 5.1 and 5.7).

To explore the role of the $\tilde{L}NV$ processes in more detail, in Fig. 5.14 we look at the projection of the allowed parameter space onto the $\Delta M - U^2$ plane with and without the $\tilde{L}NV$ processes included for the benchmark mass of $\bar{M} = 30\,\text{GeV}$.

The results of the scan with, and without $\tilde{L}NV$ processes are shown in the shaded blue and yellow regions. We find that slightly bigger mixing angles $U^2$ are allowed if $\tilde{L}NC$ effects are neglected, however, the range of allowed mass splittings is much smaller.

The $\tilde{L}NV$ processes extend the parameter space in two major ways, the lower limit on the mass splitting no longer applies, since the asymmetry can also be produced in the degenerate limit $\mu \to 0$ as was shown in 4.4.3. Furthermore, we find that large mass differences also become viable. One of the main reasons behind this is that the suppression from backreaction from 4.4.2 becomes inefficient, which allows for a larger final lepton asymmetry.

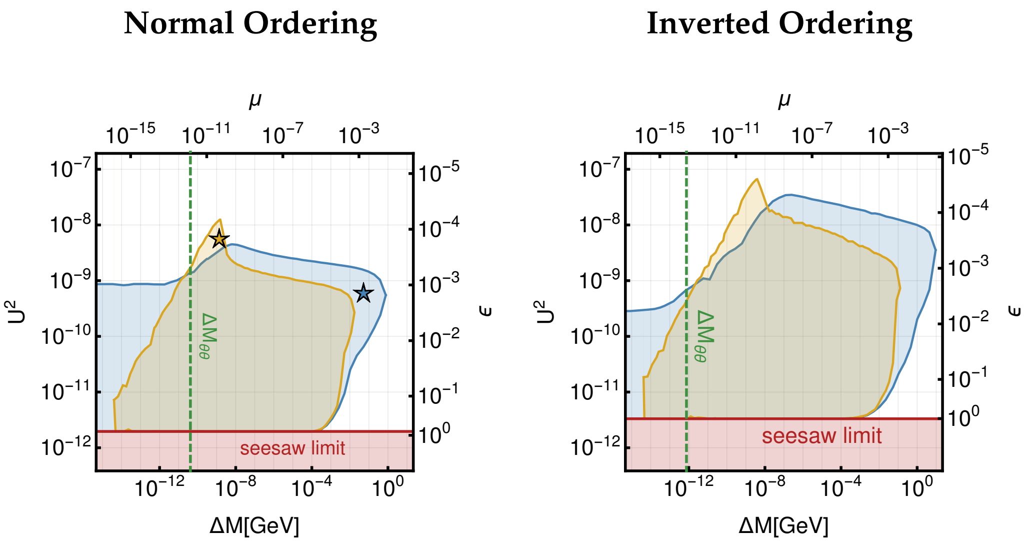


Figure 5.14: The allowed range of mass differences $\Delta M$ and mixing angles $U^2$ with (blue) and without (yellow) the inclusion of lepton number violating processes for normal and inverted ordering. We set the average mass to $\bar{M} = 30\,\mathrm{GeV}$ for the heavy neutrinos. The largest mass splittings increase by two orders of magnitude in the presence of $\tilde{L}NV$ processes, reaching the range that could be resolved by future experiments. The two benchmark point for which we presented a comparison between evolution with and without the $\tilde{L}NV$ processes in figures 4.13 are shown by the blue and yellow stars. The blue star corresponds to a point in parameter space that can only reproduce the observed BAU with the inclusion of $\tilde{L}NV$ processes, while the yellow star corresponds to a point where leptogenesis is only possible if we neglect the $\tilde{L}NV$ processes. Figure taken from [46].

# Chapter 6

# Conclusion

In this work we studied whether right-handed neutrinos with masses close to the electroweak scale could be the common origin of the neutrino masses and the BAU, with a focus on the minimal scenario with two right-handed neutrinos.

Current neutrino oscillation data already imposes strong constraints on the properties of the right-handed neutrinos. In particular, for right-handed neutrinos with masses below the electroweak scale, and large mixing angles, we find that the range of the allowed flavour mixing patterns is already constrained by existing data as shown in figures 2.4 and 2.5, and can improve significantly if the $CP$-violating phase $\delta$ is determined in the near future (*c.f.* Fig. 2.6). Comparing these predictions with the mixing angle ratios measured at a future experiment could be a first test of the low scale-seesaw mechanism.

We studied two leptogeneis mechanisms, resonant leptogenesis, that applies to right-handed neutrinos with masses above the electroweak scale, and leptogenesis through neutrino oscillations, which can be realized with right-handed neutrinos much lighter than the electroeweak scale. Following previous work, we use heavy neutrino oscillations as an adequate description of these processes. We re-derive the neutrino oscillation equations using Closed-Time-Path formalism of non-equilibrium quantum field theory. In the case of resonant leptogenesis we find that the heavy neutrino oscillation equations can be approximately solved in large parts of the parameter space. These analytic approximations can be used to calculate the decay asymmetry $\epsilon$ of heavy neutrinos. These results coincide with the $S$-matrix calculation when the mass differences are large. However, they remain finite when the mass splitting is small, regulating the apparent divergences that show up in the $S$-matrix calculation.

For neutrinos below the electroweak scale, the BAU is produced through neutrino oscillations. We identify two regimes of leptogenesis in this scenario, which we call oscillatory and overdamped. In the oscillatory regime the oscillations between the heavy neutrinos happen much earlier than the heavy neutrinos approach equilibrium, $z_{\rm eq} \gg z_{\rm vac}$. In the opposite case, in the overdamped regime, the equilibration of at least one heavy neutrino happens before they start to oscillate $z_{\rm eq} \ll z_{\rm vac}$. For each of these regimes we find semi-analytic approximations, which we can use to estimate the size of the BAU. Furthermore, we discuss the importance of $\tilde{L}$-number violation, and include it in a fully numerical study of the low-scale leptogenesis parameter space.

To determine the limits on the heavy neutrino mixing angles we perform two parameter scans, with and without the $\tilde{L}$NV effects included. For right-handed neutrino masses between 0.1 and 10 GeV, where the $\tilde{L}$-number violating effects are expected to be small, we neglect them and use the analytic approximations that describe the overdamped and oscillatory regimes. For larger masses, between 5 and 50 GeV, we include these effects, and perform the parameter scan numerically.

Finally, we confront the low-scale leptogenesis parameter space with the estimated sensitivity of existing and near-future experiments. In particular, for the currently planned future lepton colliders (CEPC, ILC, FCC-ee), we calculate the expected numbers of events for each point consistent with both the seesaw and leptogenesis mechanisms. We find that these experiments can probe large parts of the low-scale leptogenesis parameter space, and can even potentially lead to a measurement of the flavour mixing ratios $U_\alpha^2/U^2$. When combined with the constraints on the flavour mixing ratios 5.11, these measurements can be a first step towards testing the low-scale leptogenesis mechanism.

# Appendix A

# Heavy neutrino mixing angles

In the following we present the relation between the mixings $U^2_{i\alpha}$, and the parameters in the PMNS matrix $U_\nu$ for two heavy neutrinos $n_s = 2$, as found in [105]. For the trigonometric functions we use the shorthand notations $s_{ab} = \sin\theta_{ab}$ and $c_{ab} = \cos\theta_{ab}$.[1] To find expressions in the symmetric limit $\operatorname{Im}\omega \gg 1$, the relations

$$\lim_{\epsilon\to 0}\tanh(2\operatorname{Im}\omega) = 1\,, \quad \lim_{\epsilon\to 0}\cosh(2\operatorname{Im}\omega) = \sinh(2\operatorname{Im}\omega) = \frac{1}{2}\exp(2\operatorname{Im}\omega) = \frac{1}{2\epsilon}\,, \tag{A.1}$$

is particularly useful.

**Normal hierarchy**

$$\begin{aligned}
2M_{1,2}U^2_{e1,2} = {}& a_1^+\cosh(2\operatorname{Im}\omega) - a_2\sin\left(\frac{\alpha_2}{2}+\delta\right)\sinh(2\operatorname{Im}\omega) \\
&\pm\left[a_1^-\cos(2\operatorname{Re}\omega) - a_2\sin\left(\frac{\alpha_2}{2}+\delta\right)\sin(2\operatorname{Re}\omega)\right]\,, \qquad \text{(A.2a)}\\
2M_{1,2}U^2_{\mu 1,2} = {}& \left[a_3^+ - a_4\cos(\delta)\right]\cosh(2\operatorname{Im}\omega) - \left[a_5\sin\left(\frac{\alpha_2}{2}\right) - a_6\sin\left(\frac{\alpha_2}{2}+\delta\right)\right]\sinh(2\operatorname{Im}\omega)\\
&\mp\left[a_3^- + a_4\cos(\delta)\right]\cos(2\operatorname{Re}\omega)\mp\left[a_5\cos\left(\frac{\alpha_2}{2}\right) - a_6\cos\left(\frac{\alpha_2}{2}+\delta\right)\right]\sin(2\operatorname{Re}\omega)\,, \qquad \text{(A.2b)}\\
2M_{1,2}U^2_{\tau 1,2} = {}& \left[a_7^+ + a_4\cos(\delta)\right]\cosh(2\operatorname{Im}\omega) + \left[a_5\sin\left(\frac{\alpha_2}{2}\right) + a_8\sin\left(\frac{\alpha_2}{2}+\delta\right)\right]\sinh(2\operatorname{Im}\omega)\\
&\mp\left[a_7^- - a_4\cos(\delta)\right]\cos(2\operatorname{Re}\omega)\pm\left[a_5\cos\left(\frac{\alpha_2}{2}\right) + a_8\cos\left(\frac{\alpha_2}{2}+\delta\right)\right]\sin(2\operatorname{Re}\omega)\,, \qquad \text{(A.2c)}
\end{aligned}$$

[1] Note that we take $s_{ab}$ and $c_{ab}$ to be the positive real roots of $s^2_{ab}$ and $c^2_{ab}$ from Table 2.2.

where $a_1$ to $a_8$ are positive real coefficients given by active neutrino masses and their mixing angles

$$\begin{aligned}
a_1^{\pm} &= m_2 c_{13}^2 s_{12}^2 \pm m_3 s_{13}^2 \,, && \text{(A.3a)}\\
a_2 &= 2\sqrt{m_2 m_3} c_{13} s_{12} s_{13} \xi \,, && \text{(A.3b)}\\
a_3^{\pm} &= \pm m_2 (c_{12}^2 c_{23}^2 + s_{12}^2 s_{13}^2 s_{23}^2) + m_3 c_{13}^2 s_{23}^2 \,, && \text{(A.3c)}\\
a_4 &= 2 m_2 c_{12} c_{23} s_{12} s_{13} s_{23} \,, && \text{(A.3d)}\\
a_5 &= 2\sqrt{m_2 m_3} c_{12} c_{13} c_{23} s_{23} \xi \,, && \text{(A.3e)}\\
a_6 &= 2\sqrt{m_2 m_3} c_{13} s_{12} s_{13} s_{23}^2 \xi \,, && \text{(A.3f)}\\
a_7^{\pm} &= \pm m_2 (c_{23}^2 s_{12}^2 s_{13}^2 + c_{12}^2 s_{23}^2) + m_3 c_{13}^2 c_{23}^2 \,, && \text{(A.3g)}\\
a_8 &= 2\sqrt{m_2 m_3} c_{13} c_{23}^2 s_{12} s_{13} \xi \,. && \text{(A.3h)}
\end{aligned}$$

Without loss of generality we have set $\alpha_1 = 0$. We may now use the simplified notation $\alpha_2 = \alpha$ that we adopt in the main text.

### Inverted hierarchy

$$\begin{aligned}
2M_{1,2}U_{e1,2}^2 = {} & b_1^+ \cosh(2\,\mathrm{Im}\,\omega) + b_2 \sin\left(\frac{\widetilde{\alpha}}{2}\right) \sinh(2\,\mathrm{Im}\,\omega)\\
& \pm b_1^- \cos(2\,\mathrm{Re}\,\omega) \mp b_2 \cos\left(\frac{\widetilde{\alpha}}{2}\right) \sin(2\,\mathrm{Re}\,\omega) \,, && \text{(A.4a)}\\
2M_{1,2}U_{\mu 1,2}^2 = {} & \left[b_3^+ - b_4^+ \cos(\delta)\right] \cosh(2\,\mathrm{Im}\,\omega) \mp \left[b_3^- + b_4^- \cos(\delta)\right] \cos(2\,\mathrm{Re}\,\omega)\\
& - \left[b_5 \sin\left(\frac{\widetilde{\alpha}}{2}\right) + b_6 \sin\left(\frac{\widetilde{\alpha}}{2} - \delta\right) - b_7 \sin\left(\frac{\widetilde{\alpha}}{2} + \delta\right)\right] \sinh(2\,\mathrm{Im}\,\omega)\\
& \pm \left[b_5 \cos\left(\frac{\widetilde{\alpha}}{2}\right) + b_6 \cos\left(\frac{\widetilde{\alpha}}{2} - \delta\right) - b_7 \cos\left(\frac{\widetilde{\alpha}}{2} + \delta\right)\right] \sin(2\,\mathrm{Re}\,\omega) \,,\\
& && \text{(A.4b)}\\
2M_{1,2}U_{\tau 1,2}^2 = {} & \left[b_8^+ + b_4^+ \cos(\delta)\right] \cosh(2\,\mathrm{Im}\,\omega) \mp \left[b_8^- - b_4^- \cos(\delta)\right] \cos(2\,\mathrm{Re}\,\omega)\\
& - \left[b_9 \sin\left(\frac{\widetilde{\alpha}}{2}\right) - b_6 \sin\left(\frac{\widetilde{\alpha}}{2} - \delta\right) + b_7 \sin\left(\frac{\widetilde{\alpha}}{2} + \delta\right)\right] \sinh(2\,\mathrm{Im}\,\omega)\\
& \pm \left[b_9 \cos\left(\frac{\widetilde{\alpha}}{2}\right) - b_6 \cos\left(\frac{\widetilde{\alpha}}{2} - \delta\right) + b_7 \cos\left(\frac{\widetilde{\alpha}}{2} + \delta\right)\right] \sin(2\,\mathrm{Re}\,\omega) \,,\\
& && \text{(A.4c)}
\end{aligned}$$

where $b_1$ to $b_9$ are positive real coefficients given by active neutrino masses and their mixing angles

$$
\begin{aligned}
b_1^{\pm} &= m_1 c_{12}^2 c_{13}^2 \pm m_2 s_{12}^2 c_{13}^2 \,, && \text{(A.5a)}\\
b_2 &= 2\sqrt{m_1 m_2} c_{12} s_{12} \xi \,, && \text{(A.5b)}\\
b_3^{\pm} &= \pm m_1 (c_{23}^2 s_{12}^2 + c_{12}^2 s_{13}^2 s_{23}^2) + m_2 (c_{12}^2 c_{23}^2 + s_{12}^2 s_{13}^2 s_{23}^2) \,, && \text{(A.5c)}\\
b_4^{\pm} &= 2(\pm m_2 - m_1) c_{12} c_{23} s_{12} s_{13} s_{23} \,, && \text{(A.5d)}\\
b_5 &= 2\sqrt{m_1 m_2} (c_{12} c_{23}^2 s_{12} - c_{12} s_{12} s_{13}^2 s_{23}^2) \xi \,, && \text{(A.5e)}\\
b_6 &= 2\sqrt{m_1 m_2} c_{12}^2 c_{23} s_{13} s_{23} \xi \,, && \text{(A.5f)}\\
b_7 &= 2\sqrt{m_1 m_2} s_{12}^2 c_{23} s_{13} s_{23} \xi \,, && \text{(A.5g)}\\
b_8^{\pm} &= \pm m_1 (c_{12}^2 c_{23}^2 s_{13}^2 + s_{12}^2 s_{23}^2) + m_2 (c_{23}^2 s_{12}^2 s_{13}^2 + c_{12}^2 s_{23}^2) \,, && \text{(A.5h)}\\
b_9 &= 2\sqrt{m_1 m_2} c_{12} s_{12} (s_{23}^2 - c_{23}^2 s_{13}^2) \xi \,, && \text{(A.5i)}
\end{aligned}
$$

and $\widetilde{\alpha} = \alpha_2 - \alpha_1$. Therefore, the Yukawa matrices $Y$ only depend on the difference $\alpha_2 - \alpha_1$ for inverted hierarchy, which allows us to set $\alpha_1 = 0$ and use the simplified notation $\alpha_2 = \widetilde{\alpha} = \alpha$.

# Appendix B

# The Metropolis-Hastings sampling algorithm

The Metropolis-Hastings algorithm [108, 109] is method of obtaining samples of some probability distribution $\pi(x)$ (which in general does not need to be normalized).

The algorithm proposes a way of constructing a Markov chain of points $x_i$ that are approximately distributed from the distribution $\pi(x)$.

We define a conditional density $q(x|y)$ that is used to generate candidate points.

**Algorithm 1** Metropolis-Hastings algorithm

1: **Given** $x^{(i)}$
2: **Generate** $y \sim q(x_i|y)$
3: **Take**

$$x^{(i+1)} = \begin{cases} y \text{ with probability } \rho(x^{(i)}, y) \\ x^{(i)} \text{ with probability } 1 - \rho(x^{(i)}, y)\,, \end{cases} \tag{B.1}$$

where

$$\rho(x^{(i)}, y) = \min\left[\frac{\pi(y)}{\pi(x)}\frac{q(x|y)}{q(y|x)}, 1\right]\,. \tag{B.2}$$

In the limit of large $i$, the density of points $x^{(i)}$ approaches the probability distribution $\pi(x)$.

# Appendix C

# Definitions and relations between the two-point functions

The useful combinations of the two-point functions on the CTP are defined as:

$$G^A = G^T - G^> = G^< - G^{\bar{T}} \quad \text{(advanced)}\,, \tag{C.1a}$$

$$G^R = G^T - G^< = G^> - G^{\bar{T}} \quad \text{(retarded)}\,, \tag{C.1b}$$

$$G^H = \frac{1}{2}(G^R + G^A) = \frac{1}{2}(G^T - G^{\bar{T}}) \quad \text{(Hermitian)}\,, \tag{C.1c}$$

$$G^{\mathcal{A}} = \frac{1}{2\mathrm{i}}(G^A - G^R) = \frac{\mathrm{i}}{2}(G^> - G^<) \quad \text{(anti-Hermitian, spectral)}\,, \tag{C.1d}$$

$$G^F = \frac{1}{2}(G^> + G^<) \quad \text{(statistical)}^1\,. \tag{C.1e}$$

[1]Corresponds to $G^+ = G^F$ from [118].

# Appendix D

# Equilibrium Green functions

**Heavy neutrinos** To zeroth order in the Yukawa couplings, the heavy neutrino two-point functions are given by:

$$\mathrm{i}S^{<}_{Nii}(p) = -2\pi\delta(p^2 - M_{ii}^2)(\not{p} + M_{ii})\left[\vartheta(p_0)f_{Nii}(\mathbf{p}) - \vartheta(-p_0)(1 - f_{Nii}(-\mathbf{p}))\right], \tag{D.1a}$$

$$\mathrm{i}S^{>}_{Nii}(p) = -2\pi\delta(p^2 - M_{ii}^2)(\not{p} + M_{ii})\left[-\vartheta(p_0)(1 - f_{Nii}(\mathbf{p})) + \vartheta(-p_0)f_{Nii}(-\mathbf{p})\right], \tag{D.1b}$$

$$\mathrm{i}S^{T}_{Nii}(p) = \frac{\mathrm{i}(\not{p} + M_{ii})}{p^2 - M_{ii}^2 + \mathrm{i}\varepsilon} - 2\pi\delta(p^2 - M_{ii}^2)(\not{p} + M_{ii})\left[\vartheta(p_0)f_{Nii}(\mathbf{p}) + \vartheta(-p_0)f_{Nii}(-\mathbf{p})\right], \tag{D.1c}$$

$$\mathrm{i}S^{\bar{T}}_{Nii}(p) = -\frac{\mathrm{i}(\not{p} + M_{ii})}{p^2 - M_{ii}^2 - \mathrm{i}\varepsilon} - 2\pi\delta(p^2 - M_{ii}^2)(\not{p} + M_{ii})\left[\vartheta(p_0)f_{Nii}(\mathbf{p}) + \vartheta(-p_0)f_{Nii}(-\mathbf{p})\right]. \tag{D.1d}$$

$$\mathrm{i}S^{\mathcal{A}}_{Nii}(p) = \frac{\mathrm{i}}{2}2\pi\delta(p^2 - M_{ii}^2)(\not{p} + M_{ii})\,\mathrm{sgn}(p_0), \tag{D.2a}$$

$$\mathrm{i}S^{F}_{Nii}(p) = -2\pi\delta(p^2 - M_{ii}^2)(\not{p} + M_{ii})\left[\vartheta(p_0)\left(f_{Nii}(\mathbf{p}) - \frac{1}{2}\right) + \vartheta(-p_0)\left(f_{Nii}(-\mathbf{p}) - \frac{1}{2}\right)\right]. \tag{D.2b}$$

**Doublet leptons** Since the $SU(2)_L$ symmetry is unbroken at high temperatures, we should in principle take account of both elements of the lepton doublet:

$$S^{SU(2)_L}_{\ell\,AB} = \delta_{AB}S_\ell, \tag{D.3}$$

where $A, B = 1, 2$. The lepton propagators are:

$$\mathrm{i}S_\ell^<(p) = -2\pi\delta(p^2)P_\mathrm{L}\not{p}P_\mathrm{R}\left[\vartheta(p_0)f_\ell(\mathbf{p}) - \vartheta(-p_0)(1-\bar{f}_\ell(-\mathbf{p}))\right] , \tag{D.4a}$$

$$\mathrm{i}S_\ell^>(p) = -2\pi\delta(p^2)P_\mathrm{L}\not{p}P_\mathrm{R}\left[-\vartheta(p_0)(1-f_\ell(\mathbf{p})) + \vartheta(-p_0)\bar{f}_\ell(-\mathbf{p})\right] , \tag{D.4b}$$

$$\mathrm{i}S_\ell^T(p) = P_\mathrm{L}\frac{\mathrm{i}\not{p}}{p^2+\mathrm{i}\varepsilon}P_\mathrm{R} - 2\pi\delta(p^2)P_\mathrm{L}\not{p}P_\mathrm{R}\left[\vartheta(p_0)f_\ell(\mathbf{p}) + \vartheta(-p_0)\bar{f}_\ell(-\mathbf{p})\right] , \tag{D.4c}$$

$$\mathrm{i}S_\ell^{\bar{T}}(p) = -P_\mathrm{L}\frac{\mathrm{i}\not{p}}{p^2-\mathrm{i}\varepsilon}P_\mathrm{R} - 2\pi\delta(p^2)P_\mathrm{L}\not{p}P_\mathrm{R}\left[\vartheta(p_0)f_\ell(\mathbf{p}) + \vartheta(-p_0)\bar{f}_\ell(-\mathbf{p})\right] . \tag{D.4d}$$

**The Higgs Field** The propagators for the Higgs field are given by:

$$\mathrm{i}\Delta_\phi^<(p) = 2\pi\delta(p^2)\left[\vartheta(p_0)f_\phi(\mathbf{p}) + \vartheta(-p_0)(1+\bar{f}_\phi(-\mathbf{p}))\right] , \tag{D.5a}$$

$$\mathrm{i}\Delta_\phi^>(p) = 2\pi\delta(p^2)\left[\vartheta(p_0)(1+f_\phi(\mathbf{p})) + \vartheta(-p_0)\bar{f}_\phi(-\mathbf{p})\right] , \tag{D.5b}$$

$$\mathrm{i}\Delta_\phi^T(p) = \frac{\mathrm{i}}{p^2+\mathrm{i}\varepsilon} + 2\pi\delta(p^2)\left[\vartheta(p_0)f_\phi(\mathbf{p}) + \vartheta(-p_0)\bar{f}_\phi(-\mathbf{p})\right] , \tag{D.5c}$$

$$\mathrm{i}\Delta_\phi^{\bar{T}}(p) = -\frac{\mathrm{i}}{p^2-\mathrm{i}\varepsilon} + 2\pi\delta(p^2)\left[\vartheta(p_0)f_\phi(\mathbf{p}) + \vartheta(-p_0)\bar{f}_\phi(-\mathbf{p})\right] . \tag{D.5d}$$

# Appendix E

# Majorana Neutrino Self-Energy

In this appendix we briefly overview the properties of the Majorana neutrino self-energy. The self-energy of a Majorana neutrino is given by the derivative of the 2PI effective action:

$$\mathrm{i}\Sigma^{ab}_{N\,ij}(x,y) \equiv ab\frac{\delta\Gamma_2}{\delta S^{t\,ba}_{N\,ji}(y,x)}\,. \tag{E.1}$$

The heavy neutrino fields have to satisfy the general Majorana constraint:

$$N = GN^C \to S^{ab}_{N\,ij}(x,y) = GCS^{t\,ba}_{N\,ji}(y,x)G^*C^\dagger\,, \tag{E.2}$$

where $G = G^T = U^\dagger U^*$ is introduced to take account of the possible change to the Majorana condition under a unitary transformation $N \to UN$. We can therefore express the self-energy of a Majorana neutrino as a sum of two "Dirac" self energies:

$$\begin{aligned}\mathrm{i}\Sigma^{ab}_{N\,ij}(x,y) &\equiv ab\frac{\delta\Gamma_2}{\delta S^{t\,ba}_{N\,ji}(y,x)}\,, \\ &= ab\left[\frac{\partial\Gamma_2}{\partial S^{t\,ba}_{N\,ji}(y,x)} + C^tG\left(\frac{\partial\Gamma_2}{\partial S^{ab}_{N\,ij}(x,y)}\right)^t C^*G^*\right]\,,\end{aligned} \tag{E.3}$$

where $\partial$ symbolizes the partial functional derivative. In order to isolate the flavour and Dirac structure, we introduce the reduced self-energy:

$$\sum_{\alpha=e,\mu,\tau} g_w Y^*_{i\alpha}Y^t_{\alpha_j}\mathrm{i}\hat{\Sigma}^{ab}_{N\,R\,\alpha}(x,y)P_R \equiv ab\frac{\partial\Gamma_2}{\partial S^{t\,ba}_{N\,ji}(y,x)}\,, \tag{E.4}$$

where the subscript $\alpha$ tells us which of the active leptons is contributing to the self-energy, and the subscript $R$ stands for the right chirality of the contribution. By inserting both reduced self-energies, we obtain:

$$\mathrm{i}\Sigma^{ab}_{N\,ij}(x,y) = \sum_{\alpha} g_w \mathrm{Y}^{\alpha}_{+\,ij}\mathrm{i}\hat{\not{\Sigma}}^{ab}_{N\,R\,\alpha}(x,y)P_R - g_w \mathrm{Y}^{\alpha}_{-\,ij}\mathrm{i}\hat{\not{\Sigma}}^{ba}_{N\,R\,\alpha}(y,x)P_L\,, \tag{E.5}$$

where we introduced

$$\mathrm{Y}^{\alpha}_{+\,ij} \equiv Y_{i\alpha}Y^{\dagger}_{\alpha j}\,, \qquad \mathrm{Y}^{\alpha}_{-\,ij} \equiv (GY^*)_{i\alpha}(Y^tG^*)_{\alpha j}\,, \tag{E.6}$$

$$\mathrm{Y}_{+\,ij} \equiv (YY^{\dagger})_{ij}\,, \qquad \mathrm{Y}_{-\,ij} \equiv (GY^*Y^tG^*)_{ij}\,. \tag{E.7}$$

If we assume the self-energy to be translation invariant in space and time, we can apply the Wigner transform to obtain:

$$\mathrm{i}\Sigma^{ab}_{N\,ij}(k) = \sum_{\alpha} g_w \left(\mathrm{Y}^{\alpha}_{+\,ij}\mathrm{i}\hat{\not{\Sigma}}^{ab}_{N\,R\,\alpha}(k)P_R - \mathrm{Y}^{\alpha}_{-\,ij}\mathrm{i}\hat{\not{\Sigma}}^{ba}_{N\,R\,\alpha}(-k)P_L\right)\,. \tag{E.8}$$

If we define the left-chiral part of the self energy as:

$$\hat{\not{\Sigma}}^{ab}_{N\,L\,\alpha}(k) \equiv -\hat{\not{\Sigma}}^{ba}_{N\,R\,\alpha}(-k)\,, \tag{E.9}$$

we can further simplify the above equation to:

$$\mathrm{i}\Sigma^{ab}_{N\,ij}(k) = \sum_{\alpha} g_w \left(\mathrm{Y}^{\alpha}_{+\,ij}\mathrm{i}\hat{\not{\Sigma}}^{ab}_{N\,R\,\alpha}(k)P_R + \mathrm{Y}^{\alpha}_{-\,ij}\mathrm{i}\hat{\not{\Sigma}}^{ab}_{N\,L\,\alpha}(k)P_L\right)\,. \tag{E.10}$$

In equilibrium, the left and right-chiral party of the self-energies satisfy further constraints:

$$\hat{\bar{\not{\Sigma}}}_{N\,R\,\alpha}(k) = \hat{\bar{\not{\Sigma}}}_{N\,L\,\alpha}(k) \equiv \hat{\bar{\not{\Sigma}}}_{N}(k) \tag{E.11}$$

for the combinations $\mathcal{A}$, $F$, $H$, as well as $R$ and $A$. Using these relations, we can obtain the equilibrium self-energies:

$$\mathrm{i}\bar{\Sigma}_{N\,ij}(k) = g_w \mathrm{Y}_{+\,ij}\mathrm{i}\hat{\bar{\not{\Sigma}}}_{N}(k)P_R + g_w \mathrm{Y}_{-\,ij}\mathrm{i}\hat{\bar{\not{\Sigma}}}_{N}(k)P_L\,. \tag{E.12}$$

## E.1 Relation between the collision terms of the heavy and doublet neutrinos

The self-energies of the RHN and the active leptons both arise from the same 2PI effective action:

$$\mathrm{i}\Sigma^{ab}_{Nij}(k) = ab\frac{\delta\Gamma_2}{\delta S^{ba}_{N\,ij}(k)} \tag{E.13}$$

$$\mathrm{i}\Sigma^{ab}_{\ell\alpha}(k) = ab\frac{\delta\Gamma_2}{\delta S^{ba}_{\ell\alpha}(k)} \tag{E.14}$$

To show how they are connected, we introduce the four-point function $\tilde{\Gamma}$:

$$\tilde{\Gamma}^{ab}_{ij\alpha\,\mu\nu\rho\sigma}(k,p) \equiv \frac{\delta^2\Gamma}{\delta S^{ba}_{N\,ji\,\nu\mu}(k)\delta S^{ab}_{\ell\,\alpha\,\sigma\rho}(p)}\,, \tag{E.15}$$

where $a\,,b$ are the CTP indices, $i\,,j$ sterilve flavour, $\alpha$ the active flavour, and finally, $\mu\,,\nu\,,\rho\,,$ and $\sigma$ the Dirac indices. Using this four-point function one can find the self-energies of the heavy neutrinos and the doublet leptons as:

$$\begin{aligned}
\mathrm{i}\Sigma^{ab}_{N\,ij\,\mu\nu}(k) &= g_w\sum_{\alpha\rho\sigma}\int\tilde{\Gamma}^{ab}_{ij\,\alpha\,\mu\nu\rho\sigma}(k,p)S^{ab}_{\ell\,\alpha\,\sigma\rho}(p)\frac{\mathrm{d}^4p}{(2\pi)^4} \\
\mathrm{i}\Sigma^{ab}_{\ell\,\alpha\,\rho\sigma}(p) &= \sum_{ij\,\mu\nu}\int\tilde{\Gamma}^{ba}_{ij\,\alpha\,\mu\nu\rho\sigma}(k,p)S^{ab}_{N\,ji\,\nu\mu}(k)\frac{\mathrm{d}^4k}{(2\pi)^4}
\end{aligned} \tag{E.16}$$

If we insert this expression into the doublet lepton collision term (here expressed in Wightmann functions), we find that it can be expressed using the heavy neutrino propagators and self-energies:

$$\begin{aligned}
\mathscr{C} &\supset \int\frac{\mathrm{d}p^4}{(2\pi)^4}\mathrm{i}\,\mathrm{Tr}\left[\Sigma^{ab}_{\ell\,\alpha}(p)S^{ba}_{\ell\,\alpha}(p)\right] \\
&= \int\frac{\mathrm{d}p^4}{(2\pi)^4}\mathrm{i}\Sigma^{ab}_{\ell\,\alpha\,\rho\sigma}(p)S^{ba}_{\ell\,\alpha\,\sigma\rho}(p) \\
&= \int\frac{\mathrm{d}p^4}{(2\pi)^4}\frac{\mathrm{d}k^4}{(2\pi)^4}\tilde{\Gamma}^{ba}_{ij\,\alpha\,\mu\nu\rho\sigma}(k,p)S^{ab}_{N\,ji\,\nu\mu}(k)S^{ba}_{\ell\,\alpha\,\sigma\rho}(p) \\
&= \frac{1}{g_w}\int\frac{\mathrm{d}k^4}{(2\pi)^4}\mathrm{i}\Sigma^{ba}_{N\,ij\,\alpha\,\mu\nu}(k)S^{ab}_{N\,ji\,\nu\mu}(k)\,.
\end{aligned} \tag{E.17}$$

# Appendix F

# Precision of measuring flavour mixing ratios

In this appendix we briefly discuss the statistics behind measurements the flavour ratios at future colliders.

## F.1 Probability distribution for $N_{\rm sl}$ semileptonic events with $N_\alpha$ of them in flavour $\alpha$.

For decays of heavy neutrinos into flavour $\alpha$ we have two main observables, the total number of semileptonic events $N_{\rm sl}$, and the number of events with a lepton of flavour $\alpha$ in the final state $N_\alpha$. The probability distribution function (PDF) for this scenario is a product of a Poisson distribution that describes the "rare event" of producing a heavy neutrino and it decaying in the semileptonic channel, together with a binomial distribution that corresponds to the semileptonic event being of the particular flavour $\alpha$,

$$P(N_{\rm sl}, N_\alpha) = \frac{e^{-\lambda_{\rm sl}}\lambda_{\rm sl}^{N_{\rm sl}}}{N_{\rm sl}!}\binom{N_{\rm sl}}{N_\alpha}\mathrm{Br}(\alpha)^{N_\alpha}(1-\mathrm{Br}(\alpha))^{N_{\rm sl}-N_\alpha}\,, \tag{F.1}$$

where $\mathrm{Br}(\alpha) = U_\alpha^2/U^2$ is the branching ratio of semileptonic states with $\alpha$ in the final state. The expected numbers of events are $\langle N_{\rm sl}\rangle = \lambda_{\rm sl}$ and $\langle N_\alpha\rangle = \lambda_{\rm sl}\mathrm{Br}(\alpha) \equiv \lambda_\alpha$. It is interesting that if we do not keep track of the total number of semileptonic events, but calculate the distribution for $N_\alpha$ alone, we recover the Poisson distribution: the PDF reduces to a pure Poisson distribution:

$$\begin{aligned} P(N_\alpha) &= \sum_{N_{\rm sl}=N_\alpha}^{\infty} P(N_{\rm sl}, N_\alpha) \\ &= \sum_{k=0}^{\infty} \frac{\mathrm{e}^{-\lambda_{\rm sl}}\lambda_{\rm sl}^{N_\alpha+k}}{N_\alpha!k!}\mathrm{Br}(\alpha)^{N_\alpha}(1-\mathrm{Br}(a))^k \\ &= \frac{(\lambda_{\rm sl}\mathrm{Br}(a))^{N_\alpha}}{N_\alpha!}\mathrm{e}^{-\lambda_{\rm sl}}\sum_{k=0}^{\infty}\frac{[\lambda_{\rm sl}(1-\mathrm{Br}(\alpha))]^k}{k!} = \frac{\mathrm{e}^{-\lambda_\alpha}\lambda_\alpha^{N_\alpha}}{N_\alpha!}. \end{aligned} \tag{F.2}$$

The variance of $N_\alpha$ is then equal to its expectation value: $\mathrm{Var}(N_\alpha) = \langle N_\alpha\rangle = \lambda_\alpha$.

## F.2 Precision of measuring $U_\alpha^2/U^2$.

We are interested in determining the ratio $U_\alpha^2/U^2$, as well as its error, which can be determined through $\mathrm{Var}(U_\alpha^2/U^2)$. To determine the variance, we can use the usual propagation of error, noting that $N_{\rm sl}$ is not independent of $N_\alpha$, which results in:

$$\frac{\delta(U_\alpha^2/U^2)}{U_\alpha^2/U^2} = \sqrt{\frac{1}{N_\alpha} - \frac{1}{N_{\rm sl}}}. \tag{F.3}$$

Since the propagation of error assumes a large number of events, when $N_{\rm sl}$ is small, we have to calculate the expected value and variance of $\mathrm{Var}(N_\alpha/N_{\rm sl})$ from the full PDF,

$$\langle N_\alpha/N_{\rm sl}\rangle = \sum_{N_{\rm sl}=0}^{\infty}\sum_{N_\alpha=0}^{N_{\rm sl}} P(N_{\rm sl}, N_\alpha)\frac{N_\alpha}{N_{\rm sl}} = \mathrm{Br}(\alpha) = \frac{\langle N_\alpha\rangle}{\langle N_{\rm sl}\rangle}, \tag{F.4}$$

and similarly,

$$\begin{aligned} \langle N_\alpha^2/N_{\rm sl}^2\rangle &= \sum_{N_{\rm sl}=0}^{\infty}\sum_{N_\alpha=0}^{N_{\rm sl}} P(N_{\rm sl}, N_\alpha)\left(\frac{N_\alpha}{N_{\rm sl}}\right)^2 \\ &= \mathrm{Br}(\alpha)^2 + \mathrm{e}^{-\lambda_{\rm sl}}(1-\mathrm{Br}(\alpha))[1-\mathrm{Br}(\alpha)(-1+\gamma_E+\Gamma(0,-\lambda_{\rm sl})+\log(-\lambda_{\rm sl}))], \end{aligned} \tag{F.5}$$

where $\gamma_E \approx 0.58$ is the Euler constant. Finally, we may calculate the expected sensitivity:

$$\begin{aligned} \frac{\delta(U_\alpha^2/U^2)}{U_\alpha^2/U^2} &= \sqrt{\frac{\mathrm{e}^{-\langle N_{\rm sl}\rangle}(\langle N_{\rm sl}\rangle-\langle N_\alpha\rangle)[\langle N_{\rm sl}\rangle+\langle N_\alpha\rangle(1-\gamma_E-\Gamma(0,-\langle N_{\rm sl}\rangle)-\log(-\langle N_{\rm sl}\rangle)]}{\langle N_\alpha\rangle^2}} \\ &\approx \sqrt{\frac{1}{\langle N_\alpha\rangle}-\frac{1}{\langle N_{\rm sl}\rangle}}, \end{aligned} \tag{F.6}$$

which agrees with the result obtained through error propagation in the large $\langle N_{\mathrm{sl}} \rangle$ limit.

The fact that the uncertainty vanishes when $\langle N_a \rangle \to \langle N_{\mathrm{sl}} \rangle$ might seem concerning, however, note that this is the expected uncertainty. If the branching ratio is exactly $\mathrm{Br}(\alpha) = 1$, the equation $\langle N_a \rangle = \langle N_{\mathrm{sl}} \rangle$ will be satisfied, and we do not expect any events in the other channels, i.e. the uncertainty of $\langle N_a / N_{\mathrm{sl}} \rangle$ vanishes.

# Bibliography


[1] G. Hinshaw, et al., Nine-Year Wilkinson Microwave Anisotropy Probe (WMAP) Observations: Cosmological Parameter Results, Astrophys. J. Suppl. 208 (2013) 19. arXiv:1212.5226, doi:10.1088/0067-0049/208/2/19.

[2] P. A. R. Ade, et al., Planck 2015 results. XIII. Cosmological parameters, Astron. Astrophys. 594 (2016) A13. arXiv:1502.01589, doi:10.1051/0004-6361/201525830.

[3] R. H. Cyburt, B. D. Fields, K. A. Olive, T.-H. Yeh, Big Bang Nucleosynthesis: 2015, Rev. Mod. Phys. 88 (2016) 015004. arXiv:1505.01076, doi:10.1103/RevModPhys.88.015004.

[4] N. Aghanim, et al., Planck 2018 results. VI. Cosmological parametersarXiv:1807.06209.

[5] A. D. Sakharov, Violation of CP Invariance, C asymmetry, and baryon asymmetry of the universe, Pisma Zh. Eksp. Teor. Fiz. 5 (1967) 32–35, [Usp. Fiz. Nauk161,no.5,61(1991)]. doi:10.1070/PU1991v034n05ABEH002497.

[6] G. R. Farrar, M. E. Shaposhnikov, Baryon asymmetry of the universe in the standard electroweak theory, Phys. Rev. D50 (1994) 774. arXiv:hep-ph/9305275, doi:10.1103/PhysRevD.50.774.

[7] M. B. Gavela, P. Hernandez, J. Orloff, O. Pene, Standard model baryogenesis, in: '94 electroweak interactions and unified theories. Proceedings, Leptonic Session of the 29th Rencontres de Moriond, Moriond Particle Physics Meeting, Meribel les Allues, France, March 12-19, 1994, 1994, pp. 401–410. arXiv:hep-ph/9407403.

[8] P. Huet, E. Sather, Electroweak baryogenesis and standard model CP violation, Phys. Rev. D51 (1995) 379–394. arXiv:hep-ph/9404302, doi:10.1103/PhysRevD.51.379.

[9] P. Minkowski, $\mu \to e\gamma$ at a Rate of One Out of $10^9$ Muon Decays?, Phys. Lett. 67B (1977) 421–428. doi:10.1016/0370-2693(77)90435-X.

[10] M. Gell-Mann, P. Ramond, R. Slansky, Complex Spinors and Unified Theories, Conf. Proc. C790927 (1979) 315–321. arXiv:1306.4669.

[11] R. N. Mohapatra, G. Senjanovic, Neutrino Mass and Spontaneous Parity Nonconservation, Phys. Rev. Lett. 44 (1980) 912, [,231(1979)]. doi:10.1103/PhysRevLett.44.912.

[12] T. Yanagida, Horizontal Symmetry and Masses of Neutrinos, Prog. Theor. Phys. 64 (1980) 1103. doi:10.1143/PTP.64.1103.

[13] J. Schechter, J. W. F. Valle, Neutrino Masses in SU(2) x U(1) Theories, Phys. Rev. D22 (1980) 2227. doi:10.1103/PhysRevD.22.2227.

[14] J. Schechter, J. W. F. Valle, Neutrino Decay and Spontaneous Violation of Lepton Number, Phys. Rev. D25 (1982) 774. doi:10.1103/PhysRevD.25.774.

[15] M. Fukugita, T. Yanagida, Baryogenesis Without Grand Unification, Phys. Lett. B174 (1986) 45–47. doi:10.1016/0370-2693(86)91126-3.

[16] E. Cortina Gil, et al., Search for heavy neutral lepton production in $K^+$ decays, Phys. Lett. B778 (2018) 137–145. arXiv:1712.00297, doi:10.1016/j.physletb.2018.01.031.

[17] M. Drewes, J. Hajer, J. Klaric, G. Lanfranchi, NA62 sensitivity to heavy neutral leptons in the low scale seesaw model, JHEP 07 (2018) 105. arXiv:1801.04207, doi:10.1007/JHEP07(2018)105.

[18] M. LAMOUREUX, Search for heavy neutrinos with the near detector nd280 of the t2k experiment, results presented at the NEUTRINO2018 conferencedoi:10.5281/zenodo.1300449.
URL https://doi.org/10.5281/zenodo.1300449

[19] S. Alekhin, et al., A facility to Search for Hidden Particles at the CERN SPS: the SHiP physics case, Rept. Prog. Phys. 79 (12) (2016) 124201. arXiv:1504.04855, doi:10.1088/0034-4885/79/12/124201.

[20] E. Graverini, N. Serra, B. Storaci, Search for New Physics in SHiP and at future colliders, JINST 10 (07) (2015) C07007. arXiv:1503.08624, doi:10.1088/1748-0221/10/07/C07007.

[21] G. Aad, et al., Inclusive search for same-sign dilepton signatures in $pp$ collisions at $\sqrt{s} = 7$ TeV with the ATLAS detector, JHEP 10 (2011) 107. arXiv:1108.0366, doi:10.1007/JHEP10(2011)107.

[22] G. Aad, et al., Search for heavy Majorana neutrinos with the ATLAS detector in pp collisions at $\sqrt{s} = 8$ TeV, JHEP 07 (2015) 162. arXiv:1506.06020, doi:10.1007/JHEP07(2015)162.

[23] M. Aaboud, et al., Search for long-lived particles in final states with displaced dimuon vertices in $pp$ collisions at $\sqrt{s} = 13$ TeV with the ATLAS detectorarXiv:1808.03057.

[24] V. Khachatryan, et al., Search for heavy Majorana neutrinos in $\mu^{\pm}\mu^{\pm}+$ jets events in proton-proton collisions at $\sqrt{s}$ = 8 TeV, Phys. Lett. B748 (2015) 144–166. arXiv:1501.05566, doi:10.1016/j.physletb.2015.06.070.

[25] V. Khachatryan, et al., Search for heavy Majorana neutrinos in $e^{\pm}e^{\pm}$+ jets and $e^{\pm}$ $\mu^{\pm}$+ jets events in proton-proton collisions at $\sqrt{s} = 8$ TeV, JHEP 04 (2016) 169. arXiv:1603.02248, doi:10.1007/JHEP04(2016)169.

[26] A. M. Sirunyan, et al., Search for heavy neutral leptons in events with three charged leptons in proton-proton collisions at $\sqrt{s} = 13$ TeV, Phys. Rev. Lett. 120 (22) (2018) 221801. arXiv:1802.02965, doi:10.1103/PhysRevLett.120.221801.

[27] R. Aaij, et al., Search for Majorana neutrinos in $B^- \to \pi^+\mu^-\mu^-$ decays, Phys. Rev. Lett. 112 (13) (2014) 131802. arXiv:1401.5361, doi:10.1103/PhysRevLett.112.131802.

[28] A. Ossowska, Majorana Neutrino Searches at the LHCb Experiment, Acta Phys. Polon. B49 (2018) 1301–1307. doi:10.5506/APhysPolB.49.1301.

[29] J. C. Helo, M. Hirsch, S. Kovalenko, Heavy neutrino searches at the LHC with displaced vertices, Phys. Rev. D89 (2014) 073005, [Erratum: Phys. Rev.D93,no.9,099902(2016)]. arXiv:1312.2900, doi:10.1103/PhysRevD.89.073005,10.1103/PhysRevD.93.099902.

[30] E. Izaguirre, B. Shuve, Multilepton and Lepton Jet Probes of Sub-Weak-Scale Right-Handed Neutrinos, Phys. Rev. D91 (9) (2015) 093010. arXiv:1504.02470, doi:10.1103/PhysRevD.91.093010.

[31] A. M. Gago, P. Hernández, J. Jones-Pérez, M. Losada, A. Moreno Briceño, Probing the Type I Seesaw Mechanism with Displaced Vertices at the LHC, Eur. Phys. J. C75 (10) (2015) 470. arXiv:1505.05880, doi:10.1140/epjc/s10052-015-3693-1.

[32] C. O. Dib, C. S. Kim, Discovering sterile Neutrinos ligther than $M_W$ at the LHC, Phys. Rev. D92 (9) (2015) 093009. arXiv:1509.05981, doi:10.1103/PhysRevD.92.093009.

[33] C. O. Dib, C. S. Kim, K. Wang, J. Zhang, Distinguishing Dirac/Majorana Sterile Neutrinos at the LHC, Phys. Rev. D94 (1) (2016) 013005. arXiv:1605.01123, doi:10.1103/PhysRevD.94.013005.

[34] G. Cottin, J. C. Helo, M. Hirsch, Displaced vertices as probes of sterile neutrino mixing at the LHC, Phys. Rev. D98 (3) (2018) 035012. arXiv:1806.05191, doi:10.1103/PhysRevD.98.035012.

[35] A. Abada, N. Bernal, M. Losada, X. Marcano, Inclusive Displaced Vertex Searches for Heavy Neutral Leptons at the LHCarXiv:1807.10024.

[36] F. Kling, S. Trojanowski, Heavy Neutral Leptons at FASER, Phys. Rev. D97 (9) (2018) 095016. arXiv:1801.08947, doi:10.1103/PhysRevD.97.095016.

[37] J. C. Helo, M. Hirsch, Z. S. Wang, Heavy neutral fermions at the high-luminosity LHC, JHEP 07 (2018) 056. arXiv:1803.02212, doi:10.1007/JHEP07(2018)056.

[38] D. Curtin, et al., Long-Lived Particles at the Energy Frontier: The MATHUSLA Physics CasearXiv:1806.07396.

[39] A. Blondel, E. Graverini, N. Serra, M. Shaposhnikov, Search for Heavy Right Handed Neutrinos at the FCC-ee, Nucl. Part. Phys. Proc. 273-275 (2016) 1883–1890. arXiv:1411.5230, doi:10.1016/j.nuclphysbps.2015.09.304.

[40] S. Antusch, O. Fischer, Testing sterile neutrino extensions of the Standard Model at future lepton colliders, JHEP 05 (2015) 053. arXiv:1502.05915, doi:10.1007/JHEP05(2015)053.

[41] A. Abada, V. De Romeri, S. Monteil, J. Orloff, A. M. Teixeira, Indirect searches for sterile neutrinos at a high-luminosity Z-factory, JHEP 04 (2015) 051. arXiv:1412.6322, doi:10.1007/JHEP04(2015)051.

[42] T. Asaka, T. Tsuyuki, Seesaw mechanism at electron-electron colliders, Phys. Rev. D92 (9) (2015) 094012. arXiv:1508.04937, doi:10.1103/PhysRevD.92.094012.

[43] S. Antusch, E. Cazzato, O. Fischer, Displaced vertex searches for sterile neutrinos at future lepton colliders, JHEP 12 (2016) 007. arXiv:1604.02420, doi:10.1007/JHEP12(2016)007.

[44] S. Antusch, E. Cazzato, O. Fischer, Sterile neutrino searches at future $e^-e^+$, $pp$, and $e^-p$ colliders, Int. J. Mod. Phys. A32 (14) (2017) 1750078. arXiv:1612.02728, doi:10.1142/S0217751X17500786.

[45] A. Caputo, P. Hernandez, M. Kekic, J. López-Pavón, J. Salvado, The seesaw path to leptonic CP violation, Eur. Phys. J. C77 (4) (2017) 258. arXiv:1611.05000, doi:10.1140/epjc/s10052-017-4823-8.

[46] S. Antusch, E. Cazzato, M. Drewes, O. Fischer, B. Garbrecht, D. Gueter, J. Klaric, Probing Leptogenesis at Future Colliders, JHEP 09 (2018) 124. arXiv:1710.03744, doi:10.1007/JHEP09(2018)124.

[47] F. Vissani, Do experiments suggest a hierarchy problem?, Phys. Rev. D57 (1998) 7027–7030. arXiv:hep-ph/9709409, doi:10.1103/PhysRevD.57.7027.

[48] F. Bezrukov, M. Yu. Kalmykov, B. A. Kniehl, M. Shaposhnikov, Higgs Boson Mass and New Physics, JHEP 10 (2012) 140, [,275(2012)]. arXiv:1205.2893, doi:10.1007/JHEP10(2012)140.

[49] S. Iso, N. Okada, Y. Orikasa, Classically conformal $B^-$ L extended Standard Model, Phys. Lett. B676 (2009) 81–87. arXiv:0902.4050, doi:10.1016/j.physletb.2009.04.046.

[50] S. Iso, Y. Orikasa, TeV Scale B-L model with a flat Higgs potential at the Planck scale - in view of the hierarchy problem -, PTEP 2013 (2013) 023B08. arXiv:1210.2848, doi:10.1093/ptep/pts099.

[51] V. V. Khoze, G. Ro, Leptogenesis and Neutrino Oscillations in the Classically Conformal Standard Model with the Higgs Portal, JHEP 10 (2013) 075. arXiv:1307.3764, doi:10.1007/JHEP10(2013)075.

[52] V. V. Khoze, A. D. Plascencia, Dark Matter and Leptogenesis Linked by Classical Scale Invariance, JHEP 11 (2016) 025. arXiv:1605.06834, doi:10.1007/JHEP11(2016)025.

[53] D. Wyler, L. Wolfenstein, Massless Neutrinos in Left-Right Symmetric Models, Nucl. Phys. B218 (1983) 205–214. doi:10.1016/0550-3213(83)90482-0.

[54] R. N. Mohapatra, J. W. F. Valle, Neutrino Mass and Baryon Number Nonconservation in Superstring Models, Phys. Rev. D34 (1986) 1642, [,235(1986)]. doi:10.1103/PhysRevD.34.1642.

[55] R. N. Mohapatra, Mechanism for Understanding Small Neutrino Mass in Superstring Theories, Phys. Rev. Lett. 56 (1986) 561–563. doi:10.1103/PhysRevLett.56.561.

[56] M. C. Gonzalez-Garcia, J. W. F. Valle, Fast Decaying Neutrinos and Observable Flavor Violation in a New Class of Majoron Models, Phys. Lett. B216 (1989) 360–366. doi:10.1016/0370-2693(89)91131-3.

[57] E. K. Akhmedov, M. Lindner, E. Schnapka, J. W. F. Valle, Dynamical left-right symmetry breaking, Phys. Rev. D53 (1996) 2752–2780. arXiv:hep-ph/9509255, doi:10.1103/PhysRevD.53.2752.

[58] E. K. Akhmedov, M. Lindner, E. Schnapka, J. W. F. Valle, Left-right symmetry breaking in NJL approach, Phys. Lett. B368 (1996) 270–280. arXiv:hep-ph/9507275, doi:10.1016/0370-2693(95)01504-3.

[59] S. M. Barr, A Different seesaw formula for neutrino masses, Phys. Rev. Lett. 92 (2004) 101601. arXiv:hep-ph/0309152, doi:10.1103/PhysRevLett.92.101601.

[60] M. Malinsky, J. C. Romao, J. W. F. Valle, Novel supersymmetric SO(10) seesaw mechanism, Phys. Rev. Lett. 95 (2005) 161801. arXiv:hep-ph/0506296, doi:10.1103/PhysRevLett.95.161801.

[61] J. Bernabeu, A. Santamaria, J. Vidal, A. Mendez, J. W. F. Valle, Lepton Flavor Nonconservation at High-Energies in a Superstring Inspired Standard Model, Phys. Lett. B187 (1987) 303–308. doi:10.1016/0370-2693(87)91100-2.

[62] A. Pilaftsis, Radiatively induced neutrino masses and large Higgs neutrino couplings in the standard model with Majorana fields, Z. Phys. C55 (1992) 275–282. arXiv:hep-ph/9901206, doi:10.1007/BF01482590.

[63] A. Abada, C. Biggio, F. Bonnet, M. B. Gavela, T. Hambye, Low energy effects of neutrino masses, JHEP 12 (2007) 061. arXiv:0707.4058, doi:10.1088/1126-6708/2007/12/061.

[64] D. Aristizabal Sierra, A. Degee, J. F. Kamenik, Minimal Lepton Flavor Violating Realizations of Minimal Seesaw Models, JHEP 07 (2012) 135. arXiv:1205.5547, doi:10.1007/JHEP07(2012)135.

[65] C. S. Fong, M. C. Gonzalez-Garcia, E. Nardi, E. Peinado, New ways to TeV scale leptogenesis, JHEP 08 (2013) 104. arXiv:1305.6312, doi:10.1007/JHEP08(2013)104.

[66] V. Cirigliano, B. Grinstein, G. Isidori, M. B. Wise, Minimal flavor violation in the lepton sector, Nucl. Phys. B728 (2005) 121–134. arXiv:hep-ph/0507001, doi:10.1016/j.nuclphysb.2005.08.037.

[67] M. B. Gavela, T. Hambye, D. Hernandez, P. Hernandez, Minimal Flavour Seesaw Models, JHEP 09 (2009) 038. arXiv:0906.1461, doi:10.1088/1126-6708/2009/09/038.

[68] R. Ruiz, QCD Corrections to Pair Production of Type III Seesaw Leptons at Hadron Colliders, JHEP 12 (2015) 165. arXiv:1509.05416, doi:10.1007/JHEP12(2015)165.

[69] C. Degrande, O. Mattelaer, R. Ruiz, J. Turner, Fully-Automated Precision Predictions for Heavy Neutrino Production Mechanisms at Hadron Colliders, Phys. Rev. D94 (5) (2016) 053002. arXiv:1602.06957, doi:10.1103/PhysRevD.94.053002.

[70] T. Asaka, S. Blanchet, M. Shaposhnikov, The nuMSM, dark matter and neutrino masses, Phys. Lett. B631 (2005) 151–156. arXiv:hep-ph/0503065, doi:10.1016/j.physletb.2005.09.070.

[71] T. Asaka, M. Shaposhnikov, The nuMSM, dark matter and baryon asymmetry of the universe, Phys. Lett. B620 (2005) 17–26. arXiv:hep-ph/0505013, doi:10.1016/j.physletb.2005.06.020.

[72] A. Boyarsky, O. Ruchayskiy, M. Shaposhnikov, The Role of sterile neutrinos in cosmology and astrophysics, Ann. Rev. Nucl. Part. Sci. 59 (2009) 191–214. arXiv:0901.0011, doi:10.1146/annurev.nucl.010909.083654.

[73] L. Canetti, M. Drewes, T. Frossard, M. Shaposhnikov, Dark Matter, Baryogenesis and Neutrino Oscillations from Right Handed Neutrinos, Phys. Rev. D87 (2013) 093006. arXiv:1208.4607, doi:10.1103/PhysRevD.87.093006.

[74] V. A. Kuzmin, V. A. Rubakov, M. E. Shaposhnikov, On the Anomalous Electroweak Baryon Number Nonconservation in the Early Universe, Phys. Lett. 155B (1985) 36. doi:10.1016/0370-2693(85)91028-7.

[75] S. Davidson, A. Ibarra, A Lower bound on the right-handed neutrino mass from leptogenesis, Phys. Lett. B535 (2002) 25–32. arXiv:hep-ph/0202239, doi:10.1016/S0370-2693(02)01735-5.

[76] W. Buchmuller, P. Di Bari, M. Plumacher, Cosmic microwave background, matter - antimatter asymmetry and neutrino masses, Nucl. Phys. B643 (2002) 367–390, [Erratum: Nucl. Phys.B793,362(2008)]. arXiv:hep-ph/0205349, doi:10.1016/S0550-3213(02)00737-X,10.1016/j.nuclphysb.2007.11.030.

[77] K. Hamaguchi, H. Murayama, T. Yanagida, Leptogenesis from N dominated early universe, Phys. Rev. D65 (2002) 043512. arXiv:hep-ph/0109030, doi:10.1103/PhysRevD.65.043512.

[78] W. Buchmuller, P. Di Bari, M. Plumacher, Leptogenesis for pedestrians, Annals Phys. 315 (2005) 305–351. arXiv:hep-ph/0401240, doi:10.1016/j.aop.2004.02.003.

[79] G. F. Giudice, A. Notari, M. Raidal, A. Riotto, A. Strumia, Towards a complete theory of thermal leptogenesis in the SM and MSSM, Nucl. Phys. B685 (2004) 89–149. arXiv:hep-ph/0310123, doi:10.1016/j.nuclphysb.2004.02.019.

[80] J. Liu, G. Segre, Reexamination of generation of baryon and lepton number asymmetries by heavy particle decay, Phys. Rev. D48 (1993) 4609–4612. arXiv:hep-ph/9304241, doi:10.1103/PhysRevD.48.4609.

[81] M. Flanz, E. A. Paschos, U. Sarkar, Baryogenesis from a lepton asymmetric universe, Phys. Lett. B345 (1995) 248–252, [Erratum: Phys. Lett.B382,447(1996)]. arXiv:hep-ph/9411366, doi:10.1016/0370-2693(96)00866-0,10.1016/0370-2693(96)00842-8,10.1016/0370-2693(94)01555-Q.

[82] M. Flanz, E. A. Paschos, U. Sarkar, J. Weiss, Baryogenesis through mixing of heavy Majorana neutrinos, Phys. Lett. B389 (1996) 693–699. arXiv:hep-ph/9607310, doi:10.1016/S0370-2693(96)01337-8,10.1016/S0370-2693(96)80011-6.

[83] L. Covi, E. Roulet, Baryogenesis from mixed particle decays, Phys. Lett. B399 (1997) 113–118. arXiv:hep-ph/9611425, doi:10.1016/S0370-2693(97)00287-6.

[84] L. Covi, E. Roulet, F. Vissani, CP violating decays in leptogenesis scenarios, Phys. Lett. B384 (1996) 169–174. arXiv:hep-ph/9605319, doi:10.1016/0370-2693(96)00817-9.

[85] A. Pilaftsis, CP violation and baryogenesis due to heavy Majorana neutrinos, Phys. Rev. D56 (1997) 5431–5451. arXiv:hep-ph/9707235, doi:10.1103/PhysRevD.56.5431.

[86] W. Buchmuller, M. Plumacher, CP asymmetry in Majorana neutrino decays, Phys. Lett. B431 (1998) 354–362. arXiv:hep-ph/9710460, doi:10.1016/S0370-2693(97)01548-7.

[87] M. D'Onofrio, K. Rummukainen, A. Tranberg, Sphaleron Rate in the Minimal Standard Model, Phys. Rev. Lett. 113 (14) (2014) 141602. arXiv:1404.3565, doi:10.1103/PhysRevLett.113.141602.

[88] E. K. Akhmedov, V. A. Rubakov, A. Yu. Smirnov, Baryogenesis via neutrino oscillations, Phys. Rev. Lett. 81 (1998) 1359–1362. arXiv:hep-ph/9803255, doi:10.1103/PhysRevLett.81.1359.

[89] M. Tanabashi, et al., Review of Particle Physics, Phys. Rev. D98 (3) (2018) 030001. doi:10.1103/PhysRevD.98.030001.

[90] I. Esteban, M. C. Gonzalez-Garcia, M. Maltoni, I. Martinez-Soler, T. Schwetz, Updated fit to three neutrino mixing: exploring the accelerator-reactor complementarity, JHEP 01 (2017) 087. arXiv:1611.01514, doi:10.1007/JHEP01(2017)087.

[91] Nufit 3.1 (2017).
URL nu-fit.org

[92] J. A. Casas, A. Ibarra, Oscillating neutrinos and muon —> e, gamma, Nucl. Phys. B618 (2001) 171–204. arXiv:hep-ph/0103065, doi:10.1016/S0550-3213(01)00475-8.

[93] J. Lopez-Pavon, E. Molinaro, S. T. Petcov, Radiative Corrections to Light Neutrino Masses in Low Scale Type I Seesaw Scenarios and Neutrinoless Double Beta Decay, JHEP 11 (2015) 030. arXiv:1506.05296, doi:10.1007/JHEP11(2015)030.

[94] T. Appelquist, R. Shrock, Neutrino masses in theories with dynamical electroweak symmetry breaking, Phys. Lett. B548 (2002) 204–214. arXiv:hep-ph/0204141, doi:10.1016/S0370-2693(02)02854-X.

[95] T. Appelquist, R. Shrock, Dynamical symmetry breaking of extended gauge symmetries, Phys. Rev. Lett. 90 (2003) 201801. arXiv:hep-ph/0301108, doi:10.1103/PhysRevLett.90.201801.

[96] M. Shaposhnikov, A Possible symmetry of the nuMSM, Nucl. Phys. B763 (2007) 49–59. arXiv:hep-ph/0605047, doi:10.1016/j.nuclphysb.2006.11.003.

[97] T. Hambye, D. Teresi, Higgs doublet decay as the origin of the baryon asymmetry, Phys. Rev. Lett. 117 (9) (2016) 091801. arXiv:1606.00017, doi:10.1103/PhysRevLett.117.091801.

[98] S. Eijima, M. Shaposhnikov, Fermion number violating effects in low scale leptogenesis, Phys. Lett. B771 (2017) 288–296. arXiv:1703.06085, doi:10.1016/j.physletb.2017.05.068.

[99] T. Hambye, D. Teresi, Baryogenesis from L-violating Higgs-doublet decay in the density-matrix formalism, Phys. Rev. D96 (1) (2017) 015031. arXiv:1705.00016, doi:10.1103/PhysRevD.96.015031.

[100] S. Eijima, M. Shaposhnikov, I. Timiryasov, Parameter space of baryogenesis in the $\nu$MSMarXiv:1808.10833.

[101] M. Shaposhnikov, The nuMSM, leptonic asymmetries, and properties of singlet fermions, JHEP 08 (2008) 008. arXiv:0804.4542, doi:10.1088/1126-6708/2008/08/008.

[102] A. Ibarra, E. Molinaro, S. T. Petcov, TeV Scale See-Saw Mechanisms of Neutrino Mass Generation, the Majorana Nature of the Heavy Singlet Neutrinos and $(\beta\beta)_{0\nu}$-Decay, JHEP 09 (2010) 108. arXiv:1007.2378, doi:10.1007/JHEP09(2010)108.

[103] A. Ibarra, E. Molinaro, S. T. Petcov, Low Energy Signatures of the TeV Scale See-Saw Mechanism, Phys. Rev. D84 (2011) 013005. arXiv:1103.6217, doi:10.1103/PhysRevD.84.013005.

[104] P. Hernández, M. Kekic, J. López-Pavón, J. Racker, J. Salvado, Testable Baryogenesis in Seesaw Models, JHEP 08 (2016) 157. arXiv:1606.06719, doi:10.1007/JHEP08(2016)157.

[105] M. Drewes, B. Garbrecht, D. Gueter, J. Klaric, Testing the low scale seesaw and leptogenesis, JHEP 08 (2017) 018. arXiv:1609.09069, doi:10.1007/JHEP08(2017)018.

[106] O. Ruchayskiy, A. Ivashko, Experimental bounds on sterile neutrino mixing angles, JHEP 06 (2012) 100. arXiv:1112.3319, doi:10.1007/JHEP06(2012)100.

[107] T. Asaka, S. Eijima, H. Ishida, Mixing of Active and Sterile Neutrinos, JHEP 04 (2011) 011. arXiv:1101.1382, doi:10.1007/JHEP04(2011)011.

[108] N. Metropolis, A. W. Rosenbluth, M. N. Rosenbluth, A. H. Teller, E. Teller, Equation of state calculations by fast computing machines, J. Chem. Phys. 21 (1953) 1087–1092. doi:10.1063/1.1699114.

[109] W. K. Hastings, Monte Carlo Sampling Methods Using Markov Chains and Their Applications, Biometrika 57 (1970) 97–109. doi:10.1093/biomet/57.1.97.

[110] R. Acciarri, et al., Long-Baseline Neutrino Facility (LBNF) and Deep Underground Neutrino Experiment (DUNE)arXiv:1512.06148.

[111] L. W. K. on behalf of the DUNE collaboration, Sensitivity of the DUNE Experiment to CP Violation, in: TAUP 2017, 2017.
URL https://indico.cern.ch/event/606690/contributions/2613000

[112] J. Berges, Introduction to nonequilibrium quantum field theory, AIP Conf. Proc. 739 (2005) 3–62, [,3(2004)]. arXiv:hep-ph/0409233, doi:10.1063/1.1843591.

[113] E. A. Calzetta, B.-L. B. Hu, Nonequilibrium Quantum Field Theory, Cambridge Monographs on Mathematical Physics, Cambridge University Press, 2008. doi:10.1017/CBO9780511535123.
URL http://www.cambridge.org/mw/academic/subjects/physics/theoretical-physics-and-mathematical-physics/nonequilibrium-quantum-field-theory?format=AR

[114] J. S. Schwinger, Brownian motion of a quantum oscillator, J. Math. Phys. 2 (1961) 407–432. doi:10.1063/1.1703727.

[115] L. V. Keldysh, Diagram technique for nonequilibrium processes, Zh. Eksp. Teor. Fiz. 47 (1964) 1515–1527, [Sov. Phys. JETP20,1018(1965)].

[116] E. Calzetta, B. L. Hu, Nonequilibrium Quantum Fields: Closed Time Path Effective Action, Wigner Function and Boltzmann Equation, Phys. Rev. D37 (1988) 2878. doi:10.1103/PhysRevD.37.2878.

[117] B. Garbrecht, M. Herranen, Effective Theory of Resonant Leptogenesis in the Closed-Time-Path Approach, Nucl. Phys. B861 (2012) 17–52. arXiv:1112.5954, doi:10.1016/j.nuclphysb.2012.03.009.

[118] M. Drewes, B. Garbrecht, D. Gueter, J. Klaric, Leptogenesis from Oscillations of Heavy Neutrinos with Large Mixing Angles, JHEP 12 (2016) 150. arXiv:1606.06690, doi:10.1007/JHEP12(2016)150.

[119] J. M. Cornwall, R. Jackiw, E. Tomboulis, Effective Action for Composite Operators, Phys. Rev. D10 (1974) 2428–2445. doi:10.1103/PhysRevD.10.2428.

[120] T. Prokopec, M. G. Schmidt, S. Weinstock, Transport equations for chiral fermions to order h bar and electroweak baryogenesis. Part 1, Annals Phys. 314 (2004) 208–265. arXiv:hep-ph/0312110, doi:10.1016/j.aop.2004.06.002.

[121] T. Prokopec, M. G. Schmidt, S. Weinstock, Transport equations for chiral fermions to order h-bar and electroweak baryogenesis. Part II, Annals Phys. 314 (2004) 267–320. arXiv:hep-ph/0406140, doi:10.1016/j.aop.2004.06.001.

[122] A. Anisimov, W. Buchmuller, M. Drewes, S. Mendizabal, Nonequilibrium Dynamics of Scalar Fields in a Thermal Bath, Annals Phys. 324 (2009) 1234–1260. arXiv:0812.1934, doi:10.1016/j.aop.2009.01.001.

[123] B. Garbrecht, M. Garny, Finite Width in out-of-Equilibrium Propagators and Kinetic Theory, Annals Phys. 327 (2012) 914–934. arXiv:1108.3688, doi:10.1016/j.aop.2011.10.005.

[124] R. Barbieri, P. Creminelli, A. Strumia, N. Tetradis, Baryogenesis through leptogenesis, Nucl. Phys. B575 (2000) 61–77. arXiv:hep-ph/9911315, doi:10.1016/S0550-3213(00)00011-0.

[125] W. Buchmuller, M. Plumacher, Spectator processes and baryogenesis, Phys. Lett. B511 (2001) 74–76. arXiv:hep-ph/0104189, doi:10.1016/S0370-2693(01)00614-1.

[126] B. Garbrecht, P. Schwaller, Spectator Effects during Leptogenesis in the Strong Washout Regime, JCAP 1410 (10) (2014) 012. arXiv:1404.2915, doi:10.1088/1475-7516/2014/10/012.

[127] S. Eijima, M. Shaposhnikov, I. Timiryasov, Freeze-out of baryon number in low-scale leptogenesis, JCAP 1711 (11) (2017) 030. arXiv:1709.07834, doi:10.1088/1475-7516/2017/11/030.

[128] J. A. Harvey, M. S. Turner, Cosmological baryon and lepton number in the presence of electroweak fermion number violation, Phys. Rev. D42 (1990) 3344–3349. doi:10.1103/PhysRevD.42.3344.

[129] M. Beneke, B. Garbrecht, M. Herranen, P. Schwaller, Finite Number Density Corrections to Leptogenesis, Nucl. Phys. B838 (2010) 1–27. arXiv:1002.1326, doi:10.1016/j.nuclphysb.2010.05.003.

[130] M. Garny, A. Kartavtsev, A. Hohenegger, Leptogenesis from first principles in the resonant regime, Annals Phys. 328 (2013) 26–63. arXiv:1112.6428, doi:10.1016/j.aop.2012.10.007.

[131] S. Iso, K. Shimada, M. Yamanaka, Kadanoff-Baym approach to the thermal resonant leptogenesis, JHEP 04 (2014) 062. arXiv:1312.7680, doi:10.1007/JHEP04(2014)062.

[132] P. S. Bhupal Dev, P. Millington, A. Pilaftsis, D. Teresi, Flavour Covariant Transport Equations: an Application to Resonant Leptogenesis, Nucl. Phys. B886 (2014) 569–664. arXiv:1404.1003, doi:10.1016/j.nuclphysb.2014.06.020.

[133] B. Garbrecht, F. Gautier, J. Klaric, Strong Washout Approximation to Resonant Leptogenesis, JCAP 1409 (09) (2014) 033. arXiv:1406.4190, doi:10.1088/1475-7516/2014/09/033.

[134] M. Beneke, B. Garbrecht, C. Fidler, M. Herranen, P. Schwaller, Flavoured Leptogenesis in the CTP Formalism, Nucl. Phys. B843 (2011) 177–212. arXiv:1007.4783, doi:10.1016/j.nuclphysb.2010.10.001.

[135] S. Blanchet, P. Di Bari, D. A. Jones, L. Marzola, Leptogenesis with heavy neutrino flavours: from density matrix to Boltzmann equations, JCAP 1301 (2013) 041. arXiv:1112.4528, doi:10.1088/1475-7516/2013/01/041.

[136] S. Iso, K. Shimada, Coherent Flavour Oscillation and CP Violating Parameter in Thermal Resonant Leptogenesis, JHEP 08 (2014) 043. arXiv:1404.4816, doi:10.1007/JHEP08(2014)043.

[137] B. Dev, M. Garny, J. Klaric, P. Millington, D. Teresi, Resonant enhancement in leptogenesis, Int. J. Mod. Phys. A33 (2018) 1842003. arXiv:1711.02863, doi:10.1142/S0217751X18420034.

[138] A. Anisimov, D. Besak, D. Bodeker, Thermal production of relativistic Majorana neutrinos: Strong enhancement by multiple soft scattering, JCAP 1103 (2011) 042. arXiv:1012.3784, doi:10.1088/1475-7516/2011/03/042.

[139] C. P. Kiessig, M. Plumacher, M. H. Thoma, Decay of a Yukawa fermion at finite temperature and applications to leptogenesis, Phys. Rev. D82 (2010) 036007. arXiv:1003.3016, doi:10.1103/PhysRevD.82.036007.

[140] B. Garbrecht, Leptogenesis: The Other Cuts, Nucl. Phys. B847 (2011) 350–366. arXiv:1011.3122, doi:10.1016/j.nuclphysb.2011.01.033.

[141] M. Laine, Y. Schroder, Thermal right-handed neutrino production rate in the non-relativistic regime, JHEP 02 (2012) 068. arXiv:1112.1205, doi:10.1007/JHEP02(2012)068.

[142] C. Fidler, M. Herranen, K. Kainulainen, P. M. Rahkila, Flavoured quantum Boltzmann equations from cQPA, JHEP 02 (2012) 065. arXiv:1108.2309, doi:10.1007/JHEP02(2012)065.

[143] A. Salvio, P. Lodone, A. Strumia, Towards leptogenesis at NLO: the right-handed neutrino interaction rate, JHEP 08 (2011) 116. arXiv:1106.2814, doi:10.1007/JHEP08(2011)116.

[144] S. Biondini, N. Brambilla, M. A. Escobedo, A. Vairo, An effective field theory for non-relativistic Majorana neutrinos, JHEP 12 (2013) 028. arXiv:1307.7680, doi:10.1007/JHEP12(2013)028.

[145] D. Besak, D. Bodeker, Thermal production of ultrarelativistic right-handed neutrinos: Complete leading-order results, JCAP 1203 (2012) 029. arXiv:1202.1288, doi:10.1088/1475-7516/2012/03/029.

[146] B. Garbrecht, F. Glowna, P. Schwaller, Scattering Rates For Leptogenesis: Damping of Lepton Flavour Coherence and Production of Singlet Neutrinos, Nucl. Phys. B877 (2013) 1–35. arXiv:1303.5498, doi:10.1016/j.nuclphysb.2013.08.020.

[147] D. Bodeker, M. Laine, Kubo relations and radiative corrections for lepton number washout, JCAP 1405 (2014) 041. arXiv:1403.2755, doi:10.1088/1475-7516/2014/05/041.

[148] M. Laine, Thermal right-handed neutrino production rate in the relativistic regime, JHEP 08 (2013) 138. arXiv:1307.4909, doi:10.1007/JHEP08(2013)138.

[149] B. Garbrecht, F. Glowna, M. Herranen, Right-Handed Neutrino Production at Finite Temperature: Radiative Corrections, Soft and Collinear Divergences, JHEP 04 (2013) 099. arXiv:1302.0743, doi:10.1007/JHEP04(2013)099.

[150] I. Ghisoiu, M. Laine, Right-handed neutrino production rate at $T > 160$ GeV, JCAP 1412 (12) (2014) 032. arXiv:1411.1765, doi:10.1088/1475-7516/2014/12/032.

[151] J. Ghiglieri, M. Laine, Neutrino dynamics below the electroweak crossover, JCAP 1607 (07) (2016) 015. arXiv:1605.07720, doi:10.1088/1475-7516/2016/07/015.

[152] J. Ghiglieri, M. Laine, GeV-scale hot sterile neutrino oscillations: a derivation of evolution equations, JHEP 05 (2017) 132. arXiv:1703.06087, doi:10.1007/JHEP05(2017)132.

[153] S. Biondini, et al., Status of rates and rate equations for thermal leptogenesis, Int. J. Mod. Phys. A33 (05n06) (2018) 1842004. arXiv:1711.02864, doi:10.1142/S0217751X18420046.

[154] G. C. Branco, L. Lavoura, J. P. Silva, CP Violation, Int. Ser. Monogr. Phys. 103 (1999) 1–536.

[155] B. Shuve, I. Yavin, Baryogenesis through Neutrino Oscillations: A Unified Perspective, Phys. Rev. D89 (7) (2014) 075014. arXiv:1401.2459, doi:10.1103/PhysRevD.89.075014.

[156] S. Antusch, E. Cazzato, O. Fischer, Heavy neutrino-antineutrino oscillations at collidersarXiv:1709.03797.

[157] M. Anelli, et al., A facility to Search for Hidden Particles (SHiP) at the CERN SPSarXiv:1504.04956.

[158] E. Graverini, SHiP sensitivity to Heavy Neutral Leptons.
URL https://cds.cern.ch/record/2214085

[159] C. Adams, et al., The Long-Baseline Neutrino Experiment: Exploring Fundamental Symmetries of the UniversearXiv:1307.7335.

[160] T. Asaka, S. Eijima, A. Watanabe, Heavy neutrino search in accelerator-based experiments, JHEP 03 (2013) 125. arXiv:1212.1062, doi:10.1007/JHEP03(2013)125.

[161] S. Antusch, E. Cazzato, O. Fischer, Sterile neutrino searches via displaced vertices at LHCb, Phys. Lett. B774 (2017) 114–118. arXiv:1706.05990, doi:10.1016/j.physletb.2017.09.057.

[162] A. Kobach, S. Dobbs, Heavy Neutrinos and the Kinematics of Tau Decays, Phys. Rev. D91 (5) (2015) 053006. arXiv:1412.4785, doi:10.1103/PhysRevD.91.053006.

[163] M. Gronau, C. N. Leung, J. L. Rosner, Extending Limits on Neutral Heavy Leptons, Phys. Rev. D29 (1984) 2539. doi:10.1103/PhysRevD.29.2539.

[164] D. Curtin, R. Sundrum, Flashes of Hidden Worlds at CollidersarXiv:1702.02524, doi:10.1063/PT.3.3594.

[165] G. Anamiati, M. Hirsch, E. Nardi, Quasi-Dirac neutrinos at the LHC, JHEP 10 (2016) 010. arXiv:1607.05641, doi:10.1007/JHEP10(2016)010.

[166] D. Gorbunov, M. Shaposhnikov, How to find neutral leptons of the $\nu$MSM?, JHEP 10 (2007) 015, [Erratum: JHEP11,101(2013)]. arXiv:0705.1729, doi:10.1007/JHEP11(2013)101,10.1088/1126-6708/2007/10/015.

[167] A. Atre, T. Han, S. Pascoli, B. Zhang, The Search for Heavy Majorana Neutrinos, JHEP 05 (2009) 030. arXiv:0901.3589, doi:10.1088/1126-6708/2009/05/030.

[168] H. Abramowicz, et al., The International Linear Collider Technical Design Report - Volume 4: DetectorsarXiv:1306.6329.

[169] W. Kilian, T. Ohl, J. Reuter, WHIZARD: Simulating Multi-Particle Processes at LHC and ILC, Eur. Phys. J. C71 (2011) 1742. arXiv:0708.4233, doi:10.1140/epjc/s10052-011-1742-y.

[170] M. Moretti, T. Ohl, J. Reuter, O'Mega: An Optimizing matrix element generator (2001) 1981–2009arXiv:hep-ph/0102195.

[171] J. S. Marshall, M. A. Thomson, Pandora Particle Flow Algorithm, in: Proceedings, International Conference on Calorimetry for the High Energy Frontier (CHEF 2013): Paris, France, April 22-25, 2013, 2013, pp. 305–315. arXiv:1308.4537.

[172] P. Abreu, et al., Searches for heavy neutrinos from Z decays, Phys. Lett. B274 (1992) 230–238. doi:10.1016/0370-2693(92)90528-C.

[173] P. Abreu, et al., Search for neutral heavy leptons produced in Z decays, Z. Phys. C74 (1997) 57–71, [Erratum: Z. Phys.C75,580(1997)]. doi:10.1007/s002880050370.

[174] J. Gluza, T. Jeliński, Heavy neutrinos and the pp$\to$lljj CMS data, Phys. Lett. B748 (2015) 125–131. arXiv:1504.05568, doi:10.1016/j.physletb.2015.06.077.

[175] P. S. Bhupal Dev, R. N. Mohapatra, Unified explanation of the $eejj$, diboson and dijet resonances at the LHC, Phys. Rev. Lett. 115 (18) (2015) 181803. arXiv:1508.02277, doi:10.1103/PhysRevLett.115.181803.

[176] A. Das, P. S. B. Dev, R. N. Mohapatra, Same Sign versus Opposite Sign Dileptons as a Probe of Low Scale Seesaw Mechanisms, Phys. Rev. D97 (1) (2018) 015018. arXiv:1709.06553, doi:10.1103/PhysRevD.97.015018.

[177] G. Cvetič, A. Das, J. Zamora-Saá, Probing heavy neutrino oscillations in rare W boson decaysarXiv:1805.00070.